ISSN 0256-4637

VOLUME 31 NUMBER 1 January-March, 2009

Journal of Pure and Applied

Ultrasonics

Website : www.ultrasonicsindia.com

A Publication of — Ultrasonics Society of India

A Quarterly Publication of Ultrasonics Society of India

Journal of Pure and Applied

Ultrasonics

No. 1 Volume 31 Jan.-March, 2009

SUBSCRIPTION (postage paid)

Single	Rs. 550/-	US $ 50/-
Annual	Rs. 2200/-	US $ 200/-
USI Member	Free	

The submission of papers and all other correspondence regarding the Journal may please be addressed to :

Publication Secretary
Journal of Pure and Applied Ultrasonics
C/o Ultrasonics Society of India
National Physical Laboratory
Dr. K. S. Krishnan Marg
New Delhi-110012

Ultrasonics Society of India

Ultrasonics Society of India established in 1974, is engaged in the promotion of research and diffusion of knowledge concerning the field of ultrasonics and allied areas.

Membership of the Society is open to individuals without distinction of sex, race or nationality and to bodies who subscribe to the aims and objectives of the Society.
The membership fee is as follows :

Class of Membership	**Subscription (one time)**
Honorary Fellow	Nil
Fellow/Member	Rs. 1200/-
Associate Member	Rs. 500/- (for 5 yrs.)
Corporate Member	Rs. 6000/-
Fellow/Member (Foreign)	US $ 100/-
Corporate Member (Foreign)	US $ 500/-

Membership forms and the relevant information can be downloaded from the website or obtained from :

The General Secretary
Ultrasonics Society of India
National Physical Laboratory
Dr. K. S. Krishnan Marg
New Delhi-110012
e-mail : info@ultrasonicsindia.com

J. Pure Appl. Ultrason. 31 (2009) pp. 1-12

Ultrasound techniques for characterizing liquids I. broad-band spectrometers†

UDO KAATZE
Drittes Physikalisches Institut, Georg-August-Universität,
Friedrich-Hund-Platz 1, 37077 Göttingen, Germany
e-mail : uka@physik3.gwdg.de

This tutorial gives a short introduction into the broad-band ultrasonic spectroscopy of liquids. The fundamentals of acoustical methods are summarized. Preference is given to methods using continuous waves and pulse modulated signals. Related techniques, such as time-domain methods with step-like excitation of the sample and with optical monitoring of acoustical waves (Brillouin scattering), are briefly mentioned, too. Constructions of some types of sonic cells for liquids and electronic set-ups for spectral measurements are presented in detail. The merits and limitations of different techniques of measurements, covering the frequency range from almost 10 kHz up to nearly 10 GHz, are discussed. Together with applications in the relaxation properties of liquids, examples of broadband ultrasonic spectra are shown.

Key words : Ultrasonic spectroscopy, liquids, relaxations, acoustical absorption coefficient, sound velocity

INTRODUCTION

Acoustical signals couple to liquids via fundamental parameters, such as the density, viscosity, and heat capacity[1-11]. By utilizing these parameters acoustical measurements probe the native systems; labels or markers, as required by many other measurement techniques for liquids, are not necessary. Variations in the relevant liquid parameters may result from variations in the thermodynamic parameters, for example from changes in the hydrodynamic pressure, the temperature, or the pH. Variations in the sample property following thereby are often investigated by single-frequency methods which will be the focus of part II of this review.

Density, viscosity, and heat capacity of a liquid may also vary with the frequency ν of the sonic field. Such variations happen when an energy barrier exists that prevents molecules, ions, or mesoscopic structures of a liquid from instantaneously following the external field. The retarded energy transfer between different molecular states of a liquid results in a phase lag between pressure and density of a harmonic acoustic wave. Therefore, acoustic energy is absorbed and dissipated as heat. According to the fluctuation - dissipation theorem and, by analogy with the Kramers - Kronig relations[12,13], a characteristic velocity dispersion $dc/d\nu > 0$ is related with the absorption (c is the sound velocity of the liquid). In a relaxing system the relative dispersion step $[c(\nu\rightarrow 0)-c(\nu\rightarrow\infty)]/c(\nu\rightarrow\infty)$ is small and frequently does not exceed the experimental

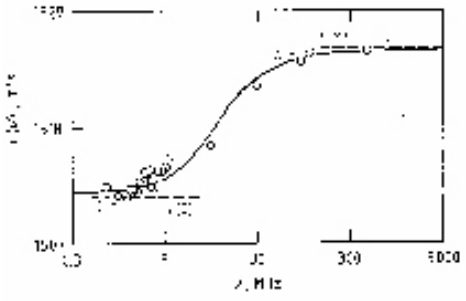

Fig.1. Sound velocity spectrum of a 0.4 mol/l solution of zinc chloride ($ZnCl_2$) in water at 25°C.[14] The line shows the dispersion as calculated from the associated absorption spectra

†Invited talk presented at NSU-XVII, B.H.U., Varanasi, Dec. 4-6, 2008.

errors. Fig. 1 displays already an extraordinarily large dispersion for aqueous systems. Because of the small dispersion amplitude of most liquid relaxations only a comparatively few broad-band sound velocity spectra exist presently. Outstanding exceptions are given, for instance 15 and 16. Because of the typically small dispersion, this part of the review is mainly restricted to ultrasonic absorption measurements.

If small effects of thermal conductivity, which play a noticeable role only in liquid metals, are neglected, the laws of conservation of mass and momentum yield the following relation for the complex propagation constant $\gamma = \alpha + i\beta$ of a sinusoidal acoustic wave within a liquid[1]

$$\left(\frac{\gamma}{i\omega}\right)^2 = \frac{\rho}{\kappa_s^{-1} + i\omega\left(\frac{4}{3}\eta^s + \eta_v\right)} \tag{1}$$

Here $i^2=-1$, α is the absorption coefficient, $\beta = 2\pi/\gamma$ where $\gamma = c/\nu$ is the wavelength, $\omega = 2\pi\nu$ is the angular frequency, ρ is the density,

$$\kappa_s = \rho^{-1} c^{-2} \tag{2}$$

is the adiabatic compressibility of the liquid, and η_s and η_v are the shear and volume viscosity, respectively. The latter is related to the curl-free part of the acoustic field. At small frequencies $(\omega \ll [\kappa_s(4\eta_s/3+\eta_v]^{-1})$ follows for the absorption along a wavelength

$$\alpha\lambda = \pi\kappa_s\omega\left(\frac{4}{3}\eta_{s0} + \eta_{v0}\right) \tag{3}$$

with η_{s0} and η_{v0} referring to very low frequencies. Because of molecular interactions, indicated by the internal energy barriers mentioned before, both the shear viscosity and the volume viscosity may be subject to relaxation and may thus depend on frequency. If we write

$$\eta_s = \eta_s(\nu) = \eta_{s\infty} + \Delta\eta_s(\nu) \tag{4}$$

and

$$\eta_v = \eta_v(\nu) = \eta_{v\infty} + \Delta\eta_v(\nu) \tag{5}$$

with $\eta_{s\infty} = \eta_s(\nu\to\infty)$ and $\eta_{v\infty} = \eta_v(\nu\to\infty)$ denoting the viscosities at frequencies well above the measurement range, eq. (3) according to

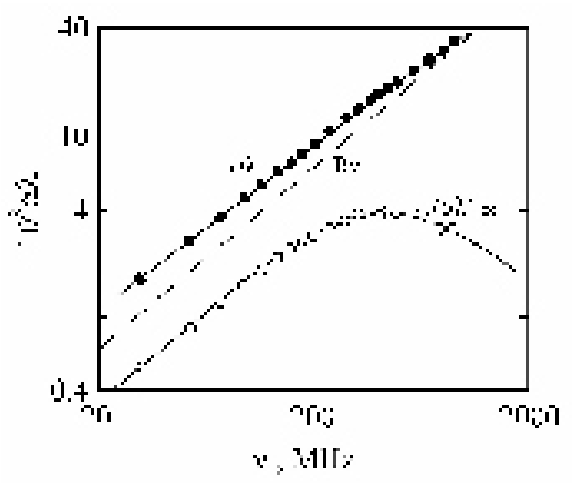

Fig.2. Ultrasonic absorption spectra of a 0.5 mol/l solution of copper chloride (CuCl2) in water at 25°C[14] Experimental total absorption-per-wavelength data are shown by points, the asymptotic high-frequency background absorption is represented by the dashed line, and the excess absorption-per-wavelength is indicated by circles. The full line is the graph of a Debye-type relaxation term eq. 8 with the following value for the parameters: $A = 7.6 \cdot 10^{-3}$, $\tau = 0.35$ ns

$$\alpha\lambda = (\alpha\lambda)_{exc}(\nu) + B\nu \tag{6}$$

can be separated into two parts. Here

$$B\nu = 2\pi^2\kappa_S\left(\frac{4}{3}\eta_{s\infty} + \eta_{v\infty}\right) \tag{7}$$

is independent of ν if the compressibility does not depend on ν. It is obvious from eq.(1) that a frequency dependent shear viscosity or volume viscosity leads also to a frequency dependent β and thus a frequency dependent c_s. As, however, briefly discussed above, the dispersion in the sound velocity of liquids is normally small. Strictly, κ_S must be replaced by $\kappa_{S\infty}$ in eq. (7).

Normally, in liquid spectroscopy we are interested in the excess absorption-per-wavelength $(\alpha\lambda)_{exc}(\nu)$ only. Nevertheless the asymptotic high-frequency term $B\nu$ in eq. (6) acts a considerable influence on the measurements. Due to its frequency dependence, proportional to ν, it dominates the total absorption-per-wavelength $\alpha\lambda$ at high frequencies and restricts measurements of liquids to frequencies below some GHz. An illustrative example, in which $(\alpha\lambda)_{exc} \approx 0.1 \cdot (\alpha\lambda)$ only at 1 GHz, is given in Fig. 2. It is the asymptotic high-frequency ("background") term $B\nu$ which necessitates different methods of measurements at low and high frequencies.

The excess absorption-per-wavelength

spectrum in Fig. 2 can be well represented by a Debye type relaxation term[17].

$$(\alpha\lambda)_{exc}(\nu) = \frac{A\omega\tau}{1+\omega^2\tau^2} \tag{8}$$

with discrete relaxation time τ. A (= $2(\alpha\lambda)_{exc}$ at $\nu = 1/(2\pi\tau)$) is the relaxation amplitude. Debye relaxation terms, and the more terms with underlying relaxation time distribution[18], are notoriously broadband. Their adequate evaluation thus requires measurements over an extended frequency range. This is the more true if the spectra of the liquids of interest display a superposition of relaxation regimes, as illustrated by the example given in Fig. 3.

CONTINUOUS WAVE METHODS

a. *Basic aspects*

At low frequencies (ν <20 MHz) the background term $B\nu$ in the absorption-per-wavelength of most liquids (eq. 6) is small. Therefore, measurement techniques are applied in which the path length of interaction between the acoustic field and the liquid is virtually increased by multiple reflections. Typically, cylindrical cells are used in which the waves propagate in a quasi-plane-wave mode along the direction of the cell axis. Because of their favourably small intrinsic loss at low frequencies spherical resonators, operated in a radial wave mode, have been also used. More recently a cell construction for the frequency range 12.5-150 kHz has been described[19]. In this paper the much more common cylindrical cavity cells[20] will be discussed in detail. In these cells the waves are reflected back and forth at the cylinder faces. Often these faces are made of piezoelectric transducers of which one acts as transmitter and the other one a receiver[15,20,21-23]. However, cavities with passive glass reflectors and separate piezoelectric devices for the coupling of the cell to the electronic set-up provide also favourable features for liquid measurements. Noteworthy is the small intrinsic loss of such resonators[24].

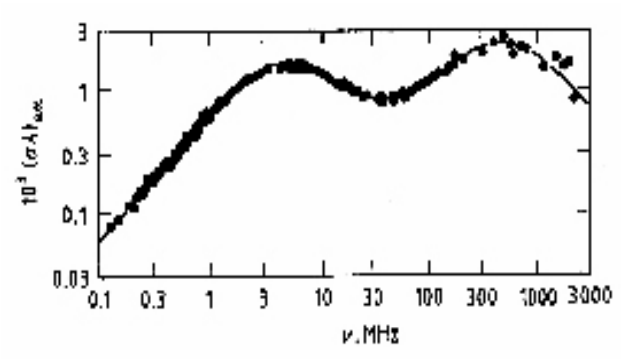

Fig.3. Ultrasonic excess absorption-per-wavelength spectrum of a 0.1 mol/l solution of manganese sulphate ($MnSO_4$) in water at 25°C.23 The line represents a superposition of two Debye relaxation terms

Assuming infinite lateral dimensions the plane wave transfer function for propagation in x-direction is

$$T_{ac}(\nu,\alpha,c,x) = \hat{T}_{ac}\frac{(1+r_r(\nu))exp(-\gamma x)}{1-r_t(\nu)r_r(\nu)exp(-2\gamma x)} \tag{9}$$

where r_t and r_r are the reflection coefficients at the transmitter/liquid and liquid/receiver interfaces, respectively, and $\hat{T}_{ac}$ is an amplitude. Normally, identical transducers are used as transmitter and receiver so that r_t=r_r := r. Because of the low conversion factor of the transducers, the amplitude of the receiver signal is very small and, therefore, electrical crosstalk cannot be neglected. Taking crosstalk with amplitude $\hat{C}$ and phase angle Φ_c into account the magnitude of the total transfer function reads

$$|T_{tot}| = \hat{T}_{ac}\left|\frac{(1+r_r(\nu))exp(-\gamma x)}{1-r_t(\nu)r_r(\nu)exp(-2\gamma x)}\right| + \hat{C}\,exp\,(i\Phi_c). \tag{10}$$

As an example a $|T_{tot}|$ - versus - x relation at 470 kHz is displayed in Fig. 4. Resonance peaks emerge in the relation at distance x_n, n = 1, 2, 3,…, which when, in a first approach, ideal reflection at the liquid/transducer interfaces ($|r|$ = 1) are assumed, follow as

$$x_n = nc/(2\nu_m). \tag{11}$$

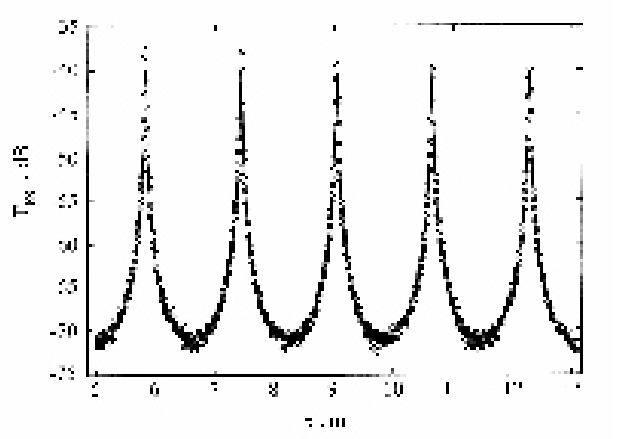

Fig.4. Magnitude of the cell transfer function (eq. 10) versus cell length x for a cell (diameter = 60 mm, frequency = 470 kHz) filled with a 0.1 mol/l aqueous solution of $MnSO_4$ at 25°C[36]

Hence the sound velocity c of the liquid can be obtained from the x_n values, whereas the absorption coefficient can be derived from the finite half-power bandwidth of the resonance peaks or, alternatively, from the decrease in the peak amplitudes with sample length x at fixed measurement frequency ν_m.

Variation of the sample length x for the measurement of the transfer function and subsequent regression analysis of this function in terms of the theoretical relation requires rather sophisticated variable path-length cells and also rather complicated routines for the fitting procedures[25]. For this reason continuous wave measurements are normally performed at fixed sample length l and varying frequency ν.

b. *Resonator transfer function, quality factor*

The transfer function of an ideal resonator ($|r| = 1$) with plane faces (eq. 9)

$$T_{ac,id} = \hat{T}_{ac}\,[\sinh(\alpha l)\cos(\omega l/c) + i\cosh(\alpha l)\sin(\omega l/c)]^{-1} \tag{12}$$

can be developed at low liquid losses ($\alpha l \gg 1$) around their resonance frequencies

$$\nu_{n,id} = nc/(2l), \quad n = 1,2,3,\ldots \tag{13}$$

to yield the half-power bandwidth

$$\Delta\nu_{n,id} = \alpha c/\pi \tag{14}$$

of the n-th resonance curve. Eqs. (13), (14) are frequently taken the basis of resonance peak evaluation. It has to be kept in mind, that for a plane X-cut quartz transducer/water interface, for example, the reflection factor magnitude $|r|$ is about 0.8 only, whereas for the 35° rotated Y-cut lithium niobate transducer/water interface $|r| \approx 0.92$. It is thus more appropriate to assume nearly ideal reflection at the transducer - air backside interface and to consider penetration of the acoustic waves into the transducers by the transfer function

$$T(\nu) = T_t(\nu)\cdot T_{ac}(\nu)\cdot T_r(\nu). \tag{15}$$

Here T_t and T_r denote the transmitter and receiver transfer functions, respectively. A nonequidistant distribution of resonance frequencies[26]

$$\nu_n = \nu_{n,id} + \frac{c}{\pi l}\arctan\left[\frac{Z}{Z_t}\cot(\pi\nu_{n,id}/\nu_t)\right] \tag{16}$$

follows with the second term on the right hand side being a correction term to the simple relation given by eq. (13). In eq. (16) Z and Z_t are the acoustic impedances of the liquid and the transducers, respectively, and ν_t is the transducer fundamental frequency of thickness vibrations. Again identical transmitter and receiver transducers are assumed.

So far finite lateral resonator dimensions and thus perfectly plane waves have been presumed. In real cells energy dissipation due to diffraction and, in addition, radiation energy losses at the transducer back faces contribute to the total half-power bandwidth, given by the relation[15].

$$\Delta\nu_n = \nu_{n,id} + Y_1 c^3 \nu^{-2} + Y_2 c. \tag{17}$$

Radiation losses, represented by the last term on the right hand side of eq. (17), become strong near νt and its overtones. Those frequency regions are normally omitted in ultrasonic resonator measurements of liquids. The effect of diffraction losses, analytically considered by the second term on the right hand side of eq. (17), is illustrated by Fig. 5 which clearly demonstrates the strong increase of the $\Delta\nu_n$ data toward low frequencies, proportional to ν^{-2}.

In resonator applications all intrinsic instrumental ("in") losses are taken into account by correcting the quality factor $Q = \nu_n/\Delta\nu_n$ using the relation

$$Q_{id}^{-1} = Q^{-1} - Q_{in}^{-1} \tag{18}$$

which is based on energy arguments. In this equation Q is the total quality factor obtained from the measurements and Q_{id} the ideal one to be used in eq. (14). Q_{in} has to be found by calibration measurements using liquids of well known absorption coefficient. Because of the strong dependence of the diffraction term in eq. (17) upon c, the reference liquid used for the calibration should match the sound velocity of the sample as close as possible. Since, according to eq. (16), the resonance frequency of the cell is a function of the liquid-to-transducer acoustic impedance ratio, the density of the reference liquid should also almost agree with that of the sample.

c. *Resonator face shape, mode spectrum*

Real cells differ from ideal cavity resonators in their finite lateral dimensions. Their mode spectrum, therefore, exhibits higher order modes

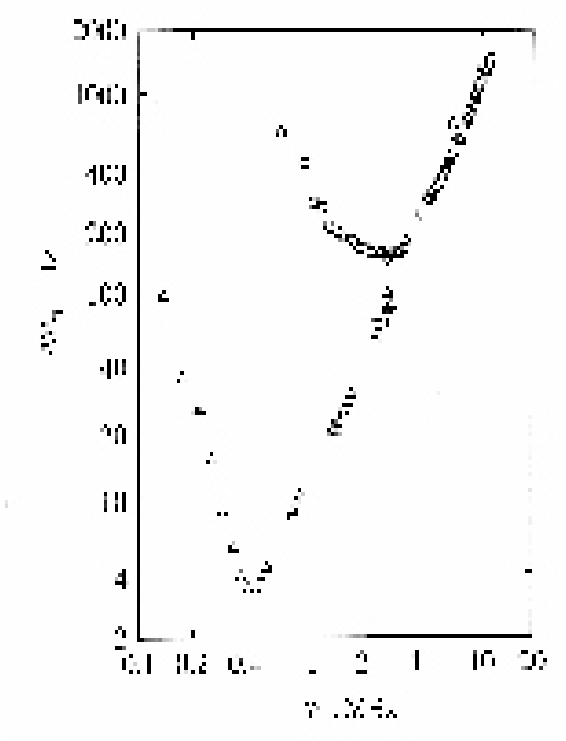

Fig. 5. Half-power bandwidth as a function of resonance frequency for a biplanar resonator cell (o, transducer diameter d_t = 16.4 mm, transducer fundamental frequency of thickness vibrations ν_t = 4 MHz) and a plano-concave cell (Δ,d_t = 80 mm, ν_t = 1 MHz).[36] Towards high frequencies the $\Delta\nu_n$ data increase due to the liquid losses, towards low frequencies diffraction losses become more and more significant

("satellites"), in addition to the principal resonances. The acoustical field of the most commonly used circular cylindrical resonators with plane faces involves radial satellite modes with resonance frequencies $\nu_{n,k}$ larger than those of the principal mode, ν_n. An example of a mode spectrum of a biplanar cavity resonator cell is given in Fig. 6. The frequency distance of the satellite modes is expressed by the relation[15].

$$\nu_{n,k} - \nu_n = \frac{1}{8\nu_n}\left(\frac{c}{R}\right)^2\left(k+\frac{1}{2}\right)(k-1) \tag{19}$$

with R denoting the cell radius and n,k = 1, 2, 3,… At small absorption ($\alpha l < 0.1$), the transfer function near a principal resonance can be developed as a sum of Lorentz terms, yielding the magnitude

$$\left|T_{ac}(\nu)\right| = \sum_{k=0}^{K}\frac{A_k}{1+i2(\nu-\nu_k)/\Delta\nu_k}\,. \tag{20}$$

In this equation k = 0 denotes the principal resonance and k = 1, 2, 3… indicate the higher

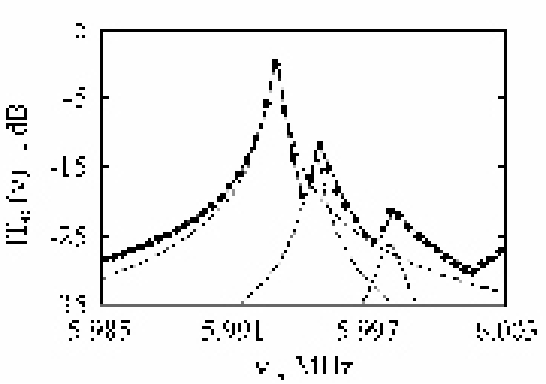

Fig.6. Magnitude of the transfer function around a principal resonance peak for a cavity resonator (d_t = 20 mm, ν_t = 4 MHz) filled with water at 25°C.[26] The dashed lines indicate Lorentz terms, the full line shows the superposition of these terms

order modes. Parameters A_k, ν_k, and $\Delta_{\nu k}$ are the amplitude, resonance frequency, and half-power bandwidth, respectively, of the k-th Lorentz term. As shown by Fig. 6 the mode spectrum at small α can be well represented by eq. (20). At higher absorption coefficient the satellite peaks may be largely masked by the principal resonance peak. Depending on the strength of the overlap of the peaks, empirical procedures are then required for a separation of the satellites from the principal resonance. The frequency distances of the higher order modes, for example, may be determined from reference measurements using liquids with small α and may then be fixed in the evaluation procedure.

An alternative method is the use of resonators with concave faces for which the mode spectrum reads

$$\nu_{n,k} = \left[n + \frac{k+1}{\pi}\xi\right]\frac{c}{2l} \tag{21}$$

with n = 1, 2, 3,…, k = 0, 1, 2,…, and

$$\xi = arccos(1-l/R)^z \tag{22}$$

where R denotes the radius of curvature of the faces and z = 1 for the half-symmetric plano-concave resonator as well as z = ½ for the symmetric biconcave resonator.

Because of the focusing effect of their faces plano-concave[22,27-29] and biconcave[23,24,30-32] resonators provide a smaller half-power bandwidth than biplanar cells[15,21,33-35] (Fig. 5). Focusing faces are particularly suitable for measurements at low frequencies (ν < 1 MHz). Another advantage of

concave faces is a considerably smaller effect from small disturbances in the cell geometry on the resonator properties. Tedious parallel adjustments of the faces, as with biplanar cells, are not necessary.

d. Data recording

Our everyday electronic devices enable easy and automated measurements and subsequent numerical analysis of the resonator transfer function around a principal resonance peak. Such mode of measurements allows for a careful consideration of the effects from higher order satellite peaks on the parameters of the principal resonance. It also permits to detect symmetries in resonance curves from electromagnetic crosstalk and irregularities in the transducer transfer functions. Fig. 7 shows an electronic set-up offering highly accurate multipoint transfer function measurements with quick and easy performance. The sinusoidal signal of frequency ν and less than 15 dBm power is provided by a highly stable synthesized signal generator (S) of a network analyzer (nwa, 1). Part of the signal is decoupled by a power splitter (2) and fed back to the reference channel (R) of the nwa receiver unit. The other part of the signal is applied to the piezoelectric transmitter of the cell (3). The receiver signal of the resonator is processed by an amplifier (4), which alleviates impedance mismatch, and is fed to the measuring channel (M) of the nwa receiver. A computer (5) controls the measurement

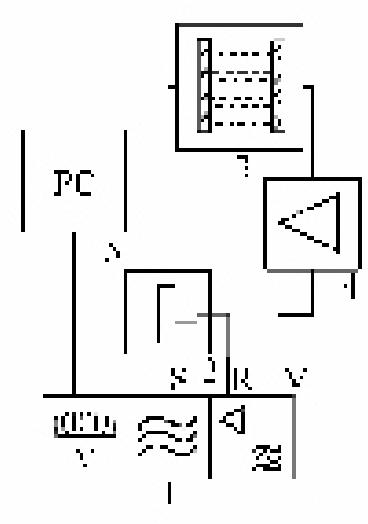

Fig.7. Scheme of a sonic resonator measurement set-up[20,36] (1, network analyzer with S, signal output port, as well as R, reference and M, measurement signal input ports; 2, signal divider; 3, cavity resonator cell; 4, amplifier; 5, process control computer)

procedure and it stores and processes the data. Complex measurements of the transfer function yield, of course, more information than scalar measurements. In principle, however, scalar measurements of the magnitude of $T(\nu)$ are also sufficient. When dealing with high quality factors ($Q > 10^5$) the resolution of the nwa must be better than 1 Hz.

e. Resonator design

As an example, Fig. 8 shows the construction of a resonator cell in which one face is a planar quartz transducer disc, the other one is a concavely ground and finely polished X-cut quartz disc of the same diameter and thickness and a radius of curvature R = 2 m.[22] The holding frame of this cell fulfils the requirements for a high mechanical stability, enables sensitive adjustment of one transducer relative to the other one, offers the possibility to suit the cell length to the acoustical properties of the liquid under test, and it allows the cell to be easily opened for inspection and transducer exchange.

Frame 15 in Fig. 8, holding the setting (5) of the plane transducer (2) fits into the main frame (13) by a ball joint (15). The setting is pressed to the main frame by three springs (17). With the aid of three finely adjustable counteracting screws (16) frame 15 and thus the piezoelectric transducer disc (2) can be precisely tipped and rotated for alignment of its surface with respect to the cell axis. As mentioned above, parallel adjustment of both transducers is compulsory for resonators with two planar faces. For that purpose the use of even more precise differential screws is recommended[21].

Various transducer mountings have been described, e.g. in[21,22]. In the configuration shown in Fig. 8 the quartz discs (2, 3) are affixed to their fittings (5) by means of elastic silicone rubber. In this way the least impediment is added to the transducers with respect to their thickness oscillations: maximizing the active diameter of vibrations and thus the beam zone of the sonic field, diffraction effects are reduced. In order to provide electrical contact to the front side of the transducers, the front side electrodes, essentially thin evaporated layers of chrome and gold, also cover the convex surfaces of the discs and zigzag shaped elastic bronze strips are embedded in the silicone layers[28]. Since silicone rubber is not chemically inert against many liquids of interest other configurations have to be also used[21,22]. As a compromise the silicone layers may be protected

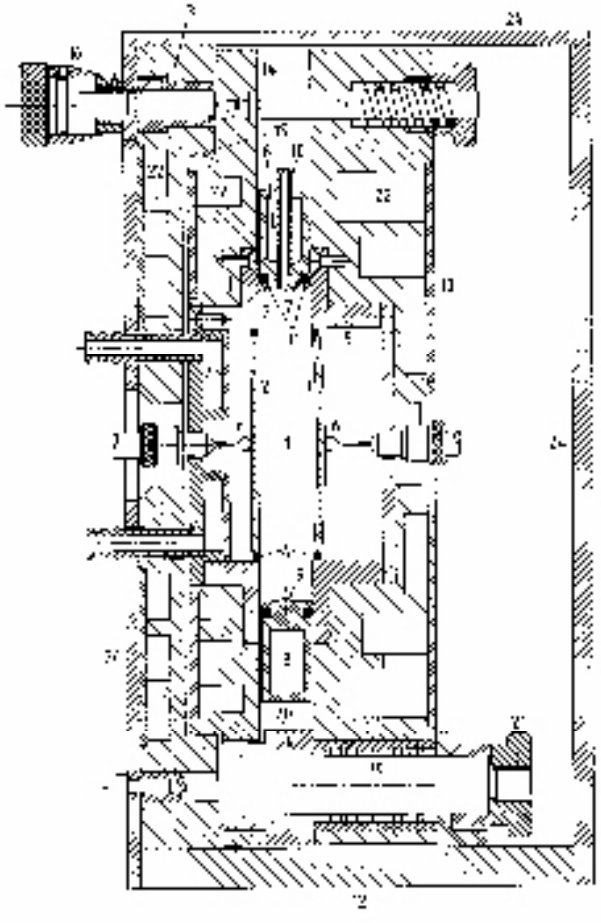

Fig.8. Cross section of a plano-concave cavity resonator cell.[22] 1, sample volume; 2, planar circular piezoelectric quartz transducer covered by coaxially evaporated thin films of chrome and gold for the electrical contacts; 3, transducer disc as 2 but concavely shaped; 4, layer of silicone rubber with bronze strips providing the electrical contact between the transducer front electrode and the holding frame; 5, transducer setting; 6, spring contact to the transducer backside ("hot") electrode; 7, cell jacket with 8, channel for circulating thermostat fluid; 9, inlet and 10, outlet for the sample liquid; 11, sealing 'o'-ring; 12, base plate; 13, main frame fixed with respect to 12; 14, adjustable frame with 15, ball joint; 16; precisely adjustable screw with 17, counteracting spring; 18, movable frame fixed against radial displacement and tilting by 19, ball bush guides; 20, gauge block establishing the distance between 13 and 18; 21, locking device; 22 and 23, thermostatic channels; 24 thermostatic shield

by O-rings as elastic seals.

Versatility and high mechanical stability at the same time is reached with the aid of three set-screws (21) fixing the movable frame (18). Gauge blocks (20) guarantee the correct distance of frame (18) to the main frame (13). Along with the cell jacket (8) the gauge blocks can be exchanged to provide another cell length. Due to their high demands in the mechanical stability resonators, in particular such with two planar faces, are sensitive to temperature variations. The holding frames, the cell jacket, and the transducer fixtures are therefore provided with channels for circulating thermostat fluid. It is recommended to place the resonator in an additional thermostatic box and to place the instrument on a solid slab which is carefully isolated against structure borne sound.

PULSE-MODULATED WAVE METHODS

a. Experimental set-up

Pulse modulation of ultrasonic waves for the separation of the measurement signal from electrical crossover and from multiple reflected waveforms is well-established in liquid measurements at frequencies between 1 MHz and 5 GHz. Since fixed-path-cell techniques require calibration measurements with reference liquids, variable path length methods are much more frequently used[20,36]. For this reason this tutorial will focus on the latter. A description of a fixed-path method with comparatively simple cell construction is given in ref[37].

Fig. 9 presents the scheme of the set-up for automatic pulse-modulated wave transmission measurements with variable path-length cells that yields absolute absorption coefficient data. The centre of the apparatus is a direct RF comparator arrangement[37-39]. that allows for a highly accurate determination of the magnitude of the cell transfer function as a function of the cell length x. If this distance between the transmitter and the receiver transducer of the cell (8, Fig. 9) is sufficiently large and if electrical crosstalk is neglected the transfer function (and thus the voltage at the receiver transducer 10) according to eq. (9) is expected to decrease exponentially with x. Hence a set of receiver voltage and corresponding cell length data yields directly the absorption coefficient α at frequency ν from the relation

$$In\left|T_{ac} / \hat{T}_{ac}\right| = -ax \tag{23}$$

The accuracy of the method is thus given by the precision of the x and receiver voltage data. As shown in the next section, the precision in the determination of the cell length can be kept small. In this RF comparator version of measurements a high accuracy of the receiver voltage data is guaranteed by substituting of the cell (8) for a precise attenuator (16). Below-cut-off piston attenuators with exactly adjustable

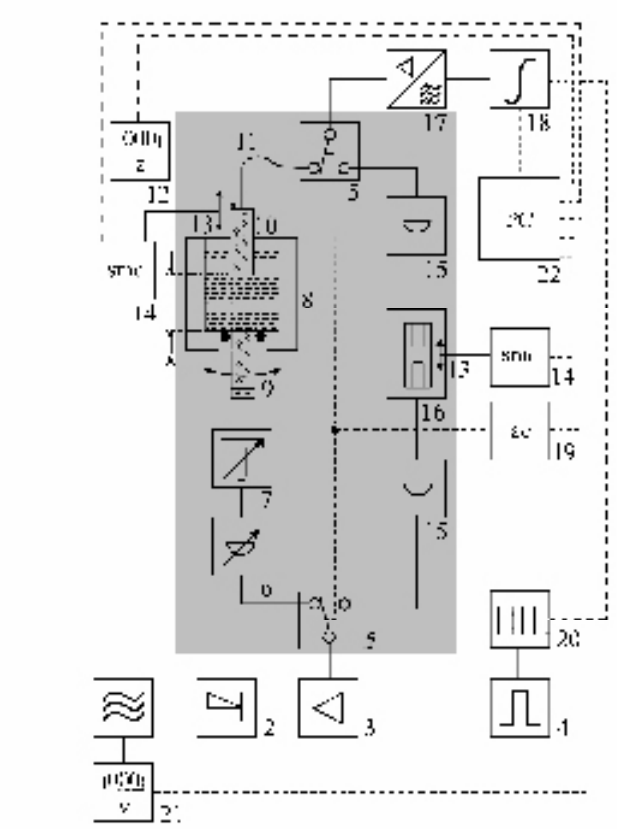

Fig.9. Block diagram of a semi-automatic comparator apparatus for absolute sonic absorption coefficient measurements at frequencies between 1 MHz and 5 GHz.[37-39] 1, signal generator; modulator; 3, broadband power amplifier; 4, pulse generator; 5, change-over switch; 6, variable attenuator; 7, impedance transformer; 8, sample cell with 9, transmitter unit provided with a device for parallel adjustment with respect to 10, receiver unit; 11, digital distance meter with 12, control unit; 13, stepping motor drive or piezo-translator with 14, control unit; 15, fixed coaxial attenuator for impedance matching; 16, high-precision adjustable below-cut-off piston attenuator; 17, superheterodyne receiver; 18, boxcar integrator; 19, switch driver and control unit; 20, trigger and control-pulse generator; 21, frequency counter; 22, process control computer

reduction of the signal amplitude[38, 40] have proven suitable for this purpose.[37-39] The high stability of modern electronics allows for a reduction of the measuring time with respect to a direct point by point comparator mode of operation. In such advanced mode of measurement the amplitudes of the signal transmitted through the cell at a number of transducer distances x (on the order of 400) are first determined. At each frequency ν the characteristic curve of the electronic devices is calibrated afterwards by switching to the parallel branch and varying the piston attenuator setting in the relevant amplitude range. Fixed attenuators (15) reduce the effect from signals that are reflected at the piston attenuator. The variable attenuator (6) enables adjustment of the signal for almost identical amplitudes in the measuring branch and the reference branch.

The sinusoidal signal with measuring frequency ν is generated by a synthesizer (1), rectangularly switched by a modulator (2) that is driven by a pulse generator (3), and amplified by a broad band amplifier (4). With the aid of two synchronously operating switches (5) the modulated signal is either transmitted through the cell or the reference branch. Afterwards it is detected by a sensitive superheterodyne receiver (17) and further processed by a boxcar integrator. Via sample-and-hold and analogue-digital boards the signal is finally stored on the computer (22). The computer controls the complete measurement process, e.g. the stepping motor or piezotranslator drives for the cell length and piston attenuator adjustment, the switches for the selection of the comparator branches, and the pulse sequences for the proper gating of the boxcar integrator as a function of signal delay due to cell length variation.

3.2 Cell construction

The construction of the sample cell depends on the frequency range of measurements. Cells for different frequency domains mainly differ from one another by the types of the piezoelectric transducers used as transmitter and receiver. Reliable constructions for the frequency range 1 MHz to 5 GHz have been presented in the literature[37-39,41]. As an example, Fig. 10 shows a device that is suitable for frequencies between 1 and 100 MHz.

For correct measurements parallel alignment of the transmitter (4, Fig. 10) and the receiver (7) transducers is mandatory. For this purpose, in correspondence to resonator cells (Figure 8), the plate (5) holding the transmitter transducer (4) is provided with a ball joint (6). Again this plate can be precisely tipped and rotated for alignment of the transducer surface with respect to the cell axis. In order to fulfil high standards in the cell length adjustment, the receiver transducer (7) is mounted on a sliding carriage (8) which, with the aid of a spindle (11) and a nut (12), can be shifted along the direction of wave propagation. Backlash-free and smooth running of the carriage is provided by three high-precision ball bush guides (9) combined with fine ground and lapped pins (10). This costly

construction maintains the receiver adjustment at cell length variations. The nut (12) is driven by a stepping motor which is coupled to the cell via a wheel (13). The cell length is measured with a resolution up to 100 nm using devices which are based on photoelectric scanning of an optical grating or sensors which consists of magnetic differential transformers.

Similar to resonators diffraction effects due to finite transducer diameters may also affect the pulse-modulated wave transmission measurements. Diffraction phenomena of circular transducers have been theoretically treated by superposing a plane wave propagating in the direction of the transducer axis and a diffraction wave excited at the transducer periphery.[42] Based on that theory the empirical formula

$$U(x) = U(0)\exp\left[-\frac{\lambda x}{2\pi A_t}\right]^{g(x)} \tag{24}$$

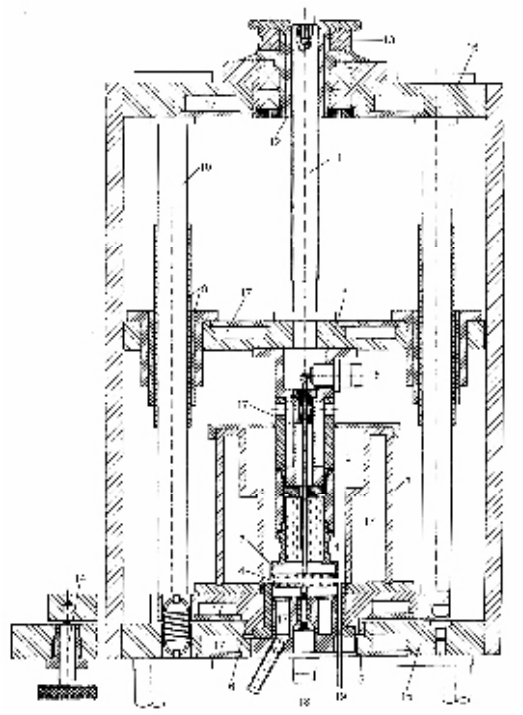

Fig.10.Cross section of a variable path-length cell for pulse modulated wave transmission measurements.[38] 1, sample volume; 2, cell jacket; 3, thermostatic coat; 4, piezoelectric transmitter transducer; 5, adjustable plate with 6, ball joint; 7, receiver transducer mounted on 8, sliding carriage; 9, high-precision ball bush guide; 10, finely lapped guiding pin; 11, spindle; 12 nut; 13, cogwheel for the coupling to the stepping motor; 14, screw for the adjustment of plate 5; 15, base plate; 16, mounting plate; 17, channel for circulating thermostat fluid; 18, electrical connector to the electronic circuit; 19, sample inlet

is used to relate the receiver voltage *U(x)* at cell length x to the one at $x = 0$. In this equation At is the transducer surface and *g(x)* is a function that can be easily found be calibration measurements using reference liquids of well known ultrasonic absorption coefficient.[38]

4. RELATED METHODS

a. Step-pulse (jump) methods

Complementary to the frequency domain techniques described above, time domain (jump) techniques are popular for the investigation of comparatively slow molecular processes. Relaxation times that can be investigated by jump methods normally are longer than 1 μs, corresponding with an upper relaxation frequency limit of about 150 kHz;[2,8] however, methods resolving relaxation times near 50 ns have been also reported.[43]

In jump methods the sample is exposed to a rapidly rising step-pulse and the approach of the new thermodynamic equilibrium is monitored by tracing of a suitable parameter. Pressure steps and temperature steps, which rapidly shift the chemical equilibrium of an elementary process of the liquid are common. Step changes in the electrical field have also been successfully applied.

Such step-pulse techniques allow for broad-band measurements by a single measurement. Therefore, if measurements, such as for biological systems, have to be rapidly done these methods offer an advantage. On the other hand, step-pulse techniques suffer from an unfavourable decay of the spectral amplitude, proportional to $1/\nu$, of the exciting signal. Reqirements with respect to system linearity and the dynamic range of the electronic set-up are thus more demanding than with spot frequency methods. The signal-to-noise ratio may be significantly increased by repetitive step-pulses or by distributing the energy of the exciting signal over programmed pulse sequences, preferably with flat spectrum. So far, however, little attention has been given to such modes of pulse measurements.

b. Brillouin scattering

Transparent samples may be also studied by utilizing the interaction of optical waves with continuous ultrasonic waves[44,45]. Bragg scattering[46] and Brillouin scattering[47] are well-tried techniques for absorption coefficient and sound velocity

measurements of liquids at hypersonic frequencies (ν > 1 GHz).

Challenging for scientific application, spontaneous Brillouin scattering permits the liquid sample to be studied in complete equilibrium. A beam of monochromatic light with small aperture is scattered from the thermal spectrum of acoustic modes. Conservation of momentum leads to a selection of sonic waves obeying Bragg's reflection law. These waves propagate in both directions of the bisector of the scattering angle. Conservation of energy leads to Doppler-shifted lines in the spectrum of the scattered light. The magnitude in the shift of the down-shifted (Stokes) and the up-shifted (anti-Stokes) line depends on the frequency of the selected ultrasonic wave. Along with the sonic wavelength from the Bragg angle the frequency yields the sound velocity of the sample. The half-power bandwidths of the Stokes and anti-Stokes lines are related to the ultrasonic absorption coefficient. An unavoidable drawback of spontaneous Brillouin scattering is the masking of the Stokes and anti-Stokes Brillouin peaks by the central Rayleigh line. According to the Landau-Placzek ratio[45],

$$\frac{I_B}{I_c} = \frac{c_p - c_v}{2v_v} \qquad (25)$$

the intensity I_B of the Brillouin lines of liquids is of the order of 10^{-6} of the intensity I_c of the central line. For this reason, stimulated and forced Brillouin scattering techniques are applied in which the signal-to-noise ratio is increased by optically inducing thermal and coherent phonons, repectively.

The smallest acoustical wavelength to be studied by Brillouin scattering is half of the optical wavelength. Hence for water, as an example, the highest ultrasonic frequency that can be obtained in experiments with visible light is about 7.5 GHz, a frequency that has been also reached with ultrasonic signals[51].

CONCLUSIONS

Various proven ultrasonic measurement methods for broadband measurements of liquids are available for the frequency range between about 10 kHz and 10 GHz. For accurate measurements, advanced ultrasonic cell design, precise mechanical machining and calibration with suitable reference liquids are required. Standing wave (resonator) techniques and pulse-modulated wave transmission techniques complement each other throughout wide ranges of frequency and absorption coefficient. Limitations with respect to sample volume exist primarily at frequencies below 1 MHz, where the sonic wavelength is large. The numerous aspects of measurements at a single (fixed) frequency or in a narrow frequency band will be covered by the second part of this tutorial.

REFERENCES

1. **Herzfeld, G. and Litovitz, T.,** Absorption and Dispersion of Ultrasonic Waves (New York: Academic, 1959)
2. **Eigen, M. and De Maeyer, L.**, Relaxation methods Techniques of Organic Chemistry vol VIII part 2, ed A Weissberger (New York: Interscience,1963) 895-1054.
3. **Lamb, J.**, Thermal relaxation in liquids Physical Acoustics, **l2A**, ed W P Mason (London: Academic, 1973).
4. **Blandamer, M.J.,** Introduction to Chemical Ultrasonics (London: Academic, 1973).
5. **Slutsky, L.J.**, Ultrasonic relaxation spectroscopy Methods of Eperimental Physics vol XIX, ed P D Edmonds (New York: Academic, 1981) pp 179-235.
6. **Stuehr, J.E.**, Ultrasonic methods Investigations of Rates and Mechanisms of Reaction, ed. C F Bernasconi (New York: Wiley, 1986) pp 247-303.
7. **Anisimov, M.A.**, Critical Phenomena in Liquids and Liquid Crystals (Philadelphia: Gordon and Breach, 1991).
8. **Strehlow, H.,** Rapid Reactions in Solutions (Weinheim: VCH, 1992).
9. **Povey, M.J.W.**, Ultrasonic Techniques for Fluids Characterisation (San Diego: Academic, 1997).
10. **Onuki, A.,** Phase Transition Dynamics (Cambridge: Cambridge University Press, 2002).
11. **Bhattacharjee, J.K**. and **Bhattacharya, S**., Nonlinear Dynamics near and far from Equilibrium (Dordrecht/New Delhi: Springer/Hindustan Book Agency, 2007).
12. **Kronig, R. de L.,** On the theory of dispersion of X-rays. *J. Opt. Soc. Am.*, **12** (1926) 547-557.

13. **Kramers, H.A**., Die Dispersion und Absorption von Röntgenstrahlen. *Phys. Z.*, **30** (1929) 522-523.

14. **Wehrmann, B.,** Ultraschallabsorptions und -Dispersionsmessungen im Frequenzbereich von 500 kHz bis 3 GHz zur Frage der Komplexbildung in wässrigen Lösungen von Zinkchlorid und Chloriden anderer 2-wertiger Metalle, PhD Thesis (Göttingen, 1991).

15. **Labhardt, A**, and **Schwarz, G.A.**, High resolution and low volume ultrasonic resonator method for fast chemical relaxation measurements Ber. Bunsenges. *Phys. Chem.*, **80** (1976) 83-92.

16 **Voleišiene, B., Migliniene** and **Voleišis, A.,** Ultrasonic study of the complexation kinetics of yttrium nitrate solutions Chemija (Vilnius) **12** (2001) 225-230.

17. **Debye, P.**, Polar Molecules (New York: Chemical Catalog, 1929).

18. **Menzel, K., Rupprecht, A.** and **Kaatze, U**., Hill-type ultrasonic relaxation spectra of liquids . *J. Acoust. Soc. Am.*, **104** (1998) 2741-2749.

19. **Polacek, R. and Kaatze, U.A.**, Small volume spherical resonator method for the acoustical spectrometry of liquids down to audio frequencies. *Meas. Sci. Technol.*, **7** (2001) 1-6.

20. **Eggers, F.** and **Kaatze, U**., Broad-band ultrasonic measurement techniques for liquids. *Meas. Sci. Technol.*, **7** (1996) 1-19.

21. **Kaatze, U., Wehrmann, B.** and **Pottel, R.,** Acoustical absorption spectroscopy of liquids between 0.15 and 300 MHz: High resolution ultrasonic resonator method. *J. Phys. E: Sci. Instrum.*, **20** (1987) 1025-1030.

22. **Eggers, F., Kaatze, U., Richmann, K.H.** and **Telgmann, T.,** New plano-concave ultrasonic resonator cells for absorption and velocity measurements in liquids below 1 MHz. *Meas. Sci. Technol.*, **5** (1994) 1131-1138.

23. **Behrends, R., Eggers, F., Kaatze, U.** and **Telgmann, T.,** Ultrasonic spectrometry of liquids below 1 MHz. Biconcave resonator cell with adjustable radius of curvature. *Ultrasonics*, **34** (1996) 59-67.

24. **Polacek, R.** and **Kaatze, U.A.,** High-Q easy-to-handle biconcave resonator for acoustic spectrometry of liquids. *Meas. Sci., Technol.* **14** (2003) 1068-1074.

25. **Schultz, J.** and **Kaatze, U.A.,** Continuous wave transmission method for the ultrasonic spectrometry of liquids. *Meas. Sci. Technol.*, **9** (1998) 1266-1276.

26. **Kaatze, U., Eggers, F.** and **Lautscham, K.,** Ultrasonic velocity measurements in liquids with high resolution - techniques, selected applications and perspectives. *Meas. Sci. Technol.*, **19** (2008) 062001-1 - 062001-21.

27. **Choi, P.K., Naito, Y.** and **Tagaki, K.,** New ultrasonic resonator method using optical diffraction for liquids. *J. Acoust. Soc. Am.*, **74** (1983) 1801-1804.

28 **Kaatze, U.** and **Wehrmann, B.,** High-Q plano-concave resonator with and without Straubel quartz for ultrasonic absorption measurements of liquids. *IEEE Trans. Instrum. Meas.*, **37** (1988) 648-651.

29. **Naito, Y., Choi, P-K.** and **Takagi, K. A.**, Plano-concave resonator for ultrasonic absorption measurements. *J. Phys. E: Sci. Instrum.*, **17** (1984) 13-16.

30. **Eggers, F. and Funck, Th.,** Ultrasonic measurements with millilitre samples in the 0.5 - 100 MHz range. *Rev. Sci. Instrum.*, **44** (1973) 969-977.

31. **Eggers, F., Funck, Th.** and **Richmann, K.H.** High Q ultrasonic liquid resonators with concave transducers. *Rev. Sci. Instrum.*, **47** (1976) 361-367.

32. **Kononenko, V.S.**, Precision method for measurements of the ultrasound absorption coefficient of liquids at frequencies of 0.1-20 MHz. *Sov. Phys.-Acoust.*, **33** (1987) 401-404.

33. **Eggers, F.,** Eine Resonatormethode zur Bestimmung von Schall-Geschwindigkeit und Dämpfung an geringen Flüssigkeitsmengen. *Acustica.*, **19** (1967/68) 323-329.

34. **Sarvazyan, A.P., Sel'kov, E.E.** and **Chalikyan, T.V**., Constant-path acoustic interferometer with transition layers for precision measurements in small liquid volumes. *Sov. Phys. Acoust.*, **34** (1988) 631-634.

35. **Eggers, F.,** Ultrasonic velocity and attenuation measurements in liquids with resonators, extending the MHz frequency

range. *Acustica*, **76** (1992) 231-40.

36. **Kaatze, U., Behrends, R.** and **Lautscham, K.**, Acoustic relaxation spectrometers for liquids. *Ultrasonics*, **39** (2001) 393-406.

37. **Kaatze, U., Lautscham, K.** and **Brai, M.**, Acoustical absorption spectroscopy of liquids between 0.15 and 3000 MHz: II. Ultrasonic pulse transmission method. *J. Phys. E: Sci. Instrum.*, **21** (1988) 98-103.

38. **Kaatze, U., Kühnel, V., Menzel, K.** and **Schwerdtfeger, S.,** Ultrasonic spectroscopy of liquids. Extending the frequency range of the variable sample length pulse technique. *Meas. Sci. Technol.*, **4** (1993) 1257-1265.

39. **Kaatze, U., Kühnel, V.** and **Weiss, G.,** Variable pathlength cells for precise hypersonic spectrometry of liquids up to 5 GHz. *Ultrasonics*, **34** (1996) 51-58.

40. **Kaatze, U.** and **Lautscham,** K., Below cut-off piston attenuator as calculable signal vernier for microwaves up to 15 GHz. *J. Phys. E: Sci. Instrum.*. **19** (1986) 1046-1050.

41. **Kaatze, U.** and **Lautscham, K.**, Acoustical absorption spectroscopy of liquids between 0.15 and 3000 MHz: III. Hypersonic comparator technique. *J. Phys. E: Sci. Instrum.*, **21** (1988) 402-406.

42. **Fay, R,**. Numerische Berechnung der Beugungsverluste im Schallfeld von Ultraschallwandlern. *Acustica,* **36** (1776/77) 209-213.

43. **Hoffmann, G.W.A.**, Nanosecond temperature-jump apparatus. *Rev. Sci. Instrum.*, **42** (1971) 1643-1647.

44. **Breazeale, M.A., Cantrell, J.H. Jr.** and **Heyman, J.S.,** Ultrasonic wave velocity and attenuation measurements Methods of Experimental Physics vol. 19 Ultrasonics ed. P D Edmonds (New York: Academic, 1981) pp 67-135.

45. **Chu, B.**, Laser Light Scattering (New York: Academic, 1991).

46. **Takagi, K.** and **Negishi, K.,** Measurement of ultrasonic velocity and absorption in liquids up to 1.5 GHz by the high resolution Bragg reflection technique. *J. Phys. D: Appl. Phys.*, **15** (1982) 757-765.

47. **Montrose, C.J., Solovyev, V.A.** and **Litovitz, T.A.,** Brillouin Scattering and relaxation in liquids. *J. Acoust. Soc. Am.,* **43** (1967) 117-130.

48. **Chiao, R. Y., Townes, C.H.** and **Stoicheff, B.P.**, Stimulated Brillouin scattering and coherent generation of intense hypersonic waves. *Phys. Rev. Lett.,* **12** (1964) 592-595.

49 **Grubbs, W.T.** and **McPhail, R.A.**, High resolution stimulated Brillouin gain spectrometer. *Rev. Sci. Instrum.,* **65** (1994) 34-41.

50. **Sonehara, T.** and **Tanaka, H.,** Forced Brillouin spectrometry using frequency-tunable continuous lasers. *Phys. Rev. Lett.,* **75** (1995) 4234-4237.

51. **Lezhnev, N.B.,** Acoustic spectrometer for the investigation of liquids in the 10 GHz frequency range. *Sov. Phys. Acoust.,* **27** (1981) 150-155.

J. Pure Appl. Ultrason. 31 (2009) pp. 13-23

Ultrasound techniques for characterizing liquids. II. survey of single frequency methods†

UDO KAATZE
Drittes Physikalisches Institut, Georg-August-Universität
Friedrich-Hund-Platz 1, 37077 Göttingen, Germany
e-mail : uka@physik3.gwdg.de

This paper focuses on acoustical methods for liquid measurements at a fixed frequency or in a small frequency band. Emphasis is particularly given to high-precision sound velocity measurements. Methods employing continuous waves and sharp pulses are discussed in detail. Related methods are also described briefly. The merits and limitations of the different methods of measurement are shown. Some examples of measurement applications are presented in order to indicate the favourable sensitivity of single methods and to reveal their extended usability in basic research and in manufacturing process.

Key words : Ultrasonic measurements, liquids characterization, sound velocity, resonator techniques, pulse methods

INTRODUCTION

High resolution ultrasonic measurements at a single-frequency or in a limited frequency band are often used for liquids characterization in basic research as well as in a broad variety of applications[1,2]. An example for fundamental studies in physical chemistry is shown in Fig. 1 where the sound velocity c and the frequency normalized absorption coefficient α/ν^2 of mixtures of water (H_2O) with dimethyl sulfoxide (DMSO) is displayed as a function of mole fraction of DMSO. For this liquid system c and α/ν^2 are independent of frequency ν within the broad frequency range from 200 kHz to 2.75 GHz[3]. The dependence of the acoustical parameters upon composition of binary mixtures is usually discussed in terms of the liquid structure. Frequently, the density ρ is simultaneously measured to obtain the adiabatic compressibility κ_S according to the Newton-Laplace equation

$$\kappa_S = \rho^{-1} c^{-2} . \qquad (1)$$

Due to the high sensitivity of sound velocimeters such measurements are favourably performed to monitor changes in sample properties. Sound velocities of aqueous surfactant solutions show a bent in the dependence upon concentration, thus clearly revealing the critical micelle concentration cmc of the system[4]. Fig. 2 displays the temperature profile of the sound velocity for a suspension of phospholipid bilayer vesicles in water. The data indicate how nicely the lipid phase transition temperature T_m is indicated by the sound velocity[5].

Recent efforts to develop easy-to-handle highly sensitive single-frequency (or small-band) sound velocity and sonic absorption coefficient measurement systems[6-11] have pushed the resolution to the order of 10^{-7}. Because of this outstanding resolution such systems are not only used in physical chemistry[12-17] as well as biophysics and biochemistry research[18-28] but also in diverse applications such as in the production of emulsions[29-33], in the pharmaceutical industry[34-39], and in the processing of foods and beverages[40-53]. A noticeable advantage of sound velocity and sonic absorption coefficient measurements, in addition to their high sensitivity, is their ability to examine optically opaque sample.

As methods to measure the sonic absorption coefficient have been described in detail in part I

†Invited talk presented at NSU-XVII, B.H.U., Varanasi, Dec. 4-9, 2008.

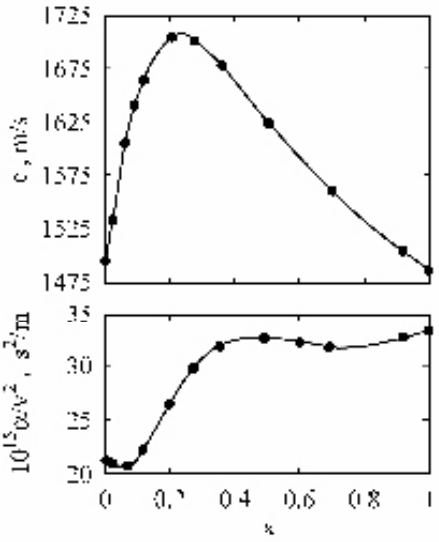

Fig.1. Sound velocity c and frequency normalized sonic absorption coefficient α/ν^2 at 1 MHz of dimethyl sulfoxide/water mixtures versus mole fraction x of DMSO[3]

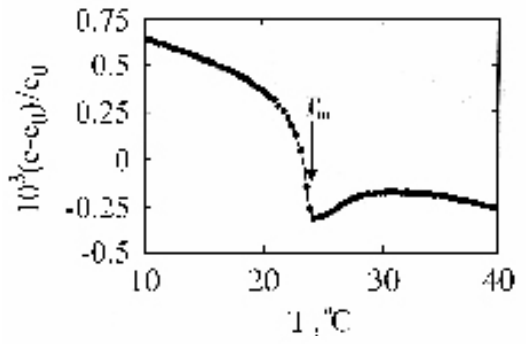

Fig. 2. Relative sound velocity $(c\text{-}c_0)/c_0$ difference versus temperature T for a 5 mg/ml solution of the phospholipid 1,4-dimyristoyl-L-3-phosphatidylcholin in water.[5] At T_m the phospholipid passes through a phase transition. c_0 is the sound velocity of water

of this tutorial[54], high resolution sound velocity measurement methods will be the focus of this part. Using these methods the absorption coefficient is often obtained as a byproduct.

SURVEY OF METHODS

a. Continuous wave methods

As outlined in part I of this tutorial, continuous wave ultrasonic measurement techniques probe standing wave patterns, in order to utilize the virtually increased path length of interaction between the sonic field and the sample. This mode of measurements permits investigations of small liquid volumes with high resolution. Again, cavity resonator techniques are used, the measurement frequencies, however, are restricted to a small range around the frequency of the minimum half-power bandwidth $\Delta\nu_h$ of the cell (Fig. 5, part I). Around that frequency the quality factor $Q = \nu_r/\Delta\nu_h$ is large, thus providing an especially long pathway of interaction. Normally, the transfer function of the resonator is measured with a network analyzer system that determine the complex output-to-input voltage ratio of the cell as sketched in the block diagram in Fig. 7 of part I.[54] The use of only one transducer as a combined transmitter and receiver and a passive reflector involves unfavourable measurement conditions for reflected signals. The sound velocity is obtained from the distance of successive resonance frequencies

$$\nu_{n+1} - \nu_n = \frac{\nu_{n\,ideal}}{\pi} \arccos \left[\frac{\left(g_{n+1}^2 - 1\right)\left(1 - g_n^2\right) - 4\, g_{n+1}\, g_n}{\left(g_{n+1}^2 + 1\right)\left(g_n^2 + 1\right)} \right] \quad n = 1,2, \tag{2}$$

with

$$g_j = \frac{Z_l}{Z_T} \arctan\left(\pi \nu_j / \nu_T\right), \quad j = 1,2,\ldots \tag{3}$$

where l is the cell length, $Z = \rho_c$ is the acoustic impedance of the liquid and Z_T as well as ν_T are the acoustic impedance and fundamental frequency of thickness vibrations, respectively, of the transmitter and receiver transducers, assumed to be identical. The absorption coefficient is again calculated from the quality factor of the resonator, using calibrations with appropriate reference liquids for the consideration of the intrinsic cell loss[2, 55]. Details of the cell construction and measurement procedure will be discussed in sect.[3].

Very accurate sound velocities have been also obtained from a variable path acoustical resonator technique[56]. Instead of varying the frequency to obtain the resonance peaks of the cell the receiver transducer is shifted along the resonator axis. The transducer shift is precisely determined using a laser interferometer. The method does not need reference measurements. At the expense of rather large sample volumes it has been applied in a remarkably broad frequency range[57, 58].

b. Pulsed wave transmission methods

By analogy with the variable path acoustical resonator technique square-pulse modulated wave transmission methods at variable sample length[54] can be also used for sound velocity determinations. Fig. 3 shows the magnitude of the normalized receiver voltage U of a liquid-filled cell as a function

of the transmitter-receiver spacing x.[59] The signal reveals characteristic ripples with periodicity $\lambda/2 = c/(2\nu)$ at small x and with periodicity λ at larger x. The former ripple structure is due to multiple reflections of the acoustic signal within the cell. At small x these reflections are not gated out because of the insufficiently short pulse duration time tp (shorter duration times would result in an enhanced effective bandwidth $\Delta\nu_p \approx 1/t_p$ of the measuring frequency). The ripple structure at large x, where the receiver voltage is small, follows from a superposition of the acoustical signal and electrical crosstalk. Hence fitting the theoretical function to the experimental $|U/\hat{U}|$-versus-x relation (Fig. 3) allows the wavelength λ of the sonic signal and thus the sound velocity $c = \lambda\nu$ to be determine from the ripple structure as well as the absorption coefficient α from the overall decrease of the signal with x.

c. Optical methods

Square-pulse modulated wave transmission methods allow measurements up to hypersonic frequencies (< 5 GHz[59]). Translucent samples may be also studied by the interaction of optical signals with continuous ultrasonic waves[60]. Spontaneous Brillouin scattering[61] probes thermal waves and thus considers the sample in complete equilibrium. Improved signal-to-noise ratios, however, are reached by Bragg scattering[62] as well as by stimulated[62-64], stimulated gain[65, 66], and forced[67] Brillouin spectroscopy.

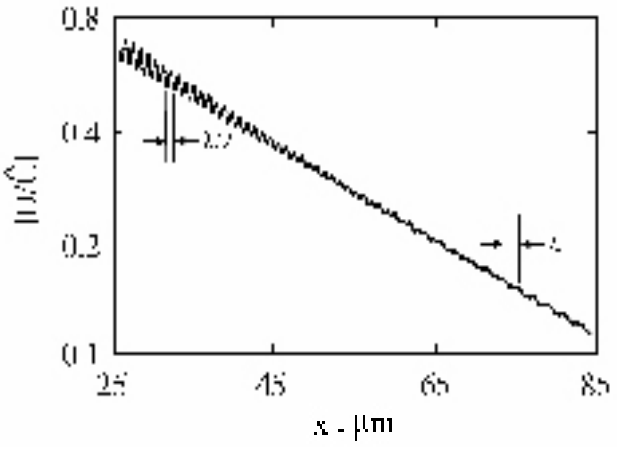

Fig.3. Log-lin plot of the magnitude of receiver voltage ratio $|U/\hat{U}|$ versus sample thickness x for pulsed wave transmission measurements at 790 MHz. The signal exhibits a characteristic ripple with periodicity $\lambda/2$ at small x and with λ at large x. These ripples result from multiple reflections of the acoustic signal within the cell and from the superposition of the acoustic signal with electrical crosstalk, respectively

Spontaneous Brillouin scattering at thermal acoustic waves, according to the Bragg condition, yields the sonic wavelength

$$\lambda = (\lambda_l/2)\, arcsin(\theta/2) \tag{4}$$

from the wavelength λ_l of the light and from the angle θ between the reflected and incident light beams (Fig. 4). Due to Doppler shift a change in the light frequency

$$\Delta\nu_L = \pm\, 2\nu_l\, (c/c_l)\, sin\,(\theta/2) = \nu \tag{5}$$

occurs with ν_l and $c_l = \lambda_l\nu_l$ denoting the frequency and phase velocity of the incident light. Hence the sound velocity $c = \lambda\nu$ of the thermal acoustic waves can be calculated from the selected angle θ and the frequency shift $\Delta\nu_l$. Sonic absorption leads to a finite half-width

$$\delta\nu_l = \pi\alpha c \tag{6}$$

of the (Stokes and anti-Stokes) Brillouin lines which can be measured to determine the absorption coefficient α. Assuming backscattering ($\theta = \pi$) as an extreme and a frequency-doubled Nd:YAG laser (λ_l = 532 nm) as light source, ν = 7.4 GHz results as the highest attainable ultrasonic frequency at which Brillouin measurements in water can be performed. Still today, separation of the Brillouin lines from the central Rayleigh line is a challenging task, as the intensity of the former, according to the Landau - Placzek ratio[60], is by a factor of the order of 10^6 smaller than that of the latter. Brillouin

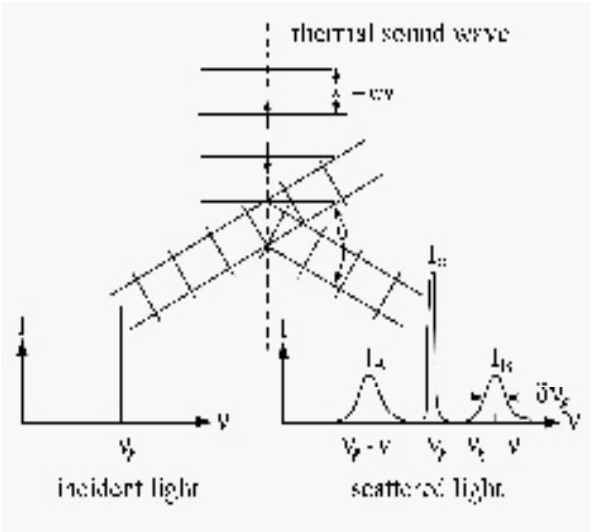

Fig.4. Scheme of Brillouin scattering by Bragg reflection of monofrequent light (frequency νl) froam thermal sound waves. The spectrum of the scattered light contains, in addition to the central Rayleigh line, the Stokes and anti-Stokes Brillouin lines

scattering methods, though most useful in basic research, are less suited for routine measurements and technical applications.

d. Pulse methods

Contrary to pulse modulated wave methods with typical t_p values between 1 and 20 μs, corresponding to a small effective bandwidth $\Delta\nu_p$ of a measurement signal with carrier frequency near 10 MHz, another category of ultrasonic techniques employs sharp pulses ($t_p \leq 1$ μs) with wider spectrum[30,43,53,68-70]. Sound velocity measurements with sharp pulses determine the time interval Δt that is required for the acoustic signal to pass a distance Δx through the sample. According to the simple relation

$$c_g = \Delta x / \Delta t \tag{7}$$

the group velocity

$$c_g = d\omega / dk \tag{8}$$

is derived from the measurements. Here $\omega = 2\pi\nu$ and $k = 2\pi/\lambda$ is the wave number. The propagation velocity c_g of sharp pulses is related to the phase velocity c, the velocity at which the phase of a single-frequency component of the sonic signal is propagating, as[2]

$$\frac{1}{c_g} = \frac{1}{c} + \frac{\nu}{c^2}\frac{dc}{d\nu} \tag{9}$$

Hence c_g equals c only in liquids with no dispersion in c. For many liquids the difference between group and phase velocity clearly exceeds the experimental errors of measurements and thus have to be considered in the quantitative evaluation of sound velocity data. On the other hand the broad frequency spectrum of sharp pulses can be utilized to determine, based on Fourier analysis of the pulse after interaction with the sample, both group and phase velocities as well as the attenuation coefficient in a considerable frequency range[30,43,53,68,69,71]. The use of sharp pulses needs broadband transducer systems as are common in sonography in medicine. Methods for the precise Δt determination (eq. 7) in sharp pulse measurement techniques will be presented below.

RESONATOR METHODS

High-precision single-frequency ultrasonic resonator techniques aim at small sample volume measurements. In many applications less than 1 ml liquid is available. For this reason large transducers, shifting the diffraction losses to low frequencies (Part I, Fig.e 5) are not normally employed. On the other hand, as precise resonance frequency determinations require small half-power bandwidths of the resonance peaks, resonator measurements are favourably performed at some MHz. Biplanar cylindrical cavity resonator cells, subject to higher-order satellite modes as described in part I, are frequently used. Measuring again the complex transfer function in a frequency range around the principal resonance peak, the disturbing satellite peaks can be taken into account. Often twin cell devices are used with one resonator filled with a reference liquid of well-known sound velocity. Assuming the effect of higher order modes to be identical in both cells, the resonance frequency of the sample cell and thus the sound velocity of the liquid is then directly determined relative to the reference without considering the complicated mode spectrum in detail. Reference measurements are particularly useful for the determination of the correct cell length. In practical applications it is impossible to control the temperature within the small fluctuation range that is needed in order to reach the exceptionally high resolution of $\Delta c/c = 10^{-7}$ which "home-made" and commercial constructions can reach today.[2] With the sample and reference resonator inserted in the same metallic block the temperature difference between both cells becomes smaller than the fluctuations in the thermostat fluid. Differences between both cavities may be close to 10^{-2} K only for temperature fluctuations on the order of 10^{-4} K in the metallic block.

An improved temperature regulation and stability is reached with Peltier elements. Fig. 5 shows a block diagram for a twin cell measurement system using a Peltier temperature control and a low priced electronic set-up[8] instead of an oversized general-purpose network analyser. The system allows an extension of additional channels for a larger number of cells because, in technical applications, measurements are often performed simultaneously in several cells.

The electronic circuit is based on the direct digital frequency synthesis (DDS) technique. One signal synthesizer (2a in Fig. 19) provides the sinusoidal measuring signal (ν), the other one (2b) the local oscillator (ν + 10 kHz) for superheterodyne mixing and amplification. The measuring signal is fed to the input transmitters of the cells. Together with the local oscillator signals the cell output signals are processed in the mixers 5as and 5ar.

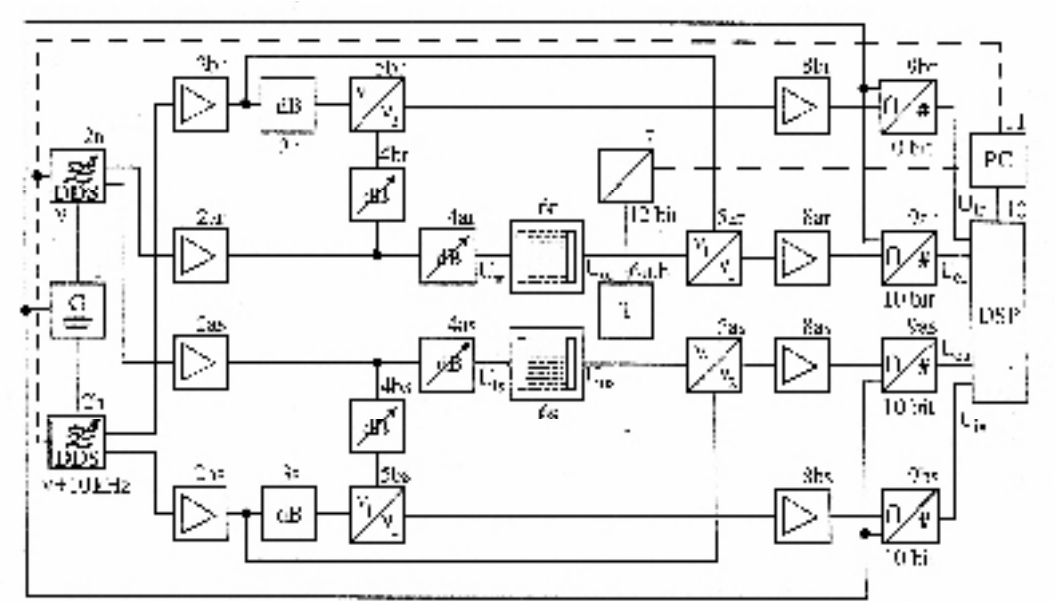

Fig.5. Block diagram for a dual channel electronic system for the determination of the complex transfer function of twin cell resonator cells;[8] s and r refer to the sample and the reference channel, respectively, a and b to the output and input signals, respectively, of the cells. 1, quartz controlled 50 MHz clock; 2, direct digital synthesizer ($\nu \leq 25$ MHz); 3, fixed attenuator; 4, variable attenuator; 5, mixer; 6, sample cell; 7, A/D converter 12 bit; 10, digital processor board, implemented in 11, computer

The resulting intermediate frequency (IF) signals (10 kHz) are proportional to the magnitudes $|U_{so}|$ and $|U_{ro}|$ of the cell output voltages. After analog/digital conversion the IF-signals are fed to a digital signal processor board (DSP). This board also receives reference signals (5bs, 5br), which are proportional to the magnitudes $|U_{si}|$ and $|U_{ri}|$ of the cell input voltages. For both the measuring and the reference channels, the real and imaginary parts of the complex transfer function $U_o(\nu)/U_i(\nu)$ are obtained by sampling U_o in phase with U_i and also at a $\pi/2$ phase shift. For a 10 kHz intermediate frequency such phase shift is equivalent to a 25 µs delay in the IF signal. In order to reach a frequency stability better than 0.1 Hz and a phase jitter below 0.01°, the DSG generators (2a, 2b) and also the analog/digital converters (9a, 9b) are controlled by a quartz stabilized 50 MHz clock (1).

In the cavity resonators described so far, the facing piezoelectric transducers are typically covered by thin layers of chrome and gold, establishing the electrical ground. In many technical and also in some scientific applications, the cavity walls should be completely non-metallic. For that reason precision - type glass cuvettes are used to form the cavity and to hold the liquid[6]. The piezoelectric transducers must then be acoustically coupled outside the cavity to the wall of the cuvette (Fig. 6). The acoustical contact can be improved by an intermediate layer for impedance matching. A disadvantage of such multilayer cells is the additional reflections of the acoustic signals between different interfaces, which results in a considerable complication of the resonance spectrum and its theoretical analysis. In practice, frequency dependent correction coefficients $\beta^*(\nu)$ and $\gamma^*(\nu)$ are used[6] in order to expand the applicability of the simple equation for the ideal resonator (see eq. 13 in part I[54])

$$c = 2l(\nu_{n+1} - \nu_n)\,(1 + \beta^*) \qquad (10)$$

Often sound velocity measurements only aim at the velocity increment δc in the sound velocity with respect to the value of the reference liquid; in this case a good approximation is reached with the corresponding frequency increment $\delta\nu_n$ for a particular resonance and a correction factor

$$\delta c/c = (1 + \gamma^*)\ \delta\nu_n/\nu_n\ . \qquad (11)$$

Those empirical correction coefficients have to be found by calibration measurements with liquids of precisely known velocity. In correspondence with calibrations for intrinsic resonator losses[54], both the sound velocity and the acoustical impedance of sample and the reference liquid should be very close in order to simulate the resonance frequencies accordingly. This condition is difficult to realize. Favourable conditions, however, exist quite often for dilute solutions with the solvent as a reference.

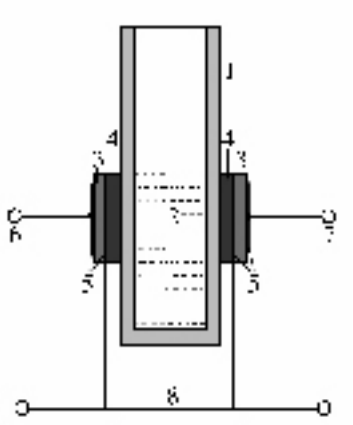

Fig.6. Sketch of a cuvette cell.[6] 1, resonator chamber body made of glass; 2, sample; 3, piezoelectric transducer; 4, intermediate coating for acoustic contact and impedance matching; 5, metallic layers for electrical contact; 6 and 7, connections to signal generator and receiver, respectively; 8, electrical ground

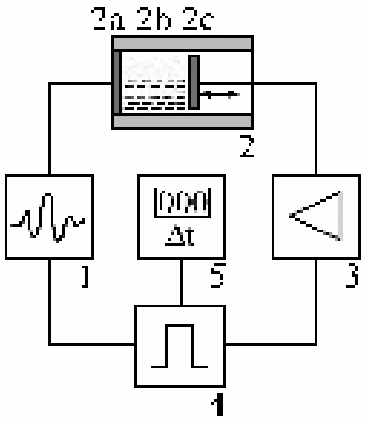

Fig.7. Block diagram of a sing-around measuring system. 2 1, signal generator; 2, sample cell; 2a-2c, transmitter transducer, sample liquid, and receiver transducer, respectively; 3, amplifier; 4, square-pulse generator; 5, counter

TRANSIENT TIME MEASUREMENT METHODS

As mentioned before, sound velocity measurements with sharp pulses are based on a precise determination of the time interval Δt, required for signal passage through the medium over a distance Δx. If Δx is accurately known, the Δt measurement, in addition to its simplicity, offers high precision for sound velocity determination. A convenient way of Δt measurements is provided by the "sing-around" method[72-74] which, in a simplified form, is sketched in Fig. 7. The sharp pulse from a signal generator (1) via a piezoelectric transmitter (2a) is fed to the specimen cell (2). The acoustic signal traverses the cell (2b), is detected by a piezoelectric receiver (2c), and is amplified afterwards for improvement of its flange steepness. The amplified signal triggers a mono-stable multivibrator (4), which generates a square pulse, incrementing a counter (5) and triggering the signal generator (1) simultaneously. The total time delay

$$\Delta t_{tot} = \Delta t + t_e \qquad (12)$$

between two subsequent signals is the sum of the desired time interval Δt in which a signal passes the sample distance Δx and a time delay t_e originating from the electronic system. The latter is determined either by calibration with a reference liquid of well known sound velocity, or, as indicated by Fig. 7, it is eliminated by a variation of the sonic path length. Two path lengths Δx_1 and Δx_2 simply yield

$$c_g = (\Delta x_1 - \Delta x_2) / (\Delta t_1 - \Delta t_2). \qquad (13)$$

For velocity data from sing-around systems, a relative error as small as 10^{-7} can be reached, provided that, as with the resonator measurements, a high sample temperature stabilization is available. In water at 25°C, for example, a change of the sound velocity by 1 part in 10^7 means by 0.15 mm/s, which corresponds to a temperature shift of only 50 μK.

Another frequently used method for velocity measurements employs sharp pulses propagating through the sample and reflected back and forth as echoes[7,9,11,30,41,75,76]. Such reflection method needs only one transducer, active both as a transmitter and receiver, and a passive sound reflector.

For both pulse-transmission and pulse-reflection measurements, the sensitivity can be enhanced utilizing multiple reflections within the cell with the relation

$$\Delta t_{tot} = 2n\Delta x/c + t_e \qquad n = 1,2,\ldots \qquad (14)$$

with n denoting the number of echoes. In contrast to resonator measurements, however, no large n values can be used in pulse measurements, because the pulses become more and more distorted when n increases. A significant source of errors in Δt measurements is the varying trigger point delay that results from pulse deformation, due to bandwidth limitations of the transducers and also of the electronic set-up, and, in addition, from the frequency dependent absorption as well as the dispersion of the sample liquid. This variance in the trigger point can be reduced by pulse correlation techniques[77] calculating the correlation function

$$C(\Delta t) = \int U(t+\Delta t)U(t)dt \qquad (15)$$

where U is the receiver signal voltage.

CONCLUSIONS

High precision sound velocimeters, often also suited for absorption coefficient measurements, are available for single frequency or narrow-band investigations. The construction of various specialized laboratory instruments has been reported in the literature. In addition, simple-to-operate commercial tools exist. Due to their sensitivity, resolution in the sound velocity can reach $\Delta c/c \approx 10^{-7}$, and their relatively simple operation, narrow-band sound velocimeters have become quite popular in many fields of material characterization and process control. This exceptionally demanding resolution is obtained with twin-cell devices and resonator techniques which actually determine the sound velocity difference between the sample and a reference. The sound velocity of the reference itself is less accurately known. Offering a method for the real-time, non-destructive, and sensitive materials characterization, small-band sound velocimetry and absorption coefficient determinations benefit additionally from their almost universal applicability. Sample property variations are usually accompanied by changes in the compressibility, density and/or sonic absorption coefficient. Another valuable advantage is its applicability to optically non-transparent samples.

REFERENCES

1. **Povey, M.J.W**., Ultrasonic Techniques for Fluids Characterisation (San Diego: Academic, 1997).
2. **Kaatze, U., Eggers, F.** and **Lautscham, K**., Ultrasonic velocity measurements in liquids with high resolution - techniques, selected applications and perspectives. *Meas. Sci. Technol.*, **19** (2008) 062001-1 - 062001-21.
3. **Kaatze, U., Brai, M., Scholle, F.D.** and **Pottel, R**., Ultrasonic absorption and sound velocity of dimethyl sulfoxide/water mixtures in the complete composition range. *J. Mol. Liquids*, **44** (1990) 197-209.
4. **Haller, J.** and **Kaatze, U.**, Complexation versus self-association: a-cyclodextrin + decyltrimethylammonium bromide aqueous solutions. *Chem. Phys. Lett.*, (2008), in press.
5. **Halstenberg, S., Heimburg, T., Hianik, Kaatze, U.** and **Krivanek, R.**, Cholesterol-induced variations in the volume and enthalpy fluctuations of lipid bilayers. *Biophys. J.*, **75** (1998) 264-271.
6. **Buckin, V.** and **Smyth, C.,** High-resolution ultrasonic resonator measurements for analysis of liquids. *Sem. Food Anal.*, **4** (1999) 113-130.
7. **Høgseth, E., Hedwig, G.** ***and*** **Høiland, H.,** Rubidium clock sound velocity meter. *Rev. Sci. Instrum,*. **71** (2000) 4679-4680.
8. **Lautscham, K., Wente, F., Schrader, W.** and **Kaatze, U.**, High resolution and small volume automatic ultrasonic velocimeter for liquids. *Meas. Sci. Technol.*, **11** (2000) 1432-1439.
9. **Benedetto, Gm, Gavioso, R.M., Guiliano Albo, P.A., Lago, S., Madonna Ripa, D.** and **Spagnolo, R.A.**, Microwave-ultrasonic cell for sound speed measurements in liquids. *Int. J. Thermophys.*, **26** (2005) 1651-65.
10. **Meyer, S., Hindle, S.A., Sandoz, J.P., Gan, T.H.** and **Hutchins, D.A.**, Non-contact evaluation of milk-based products using air-coupled ultrasound *Meas. Sci. Technol.*, **17** (2006) 1838-1846.
11. **Meier, K.** and **Kabelac, S**., Speed of sound increment for fluids with pressures up to 100 MPa. *Rev. Sci. Instrum.*, **77** (2006) 123903-1 -123903-8.
12. **Cutroni, M.** and **Mandanici, A.,** The a-relaxation process in simple glass forming liquid m-toluidine. II. The temperature dependence of the mechanical response. *J. Chem. Phys.*, **114** (2001) 7124-7129.
13. **Douhéret, G., Davis, M.I., Reis, J.C.R.** and **Blandamer,M.J.**,Isentropic compressibilities - Experimental origin and the quest for their rigorous estimation in thermodynamically ideal liquid mixtures. *Chem. Phys. Chem.*, **2** (2001) 148-161.
14. **Schmelzer, C.E.H., Zwirbla, W,, Rosenfeld, E.** and **Linde, B.B.J.,** Acoustic investigations of pseudo-stable structures in in aqueous solutions of polyethylene glycol. *J. Mol. Struct.*, **699** (2004) 47-51.
15. **Bae, R.J**, Ultrasonic velocity and absorption measurements in an aqueous solution of

poly (sodium 4-styrenesulfonate). *Macromol. Res.,* **12** (2004) 559-563.

16. **Pfeiffer, H.** and **Heremans, K.,** The sound velocity in ideal mixtures from thermal volume fluctuations. *Chem. Phys. Chem.*, **6** (2005) 697-705.

17. **Hanke, E., Schulz, U.** and **Kaatze, U.**, Structural aspects of poly (ethylene glycol) - water mixtures. Isentropic compressibility study. *Chem. Phys. Chem.*, **8** (2007) 553-560.

18 **Lee, A.** and **Chalikian, T.V**., Volumetric characterisation of the hydration properties of heterocyclic bases and nucleosides. *Biophys. Chem.*, **92** (2001) 209-227.

19 **Pfeiffer, H.** and **Heremans, K.,** Apparent sound velocity of lysozyme in aqueous solutions. *Chem. Phys. Lett.,* **361** (2002) 226-230.

20. **Taulier, N. and Chalikian, T.V.**, Compressibility of protein transition. *Biochem. Biophys. Acta.,* **1595** (2002) 48-70

21. **Schrader, W., Ebel, H., Grabitz, P., Hanke E., Heimburg, T., Hoeckel, M., Kahle, M., Wente, F.** and **Kaatze, U.,** Compressibility of lipid mixtures studied by calorimetry and ultrasonic measurements. *J. Phys. Chem.*, **B 106** (2002) 6581-6586.

22. **Chalikian, T.V**., Volumetric properties of proteins. *Ann. Rev. Biophys. Biomol. Struct.*, **32** (2003) 207-235.

23. **Hianik, T., Rybár, P., Benediktyová, Z., Svobodá, L.** and **Hermetter, A.**, Effects of oxidation on changes of compressibility of bovin serum albumin. *Gen. Physiol. Biophys.,* **22** (2003) 67-76.

24. **Hedwig, G.R.** and **Høiland, H.**, Thermodynamic properties of peptide solutions. Part 18. Partial molar isentropic compressibilities of Gly-X-Gly tripeptides (X = Tyr, Pro, Gln, Asp and Glu), and GlyLysGly acetate in aqueous solution at 25° C. *J. Sol. Chem.*, **34** (2005) 1297-1310.

25. **Sarvazyan, A., Tatarinov, A.** and **Sarvazyan, N.,** Ultrasonic assessment of tissue hydration status. *Ultrasonics,* **43** (2005) 661-671.

26. **Taulier, N., Beletskaya, I.V.** and **Chalikian, T.V.,** Compressibility changes accompanying conformational transitions of apomyoglobin. *Biopolym.,* **39** (2005) 218-229.

27. **Smirnovas, V., Winter, R., Funck, T.** and **Dzwolak, W.** Thermodynamic properties underlying the a-helix-t-ß-sheet transition, aggregation and amyloidogenesis of polylysine as probed by calorimetry, densimetry and ultrasound velocimetry. *J. Phys. Chem.,* **B 109** (2005) 19043-19045.

28. **Smirnovas, V., Winter, R., Funck, T.** and **Dzwolak, W**., Protein amyloidogenesis in the context of volume fluctuations: A case study of insulin. *Chem. Phys. Chem.*, **7** (2006) 1046-1049.

29. **Amararene, A., Gindre, M., Le Huéron, J.Y., Urbach, W., Valdez, D.** and **Waks, M.,** Adiabatic compressibility of AOT [sodium bis (2-ethylhexyl) sulfosuccinate] reverse micelles: Analysis of a simple model based on micellar size and volumetric measurements. *Phys. Rev.,* **E 61** (2000) 682-689.

30. **Tong, J.** and **Povey, M.J.W**., Pulse echo comparison method with FSUPER to measure velocity dispersion in n-tetradecane in water emulsions. *Ultrasonics,* **40** (2002) 37-41.

31. **Galán, J.J., Del Castillo, J.L., González-Pérez, A., Czapkiewicz, J.** and **Rodríguez, J.R.**, Density and sound velocity studies of aqueous solutions of tetradecy ltrimethylammonium nitrate at different temperatures. *J. Sol. Chem.*, **32** (2003) 919-927.

32. **Challis, R.E., Povey, M.J.W., Mather, ML. and Holmes, A.K.,** Ultrasound techniques for characterizing colloidal dispersions. *Rep. Prog. Phys.,* **68** (2005) 1541-1637.

33. **Panchal, K.N., Desai, A.** and **Nagar, T.** Sphere-to-rod transition in cationic micelles: Quaternary ammonium halides + phenol + water systems, *J. Dispersion Sci. Technol.,* **27** (2006) 963-970.

34. **Povey, M.J.W.**, Particulate characterisation by ultrasound. *Pharmac. Sci. Technol. Today,* **3** (2000) 373-380.

35. **Serris, E., Perier-Camby, L., Thomas, G., Desfontaines, M.** and **Fantozz, G.,** Acoustic emission of pharmaceutical powders during compaction. *Powder Technol.,* **128** (2002) 269-299.

36. **Labeit, D., Watanabe, K., Witt, C., Fujita, H., Wu, Y., Lahmers, S., Funck, T., Labeit, S.** and **Ganzier, H.**, Calcium-dependent molecular

spring elements in the giant protein titin. *PNAS,* **100** (2003) 13716-13721.

37. **Han, F., Taulier, N**. and **Chalikian, T.V.,** Association of the Minor Groove Binding Drug Hoechst 33258 with d (CGCGAATTCGCG) 2: Volumetric, Calorimetric, and Spectroscopic Characterisations. *Biochem.*, **44** (2005) 9785-9794.

38. **Medendorp, J.** and **Lodder, R.A.**, Acoustic-resonance spectrometry as a process analytical technology for rapid and accurate tablet identification. *AAPS Pharm. Sci. Tech.* **7** (2006) E1-9.

39. **Shah, R.B., Zidan, A.S., Funck, T., Tawakkul, M.A., Nguyenpho, A**. and **Khan, M.A.**, Quality by design: characteization of self-nano-emulsified drug delivery systems (SNEDDs) using ultrasonic resonator technology. *Intern. J. Pharm.*, **341** (2007) 189-194.

40. **Povey, M.J.W.,** The elastic properties of foods Handbook of Elastic Properties of Solids, Liquids, and Gases Vol. III: Elastic Properties of Solids: Biological and Organic Materials, Earth and Marine Sciences ed. Levy, M., Bass, H. and Stern, R. (New York: Academic, 2001).

41. **Létang, C., Piom, M., Verdier, C.** and **Lefebvre, L.**, Characterization of wheat-flour-water doughs: A new method using ultrasound. Ultrasonics, **39** (2001) 133-141.

42. **Sigfusson, H., Ziegler, G.R.** and **Coupland, J.N.**, Ultrasonic monitoring of unsteady-statecooling of food products. *Trans. ASAE*, **44** (2001) 1235-1240.

43. **Bakkali, F., Moudden, A., Faiz, B., Amghar, A., Maze, G., Montero de Espinosa, F**. and Akhnak, M., Ultrasonic measurement of milk coagulation time. *Meas. Sci. Technol.*, **12** (2001) 2154-2159.

44. **Benedito, J., Carcel, J.A., Gonzalez, R.** and **Mulet, A.**, Application of low intensity ultrasonics to cheese manufacturing processes. Ultrasonics, **40** (2002) 19-23.

45. **Zhao, B., Basir, O.A.** and **Mittal, G.S.**, Correlation analysis between beverage apparent viscosity and ultrasound velocity. *Intern. J. Food Prop.*, **6** (2003) 443-448.

46. **Cho, B.K**. and **Irudayaraj, J.M.K**., Foreign object and internal disorder detection in food materials using noncontact ultrasound imaging. *J. Food Sci.,* **68** (2003) 967-974.

47. **Cho, B.K**. and **Irudayaraj, J.M.K**., A noncontact ultrasound approach for mechanical property determination of cheeses. *J. Food Sci.*, **68** (2003) 2243-2247.

48. **Lehmann, L,, Kudryashov, E**. and **Buckin, V**.,Ultrasonic monitoring of the gelatinisation of starch. *Progr. Colloid Polym. Sci.,* **123** (2004) 136-40.

49. **Ross, K.A., Pyrak-Nolte, L.J**. and **Campanella, O.H**., The use of ultrasound and shear oscillatory tests to characterize the effect of mixing time on the rheological properties of ough Food. *Res. Intern.,* **37** (2004) 567-577.

50. **Lehmann, L.** and **Buckin, V.,** Determination of the heat stability profiles of concentrated milk and milk ingredients using high resolution ultrasonic spectroscopy. *J. Diary Sci.*, **88** (2005) 3121-3129

51. **Krasaekoopt, W., Bhandari, B**. and **Deeth, H.**, Comparison of gelation profile of yoghurts during fermentation measured by rva and ultrasonic spectroscopy. *Intern. J. Food Prop.,* **8** (2005) 193-198.

52. **Dwyer, C., Donelly, L**. and **Buckin, V.**, Ultrasonic analysis of rennet-induced pre-gelation and gelation processes in milk. *J. Diary Res.*, **72** (2005) 303-310.

53. **Taifi, N., Bakkali, F., Faiz, B., Moudden, A., Maze, G.** and **Décultot, D.**, Characterization of the synthesis and the firmness of the milk gel using an ultrasonic technique. *Meas. Sci. Technol.,* **17** (2006) 281-287.

54. **Kaatze, U.,** Ultrasonic measurement techniques for liquids. I. Broad-band spectroscopy, this issue (2009).

55. **Eggers, F.** and **Kaatze, U.,** Broad-band ultrasonic measurement techniques for liquids. *Meas. Sci. Technol.*, **7** (1996) 1-19.

56. **Voleišis, A.** and **Yaronis, E**., Precise ultrasonic interferometer for testing liquids over a frequency range of 1 - 700 Mc/s, Proc 7th Intern. *Congress Acoustics*, (Budapest, 1971) 501-504.

57. **Voleišiene, B., Migliniene,** and **Voleišis, A.**, Ultrasonic study of the ionic association in aqueous solutions of lanthanide salts. *J.*

Acoust. Soc. Am., **105** (1999) 962.

58. **Voleišiene, B., Migliniene,** and **Voleišis, A.**, Ultrasonic study of the complexation kinetics of yttrium nitrate solutions Chemija (Vilnius), **12** (2001) 225-230.

59. **Kaatze, U., Kühnel, V.** and **Weiss, G.**, Variable pathlength cells for the hypersonic spectrometry of liquids up to 5 GHz. **Ultrasonics, 34** (1996) 51-58.

60. **Chu, B.**, Laser Light Scattering (New York: Academic, 1991).

61. **Montrose, C.J., Solovyev, V.A**. and **Litovitz, T.A.**, Brillouin Scattering and relaxation in liquids. **J. Acoust. Soc. Am., 43** (1967) 117-130.

62. **Takagi, K.** and **Negishi, K**., Measurement of ultrasonic velocity and absorption in liquids up to 1.5 GHz by the high resolution Bragg reflection technique. *J. Phys. D: Appl. Phys.*, **15** (1982) 757-765.

63. **Chiao, R.Y., Townes, C.H.** and **Stoicheff, B. P.**, Stimulated Brillouin scattering and coherent generation of intense hypersonic waves. *Phys. Rev. Lett.,* **12** (1964) 592-595.

64. **Grubbs, W.T.** and **McPhail, R.A**., High resolution stimulated Brillouin gain spectrometer. *Rev. Sci. Instrum.,* **65** (1994) 34-41.

65. **Ratanaphruks, K., Grubbs, W.T.** and **MacPhail, R.A.,** CW stimulated Brillouin gain spectroscopy of liquids. *Chem. Phys. Lett.,* **182** (1991) 371-378.

66. **Faris, G.W., Gerken, M., Jirauschek, C., Hogan, D.** and **Chen, Y**., High-spectral-resolution stimulated Rayleigh-Brillouin scattering at 1μm. *Opt. Lett.,* **26** (2001) 1894-1896.

67. **Sonehara, T**. and **Tanaka, H.**, Forced Brillouin spectrometry using frequency-tunable continuous lasers. *Phys. Rev. Lett.*, **75** (1995) 4234-4237.

68. **Sachse, W**. and **Pao, Y.H**., On the determination of phase and group velocities of disperse waves in solids. *J. Appl. Phys.,* **49** (1978) 4320-4327.

69. **Kline, R.A.**, Measurement of attenuation and dispersion using an ultrasonic spectroscopy technique. **J. Acoust. Soc. Am., 76** (1984) 167-172.

70. **Goodenough, T.I.J., Rajendran, V.S., Meyer, S.** and **Prête, D**., Development of a multi-frequency pulse diagnostic ultrasound. *Ultrasonics*, **43** (2005) 165-171.

71. **Elias, Mm** and **Garcia-Moliner, F.**, Wave packet propagation and frequency dependent internal friction. *Physical Acoustics,* **V**, ed. Mason, W.P. and Thurston, R. (New York: Academic, 1968) 163-219.

72. **Greenspan** and **Tschiegg, C.E.,** Sing-around ultrasonic velocimeter for liquids. *Rev. Sci. Instrum.,* **28** (1957) 897-901

73. **Aindow, J.D.** and **Chivers, R.C.**, A narrow-band sing-around ultrasonic velocity measurement system. *J. Phys. E: Sci. Instrum.*, **15** (1982) 1027-1030.

74. **Ernst, S., Marczak, W., Manikowski, R**., **Zorçbski, E**. and **Zorçbski, M.A**., Sing-around apparatus for group velocity measurements in liquids. Testing by standard liquids and discussion of errors. *Acoust. Lett.,* **15** (1992) 123-130.

75. **Horváth-Szabó, G., Høiland, M.** and **Høgseth, E.**, An automated apparatus for ultrasound velocity measurements improving the pulse-echo-overlap method to a precision better than 0.5 ppm in liquids. *Rev. Sci. Instrum.*, **65** (1994) 1644-1648.

76. **Tardajos, G., Gonzales Gaitano, G.** and **Montero de Espinosa, F.**, Accurate, sensitive and fully automatic method to measure sound velocity and attenuation. *Rev. Sci. Instrum.,* **65** (1994) 2933-2938.

77. **Hosoda, M. Takagi, K., Ogawa, H., Nomura, H.** and **Sakai, K**., Rapid and precise measurement system for ultrasonic velocity by pulse correlation method designed for chemical analysis. *Jpn. J. Appl. Phys.*, **44** (2005) 3268-3271.

J. Pure Appl. Ultrason. 31 (2009) pp. 24-30

Ultrasonic internal rotary inspection system (IRIS) for heat exchanger and steam generator tubes

A. JOSEPH, GOVIND K. SHARMA and T. JAYAKUMAR*
Non-Destructive Evaluation Division
Indira Gandhi Centre for Atomic Research, Kalpakkam - 603 102, Tamil Nadu
*e-mail: tjk@igcar.gov.in

Ultrasonic Internal Rotary Inspection System (IRIS) is used for inspection of tubes of heat exchangers and steam generators. The system displays circumferential cross section of tubes (wall thickness of tubes) at any given axial position and reveals both uniform and localised (pitting) corrosion. In this paper, the operating principle of IRIS and comparison of wall thickness measurements by physical and IRIS methods are briefly explained. Details of studies carried out on the resolution capabilities of IRIS in stainless steel and brass tubes having artificial defects (holes) are discussed. The results obtained from a study carried out on a carbon steel tube with artificial defects under baffle plate are also discussed in this paper.

Key words :

INTRODUCTION

Industries like Petrochemicals, Fertilizer, Power and other industries are equipped with various heat exchangers and steam generators for effective heat transfer and also as a part of process requirement. Non destructive evaluation (NDE) and condition monitoring of the heat exchanger/steam generator tubes is necessary for the successful operation of the plants. Eddy current testing (ECT) is a widely used technique for inspection of heat exchanger tubes. However, defect interpretation and evaluation using ECT needs more expertise and relies upon the skill of the NDT personnel. Also, with eddy current testing, the exact circumferential position of the defect cannot be identified and only the axial position along the length of the tube can be identified, unless segmented type probes are employed. Due to presence of baffle plates (support plates), defect detection in tubes of heat exchangers poses a lot of difficulties in eddy current testing. Though multi frequency eddy current testing could solve this problem of defect detection under baffle plates, evaluation of the defect becomes difficult particularly in the case of carbon steel tubes because of large variations in the permeability of carbon steel. Since the characteristics of the natural defects differ from that of the artificial reference defects used in the standard calibration tubes, quantitative assessment of the actual defects would be difficult.

Ultrasonic Internal Rotary Inspection System (IRIS) is relatively a new ultrasonic equipment used for inspection of tubes of heat exchangers and steam generators. The equipment has the capability of detecting wall thinning and pitting due to corrosion in tubes. The advantages of this system are: (i) it can measure the remaining wall thickness of the tubes up to 500 μm with an accuracy of better than 50 μm (ii) it can indicate the reduction in wall thickness taken place either from outer surface or inner surface of the tubes or both (iii) it can also reveal the circumferential position of the defects such as localised pitting and (iv) it can reveal defects under baffle plates (support plates).

*Fellow, Ultrasonics Society of India

The operating principle of the IRIS is briefly explained in this paper. Artificial defects (holes and notches) of various diameters with different gaps between the defects were machined in the circumferential plane of the tubes. Details of studies carried out on the artificial defects and the results obtained on the resolution capabilities of IRIS are discussed in this paper. This paper also describes the results of an experiment conducted in a carbon steel tube having artificial defects under baffle plates.

OPERATING PRINCIPLE OF IRIS

The operating principle of the IRIS is similar to the measurement of thickness using immersion ultrasonic pulse echo technique[1-2]. Immersion ultrasonic transducer is kept inside a tube filled with water. The high frequency broad band (10 to 25 MHz) ultrasonic immersion transducer converts a pulse of electrical energy into ultrasonic vibrations (pulses). The ultrasonic pulses travel through the water to the tube wall and from the inner surface of the tube, a part of the energy of the pulse is reflected back to the transducer. A small part of the ultrasonic wave, i.e. about one-tenth travels through the tube wall and is reflected from the outer surface of the tube. Again, a small part of about one tenth of this pulse is transmitted into the water and then reaches back to the transducer. The two ultrasonic pulses (from inner and outer surfaces) reflected back to the transducer generate electrical signals, which are separated by the time required for the ultrasonic wave to make a round trip through the tube wall. Since this time is proportional to the wall thickness, the thickness can be obtained by measuring the time delay between the inner and outer surface reflections. This is done electronically in the IRIS system. If there is a wall thinning from ID/OD surface or both, there will be a corresponding change in the time delay.

The IRIS system consists of the following: (i) The test head with probe, mirror, water turbine and probe centering device (ii) the water supply regulator, water pump and cables and (iii) the oscilloscope and associated electronics. The schematic of the test head with a high frequency ultrasonic transducer and rotating mirror is shown in Fig. 1. A small turbine rotor is connected to a mirror. The turbine is rotated by water, pumped by a submersible compressor pump with a delivery pressure of about 0.55 MPa (80 psi). The high pressure water is pumped through a small diameter, high pressure PVC tube. This tube, which is attached to the test head, enables the turbine to rotate at a speed of 1800 rpm. Thus, the attached mirror with the turbine is also rotated at 1800 rpm. Each rotation of the mirror constitutes one revolution of the ultrasonic beam and shows a rectilinear picture (B-scan) of the cross section of the tube wall in the oscilloscope screen. A wire marker in the turbine interrupts the beam during each revolution, thus providing the pulse for initiating the trigger in oscilloscope display.

The equipment is calibrated with the standard tube supplied with the system. This allows the operator to check whether all the components of the system are functioning correctly and that the individual controls are set at appropriate levels. It is recommended that wherever possible, a sample of the same tube as that to be inspected is made

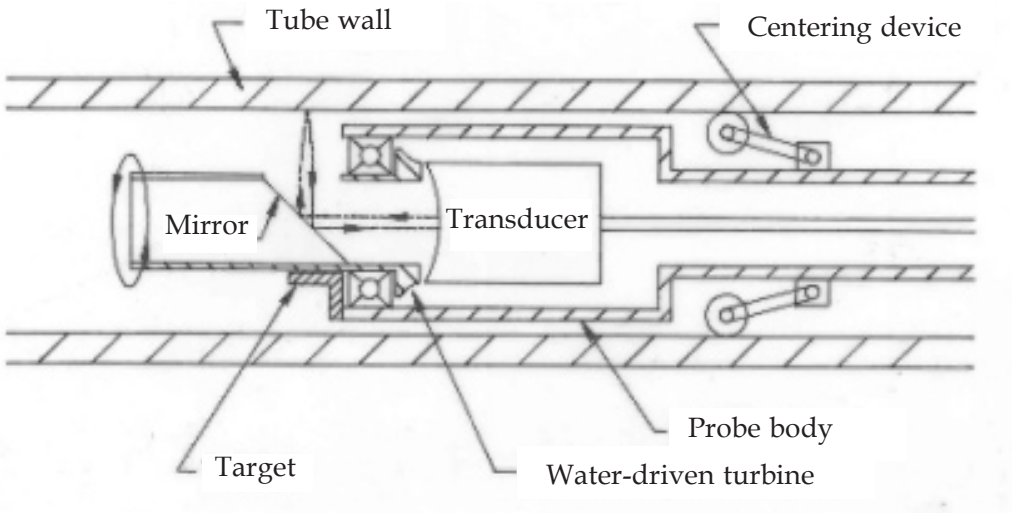

Fig.1. Schematic of the IRIS head with a high frequency ultrasonic transducer and rotating mirror

available as a specific calibration standard. By selecting suitable levels in different controls like trigger, attenuation, damping, tube diameter etc., a clear rectilinear display (B-scan) can be obtained on the oscilloscope screen (Fig. 2). The left boundary of the display represents the condition of the inner surface of the tube and the right extreme trace represents the condition of the outer surface. The height of the display represents the circumference and the wall thickness of the tube is represented by the width of the display.

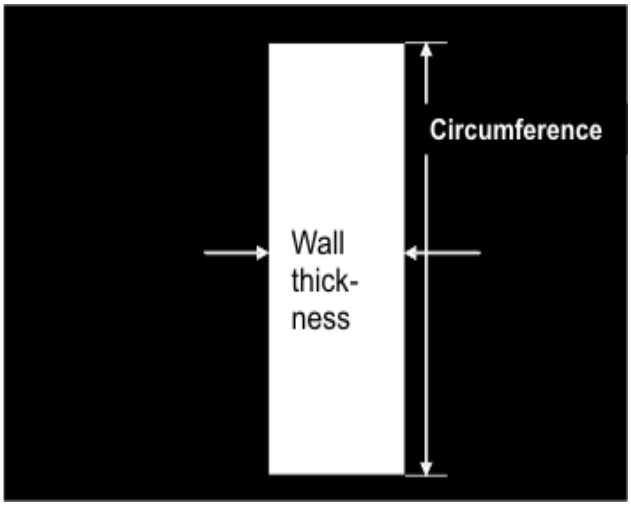

Fig. 2. Schematic of rectilinear display of a tube cross section and circumference on the oscilloscope screen of IRIS system

PRE INSPECTION PREPARATIONS (CLEANING OF TUBES)

The pre inspection preparation (cleaning) depends on the type of tube that is to be inspected. In all the cases, the preparations involve cleaning the tube inner surface such that the tube is totally free from loose scales, debris and other process fluids. A clean well defined boundary between the fled water and the inside diameter of the tube produces a sharp and relatively high amplitude front wall echo. Any rust on either the inner or outer surface of the tube reduces the reflectivity of the boundary, and produces a less defined front/ back wall echo. Accurate measurement of the wall thinning allows the inspector to decide whether the tube has reached its critical limit or not. The system's capability to identify wall loss on both ID and OD sides enables to take corrective action on the control of the environment to which the tubes are exposed to on the OD and ID sides to reduce the extent of corrosion, thus extending the life of the tubes. If the calibration has been carried out correctly, no other factor has a greater influence on the resolving power of the IRIS than the condition of the inner surface of the tube. It is recommended that high pressure water jetting of the inner surface of the tubes should be sufficient to remove loose scales and layers. In exceptional cases, where the internal deposits are adherent, it is necessary to use wire brushing of the inner surface. Chemical cleaning and sand blasting are highly effective methods for cleaning.

EXPERIMENTS

Comparison of wall thickness measurements by physical and IRIS methods

After calibration of the IRIS equipment with the help of calibration tubes, studies were conducted on tubes of various materials and thicknesses. B-scan displays were obtained from perspex, stainless steel, brass and carbon steel tubes and wall thickness was measured from the IRIS display (change in the width of the CRT pattern). The thickness values obtained are given in Table 1. The wall thicknesses of the tubes were also measured by physical methods and the values have been correlated with the values obtained using IRIS (Table 1). In order to asses the sensitivity of the wall thickness using IRIS, a comparative study was also done on a corroded carbon steel tube by using optical method. The position of the tube where IRIS measurements were made was marked and a small specimen was cut. The specimen was moulded and then marked in 30°/60° segments and the thickness was obtained by optical measurements. The thickness values obtained on a corroded carbon steel sample using optical and IRIS methods are given in Table 2. The comparative study clearly indicated that there is good correlation for wall thickness measurements made by conventional physical method and the IRIS method.

Austenitic stainless steel and brass tubes

Table 1. Wall thickness measurements by 'Optical' and 'IRIS' methods

Material	Wall thickness measured by physical method (mm)	Wall thickness measured by IRIS method (mm)
Perspex	3.30	3.30
Stainless steel	3.30	3.28
Brass	1.70	1.69
Carbon steel	2.66	2.65

Table 2. Comparison of wall thickness (WT) measured using 'Optical' and 'IRIS' methods for a corroded carbon steel specimen

Reference Point	0°	60°	120°	180°	240°
WT by Optical method	2.20	1.72	2.37	1.41	1.43
WT by IRIS method	2.25	1.79	2.42	1.45	1.51

were chosen for the circumferential resolution studies. These materials are widely used for heat exchangers in nuclear as well as in refrigeration industry. An AISI type 304 stainless steel tube and a brass tube having 25mm internal diameter (ID) and wall thickness (WT) of 1.0 mm and 0.9 mm respectively were used for the study. Three sets of artificial defects (holes) of various diameters (1.0, 2.0, and 3.0 mm) were made in a circumferential plane with different gaps 0.5, 1.0, 2.0 and 3.0 mm between the holes to determine the circumferential resolution capability of IRIS. The distance between any set of two holes was made in such a way that there exists a uniform gap between the three sets of holes. Fig. 3 shows the tubes used for the resolution study. All the three sets of holes (artificial defects) of various diameters (1.0, 2.0 and 3.0 mm) with different gaps 0.5, 1.0, 2.0 and 3.0 mm between the holes were easily detected by IRIS. The B-scan display of the holes obtained for 0.5mm gap is seen as a merged image (Fig. 4) but the displays of the holes with gaps of 1.0, 2.0 and 3.0 mm were clearly visible as separate images (Figs. 5 to 7). Hence, the circumferential resolution capability of IRIS is 1mm i.e. defects with 1.0mm and more gaps between them can be easily resolved in IRIS inspection.

Carbon steel tube with artificial defect under baffle plate

As indicated earlier, due to presence of baffle plates (support plates), the defect detection in tubes of steam generators/heat exchangers poses a lot of difficulties in eddy current testing

Fig. 3. Stainless steel and brass tubes used for the resolution study

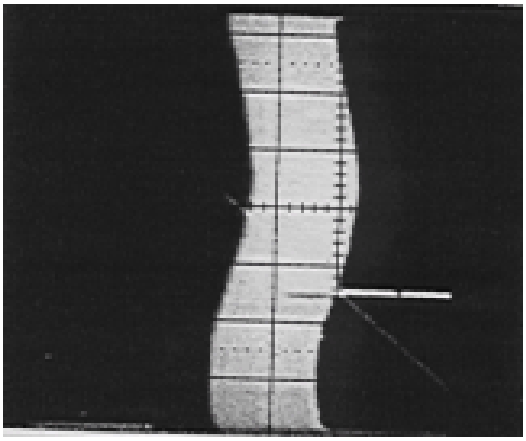

Fig. 4. Cross sectional image of a stainless steel tube with 0.5mm gap between defects

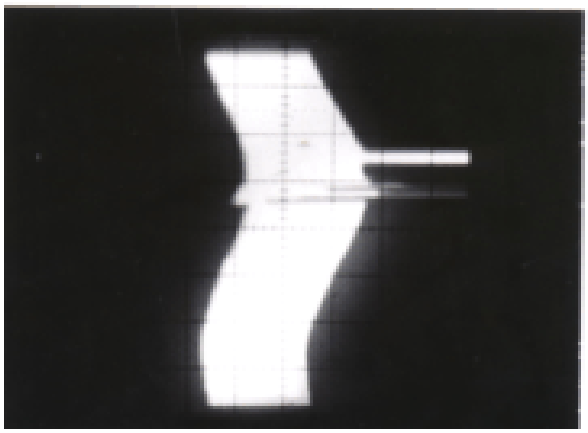

Fig. 5. Cross sectional image of a stainless steel tube with 1.0 mm gap between defects

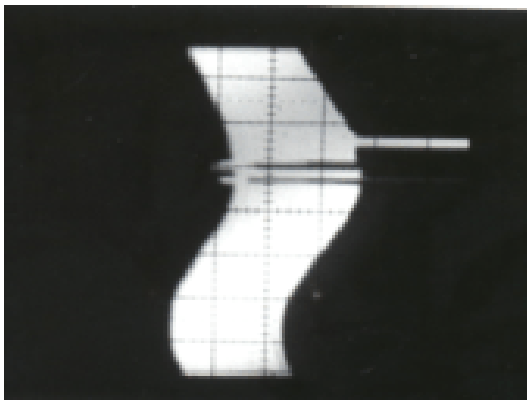

Fig. 6. Cross sectional image of a stainless steel tube with 2.0 mm gap between defects

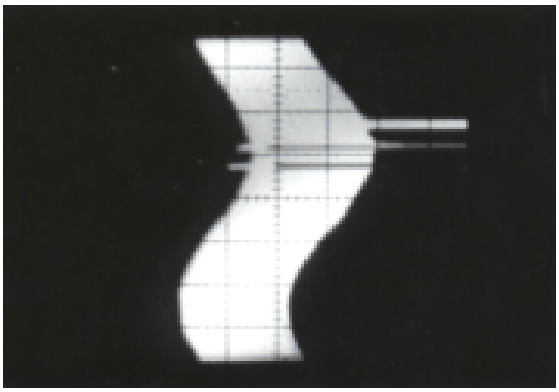

Fig.7. Cross sectional image of a stainless steel tube with 0.3mm gap between defects

[3]. Though multi frequency eddy current testing could solve this problem of defect detection under baffle plates, evaluation of the defect becomes difficult particularly in the case of carbon steel tubes because of large variations in the permeability of carbon steel materials. In order to assess the feasibility of using IRIS as an alternate /complimentary method for ECT, the following studies were conducted: (i) carbon steel heat exchanger tube having baffle plate with uniform gap between the tube and the plate (ii) carbon steel tube with baffle plate making contact on the OD of the tube at some points and (iii) carbon steel tubes having defects at the point on the tube where baffle plate makes a contact.

The studies indicated that whenever a uniform gap exist between the baffle plate and the tube, the presence of baffle plate is not at all seen in the B-scan picture and only the cross section of the tube is seen from the measurements. Whenever the tube comes into contact with the plate by way of sagging/swelling, the cross sectional image of the tube and the place of contact of the baffle plate are clearly displayed by IRIS (Fig. 8). Fig. 9 and 10 show the B-scan images of two defects of size 10% and 20% WT under the support plate with an uniform gap between the baffle plate and the tube (baffle plate does not have contact with the tube). The presence of the baffle plate is seen (Fig. 11) by IRIS due to through and through nature of the defect in the tube wall even though there is a uniform gap between the baffle plate and the tube. In this case, the shift in the baffle plate signal from the tube wall can very well be correlated to the gap between the baffle plate and the tube. From the above laboratory studies, it can be concluded that IRIS can be used with more reliability as compared to eddy current testing for inspection of carbon steel tubes with support plates. The IRIS can be advantageously used to know the

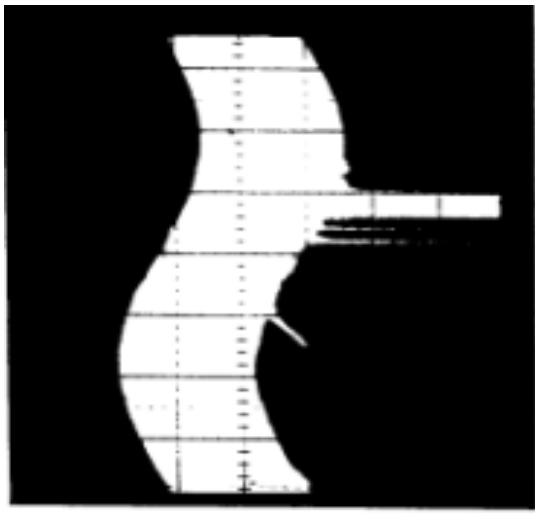

Fig.8. Cross sectional image of carbon steel tube with baffle plate contact

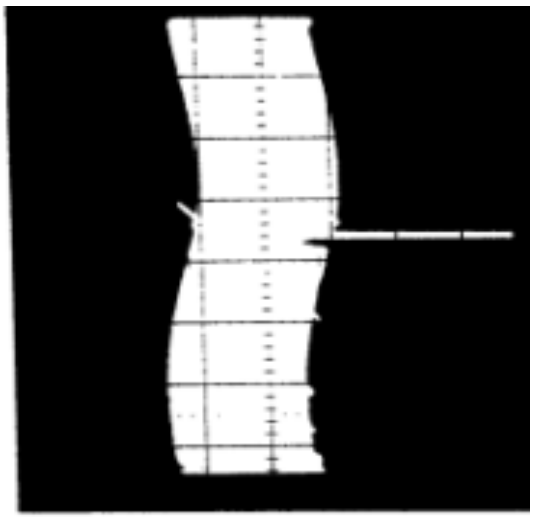

Fig.9. Cross sectional image of carbon steel tube with a 10% WT defect from OD (baffle plate not having contact with tube)

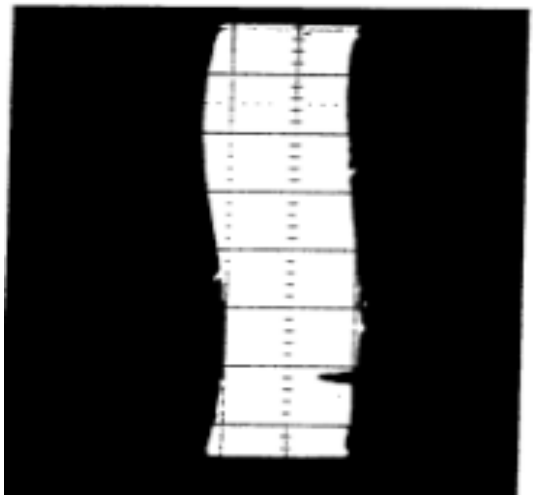

Fig.10. Cross sectional image of carbon steel tube with 20% WTdefect from OD. (baffle plate not having contact with tube)

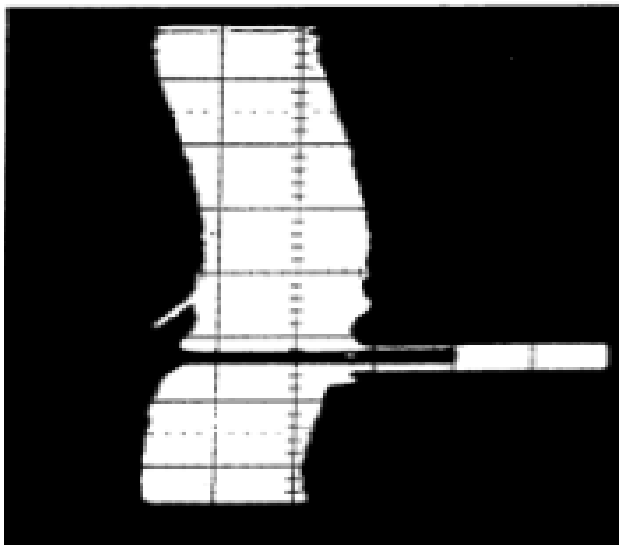

Fig. 11. Cross sectional image of carbon steel tube with a through and through defect under baffle plate

defect nature, depth and circumferential position under the baffle plate, thus making it possible for comprehensive assessment.

ADVANCES IN INTERNAL ROTARY INSPECTION SYSTEM FOR TUBES

Computers are used to convert the earlier analog IRIS equipment to digital IRIS equipment. The digital IRIS provides detailed information of a defective area to the operator for extensive analysis on a composite display. All the measurements made during a complete scan in full length of a tube are stored and then displayed on a computer screen. Computer software is used for producing real time rectangular or circular pictures. Alternatively, it is also possible to obtain

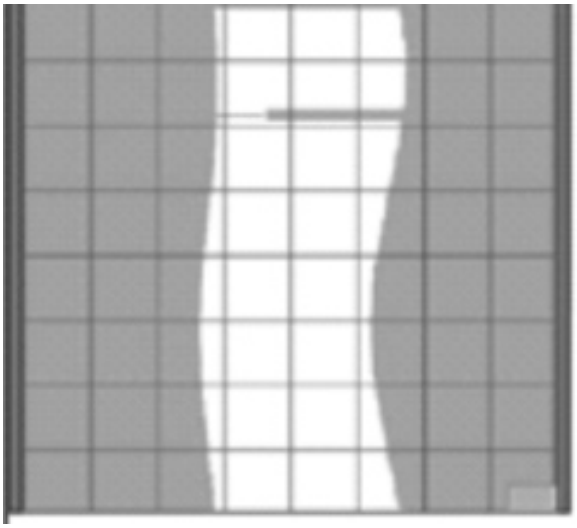

Fig.12.Typical Rectangular display of a tube cross section (B-Scan) obtained using computer software of IRIS

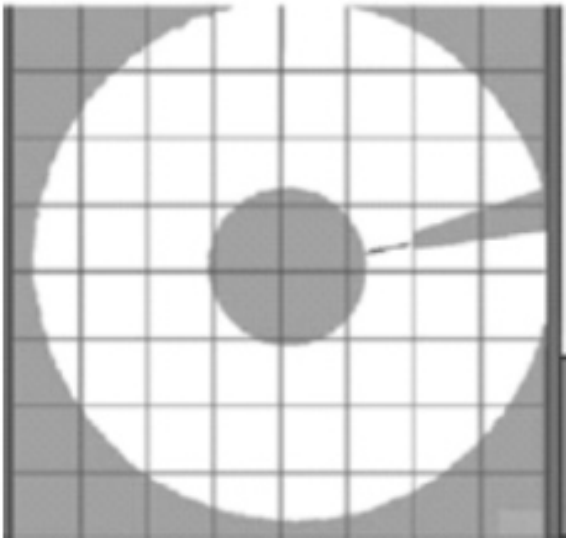

Fig.13.Typical Circular display of a tube cross section (B-Scan) obtained using computer software of IRIS

the C-Scan images. The latest trends in the IRIS show a great comfort in the testing. The signals can be stored in a computer at the work place and analysed later in a laboratory. Bends in the tubes cannot be examined but it is possible for the probe to negotiate the bends in bigger tubes and inspect straight portions ahead. The IRIS technique is used as a complimentary method to verify the results of other techniques. The IRIS can give additional information on the geometry of the defects.

CONCLUSION

Ultrasonic IRIS is an instrument best used for trend analysis on the loss of thickness and isolated defects, if any, in heat exchanger/ steam generator tubes for failure prediction, prevention and life assessment and extension. The circumferential resolution of the IRIS is 1.0mm gap between two defects of 1mm and bigger sizes. The instantaneous cross sectional image of the tube obtained by the IRIS shows the remaining wall thickness and condition of the tubes. This enables the plant personnel to monitor the heat exchanger tubes and to take decision on the plugging of the affected tubes, thus avoiding sudden failures and unwanted shutdowns. The information obtainable by the IRIS on the exact location of the defects and its capability to detect defects under baffle plates makes it inherently superior to ECT.

ACKNOWLEDGMENTS

The authors wish to thank Dr. P. R. Vasudeva Rao, Director, Materials and Metallurgy Group and Dr. Baldev Raj, Director, IGCAR for their

constant encouragement and support. The authors like to acknowledge the help received from Mr. P. Sukumar and the former colleagues Mr. C. V. Subramanian, Mr. A. S. Ramesh and Mr. M. Thavasimuthu.

REFERENCES

1. **Subramanian, C.V, Joseph, A., Ramesh, A. S., Jayakumar T., Kalayanasundaram P**., and **Baldev Raj**, "Wall thickness measurements of tubes by internal rotary inspection system (IRIS) a comparative study with metallography", New Delhi; *Proc. 14th World Conference on Non destructive Testing*, **2** (1996) 985-988.

2. Pan American Industries, Inc., Huston, Texas, USA, Operating Manual for IRIS.

3. **Ramesh, A.S., Subramanian, C.V., Joseph, A., Jayakumar, T., Kalyanasundaram, P**. and **Baldev Ra**j, "Wall thickness measurements of tubes by internal rotary inspection system (IRIS)", *Journal of Non-deaructive Evaluation*, **19 (3-4)** (1998) 22-26.

J. Pure Appl. Ultrason. 31 (2009) pp. 31-35

Nondestructive characterization of a lyotropic liquid crystalline system

GIRIDHAR MISHRA*, R.R. YADAV** and S.K. KOR
Physics Department, University of Allahabad, Allahabad-211 002, India
*e-mail: giridharmishra@rediffmail.com

In the present work, the characterization of a calamitic liquid crystal mixture - sodium lauryl sulphate (SLS)/ decanol/ water - has been reported using ultrasonic velocity and absorption measurements as a function of temperature and concentration. The experimental tools used were, ultrasonic interferometry for the velocity and pulse-echo technique for the absorption measurements. The results are discussed in terms of the temperature and concentration dependent lyotropic liquid crystal formed in the material system.

PACS code: *43.35.Bf, 43.35.+d, 42.70.Df, 64.70.Md, 61.30St*

Key words : Ultrasonic velocity, ultrasonic absorption, lyotropic liquid crystals, Pulse - echo technique

INTRODUCTION

Liquid crystals having anisotropy of physical properties show a large number of mesophases. Liquid crystalline mesophases are characterized by different structures and different spatial symmetries, displaying a great variety of textures. They possess different morphological, optical and structural peculiarities. Mixtures of amphiphilic molecules, having hydrophilic head and hydrophobic tail, form in aqueous solutions anisotropic miceller aggregates, which may orient mutually under proper temperature/ concentration conditions, giving lyotropic nematic phases[1-2]. For a liquid crystal, determination of temperature/concentration dependent characteristics at constant pressure is an important part of the study of its thermodynamic properties and phase transitions. Such measurements have been made in different lyotropic systems including n-octylamine/water[3] and CTAB/water[4]. Sodium lauryl sulfate is probably the most researched anionic surfactant compound. It has recently found application as a surfactant in gas hydrate or methane hydrate formation reactions increasing the rate of formation as much as 700 times. On the basis of temperature- concentration phase diagrams given by L.J. Yu and A. Saupe, two uniaxial and one biaxial nematic phases have been observed[5]. The shape of the micelles in the nematic phase could not be explained exactly till today. In the work of T. Bica et al.[6] they have assumed that oblate micelles give the nematic discotic phase while prolate micelles give the nematic calamitic phase. Ultrasonics is a versatile tool for studying the properties of solids, liquid and liquid crystals[7-15]. The theory for absorptions and dispersions are well established in solids and liquids but for liquid crystals there are various theories to understand the ultrasonic absorption as a function of temperature, frequency and concentration. Two main types of liquid crystals, thermotropic[16] and lyotropic liquid crystals[12], have been studied by ultrasonic technique. In thermotropic liquid crystals[17] the main criterion is the temperature, as the temperature is varied the liquid crystalline properties are seen. In lyotropic liquid crystals, concentration of a component in the material is the main criterion but temperature also plays some role in few cases. Ultrasonic

*Member, **Fellow, Ultrasonics Society of India

absorption measurements in materials, especially in liquid crystalline phases are important because of its widespread use in medical and biological fields. Accumulation of absorption data and the classification of the cases of absorption are therefore desired in various systems. We have made the ultrasonic absorption and velocity measurements at different temperatures and the concentrations of the lyotropic solutions. The acoustical anisotropy has been discussed in relation to identify the liquid crystalline phases depending upon the temperature/concentration.

EXPERIMENTAL

1. *Materials and sample preparation*

In the present ultrasonic study sodium lauryl sulphate (SLS) (99% purity), used without further purification, 1-decanol and doubly distilled water were used to prepare the lyotropic solutions of different concentrations. SLS and water were mixed in a vessel until the mixture becomes homogeneous. The appropriate quantity of 1-decanol was added to the clear homogeneous solution. Finally this mixture was again mixed for 10 hours with the help of magnetic stirrer. The concentrations of all the three components in different samples are shown in Table 1:

2. *Experimental technique*

Ultrasonic velocity measurements have been made by using the variable path interferometer[18] at a frequency of 2.0 MHz. Knowing the wavelength and frequency the ultrasonic velocity can be obtained. Temperature of the sample is kept constant by circulating water around the ultrasonic cell at constant temperature from thermostat. The temperature variation is accurate to ± 0.5°C and velocity to ±0.1%. Standard pulse technique, first developed by Pellam and Galt[19], has been used for ultrasonic absorption measurements. The output of the receiving crystal is amplified, demodulated and fed to the Y- axis of the C.R.O. The original pulse along with the reflected pulses is observed on an oscilloscope. The ultrasonic intensity decreases exponentially with the path length thus the intensity at particular distance between output quartz crystal and the reflector can be written as

$$I_x = I_0 e^{-2ax} \tag{1}$$

where x is the distance between output quartz crystal and the reflector. I_o is the max. intensity and α is absorption coefficient. If I_{x1} and I_{x2} are the intensities of ultrasonic waves at x_1 and x_2 distances, then from eqn. (1) we can write

$$I_{x_1} = I_0 e^{-2ax_1} \tag{2}$$

$$I_{x_2} = I_0 e^{-2ax_2} \tag{3}$$

On solving eqn. (2) and (3) one can easily obtain the following expression of ultrasonic absorption as-

$$\alpha = \frac{I}{2(x_2 - x_1)} In \frac{I_{x_2}}{I_{x_1}} \tag{4}$$

The absorption coefficient calculated using eqn. (4) was further used to estimate α/f^2, the absorption. The accuracy in the absorption measurement is ± 5%. Several known values of standard liquids including water were checked so as to ascertain the accuracy in absorption and velocity measurements.

Table 1. Concentrations of SLS, water and decanol used for making samples

S.No.	SLS (wt%)	water (wt%)	decanol (wt%)
1.	24.55	70.96	4.49
2.	24.65	70.86	4.49
3.	24.75	70.76	4.49
4.	24.85	70.66	4.49
5.	24.95	70.56	4.49
6.	25.05	70.46	4.49
7.	25.15	70.36	4.49
8.	25.25	70.26	4.49
9.	25.35	70.16	4.49
10.	25.45	70.06	4.49

EXPERIMENTAL RESULTS AND DISCUSSION

The measurements have been made at 0.1gm interval of SLS concentration in 1-decanol and water. The concentration dependence of the ultrasonic velocity measurement at room temperature with error bar is shown in Fig. (1). The plot shows that there is a minimum in ultrasonic velocity at 25.05 wt% concentration of SLS. This is referred as critical concentration. Fig. (2) shows the results of the temperature dependence of the ultrasonic velocity. The distinct minima are observed at 25°C and 40°C for the sample having 25.05 wt% of SLS and 1-decanol+ water. The liquid crystal formation in a mixture depends

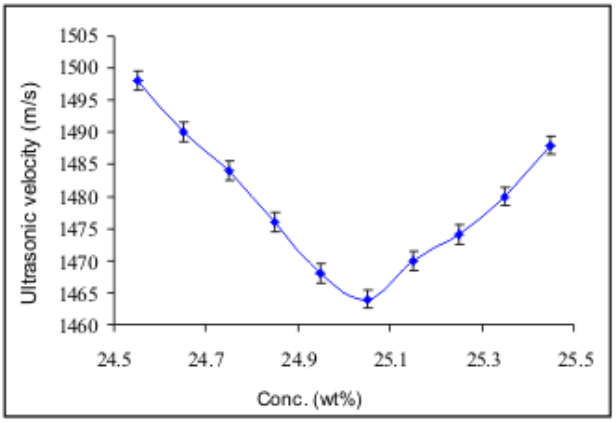

Fig. 1. Concentration dependent ultrasonic velocity at 25°C

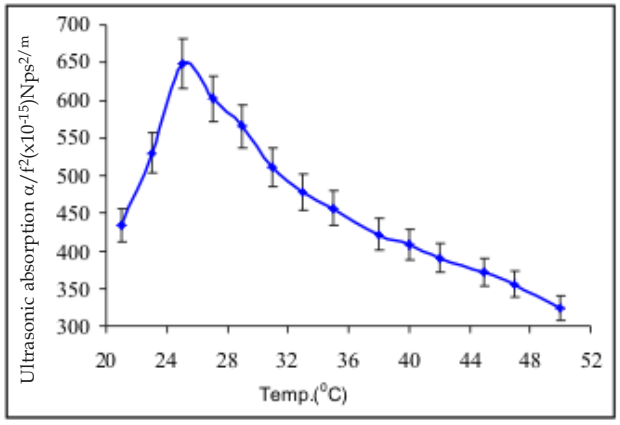

Fig. 3. Temperature dependent ultrasonic absorption at critical concentration

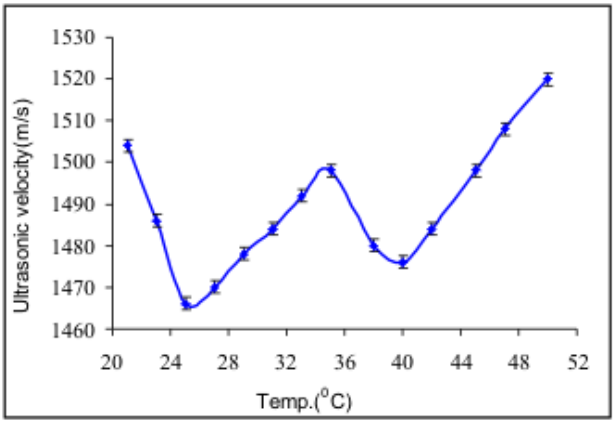

Fig. 2. Temperature dependent ultrasonic velocity at critical concentration

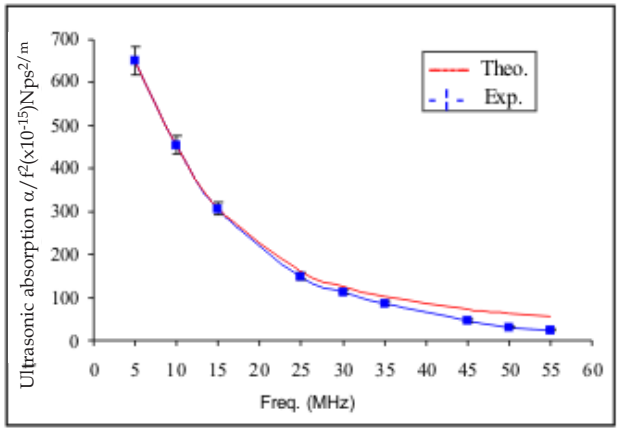

Fig.4. Frequency dependent ultrasonic absorption at 25°C for 25.05 wt%of SLS, theoretical and experimental curves

on two factors, first the ability of molecules to pack into a single liquid crystal lattice and secondly the mean orientational cohesive energy of the mixture[20]. During the phase transition the disordered liquid state is converted into ordered state having a long range orientational order of the molecules and hence an anomalous change in velocity occurs at the critical concentration as a result of sudden change in structure. The increase in the sound velocity after the minimum is caused by the increase in the degree of order among the molecules. As the molecules become more parallel with increasing concentration implying that the degree of order increases, the intermolecular distance decreases resulting in an increased sound velocity.

Next the ultrasonic absorption measurements have been made at critical concentration for different temperatures and frequencies as shown in Fig. (3) and Fig. (4), respectively. Fig. (3) shows that there is maximum absorption at 25°C for the sample having 25.05 wt% of SLS and 1-decanol+ water.

The plot of (α/f^2) versus frequency is shown in Fig. (4). As the curve in Fig. 4 is relaxation type, the ultrasonic absorption can be given by a single relaxation equation[21]:

$$\frac{\alpha}{f^2} = \frac{A}{1+(f/f_c)^2} + B \qquad (5)$$

where (α/f^2) is the absorption at frequency f_c, where fc is the relaxation frequency, A is the relaxation amplitude and B is the ultrasonic absorption at very high frequency which is same as the solvent absorption. Eq. 5 is fitted to the experimental data and the values of constants estimated are as given in Table 2.

A perusal of Fig. 2 shows that the ultrasonic velocity is minimum at 25°C in the 25.05 wt%

Table 2. Values of different constants for the lyotropic liquid crystalline systems

f_c MHz	A 10^{-15}Nps^{2}m^{-1}	B 10^{-15}Nps^{2}m^{-1}
11.9	736.37	24.54

concentration of SLS in water/decanol system. Similarly a perusal of Fig. 3 shows the ultrasonic absorption maximum at the same temperature, 25°C. This type of ultrasonic propagation behavior may be appeared due to the micelles formations at critical concentration/temperature of the system.

Such relaxation type behavior of ultrasonic absorption maxima and velocity minima is similar to those previously observed in thermotropic liquid crystals, binary liquids and liquid gas system at critical points[3-4,22]. Thus molecular texture of the micellar solution can be correlated to the liquid crystalline phase of the present solutions. Beica et al6 have shown the liquid crystalline behavior of the above mentioned system at the 25.05 wt% concentration of SLS in decanol and water at temperature ~ 24 °C which is very close to our acoustical analysis of the liquid crystalline phase of the system. The temperature is slightly different as the accuracy in the measurement of the temperature in our experiment is ±0.5° C. Thus our acoustical study of the liquid crystalline system SLS/decanol/water is established very well.

This study using the simple and nondestructive ultrasonic technique can be used for the online identification of the liquid crystalline phase of the system.

ACKNOWLEDGEMENT

The authors are grateful to the Department of Science and Technology, Govt. of India (DST project no. SR/S2/CMP-0069/2006) for the financial support to carry out the work successfully.

REFERENCES

1. **Lawson, K.D.** and **Flautt, T.J.,** Magnetically oriented lyotropic crystalline phases, *J. Am. Chem. Soc.*, **89** (1967) 5489.

2. **Rodriguez, C.R., Pusiol, D.J., Figueiredo Neto, A.M.,** and **Martin, C.A.,** Micellar anisotropy in lyotropic uniaxial nematic phases studied by transversal NMR relaxation dispersion, *Phys. Rev.,* **69** (2004) 041708.

3. **Nishikawa, S.,** Ultrasonic absorption in aqueous solutions of n-octylamine structural relaxation in mesomorphic state, *J. Colloid Interf.,* **45** (1973) 259.

4. **Yadawa, P.K.,** Ph.D. Thesis, University of Allahabad, Allahabad, India (2007).

5. **Yu, L.J.** and **Saupe,A.**, Observation of a biaxial nematic phase in potassium laurate-1-decanol-water mixtures, *Phys. Rev. Lett.*, **45** (1980)1000.

6. **Beica, T., Moldovan, R., Puica, M.R.** and **Frunza, S.**, Temperature dependence of the density of calamitic and discotic nematic lyotropic liquid crystals containing sodium lauryl sulphate/decanol/water, *Liq. Cryst.,* **10** (2002) 1275.

7. **W.P. Mason,** Physical Acoustics, vol. III B. New York: Academic Press, (1965).

8. *I.E.E.E., Special issue on Ultrasonics,* **53** (1966).

9. **Pandey, D.K., Yadawa, P.K.** and **Yadav, R.R.**, Acoustical wave propagation in Laves-phase compounds, *Materials Letters,* **61** (2007) 4747.

10. **Bhatia, A.B.,** An Introduction to the Theory of Sound Absorption and Dispersion in Gases, Liquids and Solids, Dover, New York (1985).

11. **Hertzfeld, K.F.** and **Litovitz, T.A.**, Absorption and Dispersion of Ultrasonic Waves. New York Academic Press (1965).

12. **Lubensky, T.C.,** Liquid crystal physics at the millennium, *Mol. Cryst.*, **1** (2001) 364.

13. **Miyano, K.** and **Ketterson, J.B.,** *Physical Acoustics,* **A6** (1972) 2401.

14. **Edmonds, P.D.** and **Orr, D.A.,** Ultrasonic absorption and dispersion at phase transition in liquid crystalline components, *Mol. Cryst.,* **2** (1966)135.

15. **de Gennes, P.G.,** The Physics of Liquid Crystals, Oxford University Press (1974).

16. **de Gennes, P.G.** and **Frost, J.,** The Physics of Liquid Crystals, Oxford University Press,(1993).

17. **Kor, S.K.** and **Pandey, S.K.,** Ultrasonic investigation of cholesteric liquid crystals, *J.Chem. Phys.,* **64** (1975)1333.

18. **Fox, F.E.,** Ultrasonic interferometry, *Phys. Rev.,* **52** (1937) 973.

19. **Pellam, J.R.** and **Galt, J.K.**, Ultrasonic propagation in liquids: I. Application of pulse technique to velocity and absorption measurements at 15 megacycles, *J.Chem. Phys.,* **14** (1946) 608.

20. **Dave, J.S.** and **Dewar, M.J.S.,** Mixed liquid crystals, *J. Chem. Soc.,* (1954) 4617.

21. **Beyer, R.T.** and **Letcher, S.V.**, Physical Ultrasonics, Academic Press, New York, 1969 (p.129).

22. **Cao, Y.N., Diebold, G.J.** and **Zimmt, M.B.,** Transient grating studies of ultrasonic attenuation in reverse micellar solutions, *Chem. Phys. Lett.,* **276(5)** (1997) 388.

A Brief Report on the Seventeenth National Symposium on Ultrasonics (NSU-XVII)

17th National Symposium on Ultrasonics, (NSU-XVII) was jointly organized by the Department of Physics, Banaras Hindu University, Varanasi and Ultrasonics Society of India during Dec. 4-6, 2008, at Department of Physics B.H.U.,Varanasi. The objective of the symposium was to provide a common platform to scientists, technologists, academicians, users and manufacturers of ultrasonic instruments, devices and materials for industrial, medical and other applications. Due to wide ranging applications of ultrasonics from synthesis to characterization of nanomaterial materials, the focal theme of the Symposium "Ultrasound and Nanomaterials" was in line with the current focus of scientists, technologists and academicians all over the world. A broad range of topics were covered under the following categories:

Ultrasonic Instrumentation, Sensors and Transducers, MEMS and NEMS, Materials and Devices, Biomedical Ultrasonics, Ultrasonic Imaging, Physical acoustics, NDE, Modeling and Simulation, Signal processing, Underwater Ultrasonics, Standards and Calibrations, Acousto-optics, photoacoustics, Ultrasound and nanomaterials, Laser Ultrasonics etc..

The symposium was inaugurated by Prof. B.D. Singh (Rector, Banaras Hindu University, Varanasi). In his inaugural address he pointed out the importance and need of interdisciplinary research among various disciplines of Science. Dr. Rajendra Kumar Singh (Convener and Organizing Secretary of the Symposium) discussed at length the objectives and the main theme of the Symposium. Prof. Udo Kaatze (Gottingen, Germany), the Chief Guest of the Symposium called upon scientists to advance the knowledge in the experimental field in this applied discipline. Dr. P.P. Chandrachoodan (Programme Director BRNS DAE) present as guest of honor during the occasion emphasized the need of more research in the field on applied aspects. Dr. Krishan Lal, (President, USI) described in detail the activities of the Ultrasonics Society of India in promoting the cause of ultrasonics. Mr. S.K. Singhal, Secretary, USI, informed the Society has instituted Dr. Parthasarathy, Dr. M. Pancholi awards and will be announced during the Symposium for best contributory paper presentation.

12 plenary, 1 tutorial and 14 invited talks by the scientists from India and abroad (10) were delivered along with more than 85 contributed papers were presented in oral and poster sessions, covering a wide variety of topics related to the science and technology of the Ultrasonics. An exhibition on instruments was organized in which several exhibitors including manufacturer of ultrasound instruments displayed their products.

In the plenary talk delivered by Prof. Udo Kaatze (Germany) on "broad band spectroscopy of liquids" he described different acoustical techniques in the wide frequency range from 10 KHz-10 GHz. He discussed in detail the applicability of these techniques as universal research tool for the investigation of molecular processes of many chemical, biochemical and physicochemical systems. During his talk he paid special attention to the chemical relaxations of ionic and molecular reactions including mechanisms of structural isomerization, association and complexation as well as stacking processes and micelle formation. Prof. J.K. Bhattacharjee (S.N. Bose Centre, Calcutta) gave very illustrative talk on critical ultrasonics. He discussed the primary mechanisms responsible for damping of sound waves in a fluid. In his talk he elaborated on the resonance absorption of sound wave and told that when time period of sound wave matches the relaxation time resonance occurs and fluid absorbs sound energy from the propagating sound wave. He explained how near the critical point (liquid-gas critical point or critical demixing point of the binary liquid mixtures) the fluctuation gets much correlated and are infinitely long ranged.

Prof. Weon Bae Ko (South Korea) described the synthesis of metal nano particles with various surfactants and metal salts in water under ultrasonic irradiation. Dr. T. Jayakumar (IGCAR, Kalpakkam) threw light on advances in ultrasonic NDE techniques for evaluation of flaws, microstructures and residual stresses in materials and components. He explained how the advanced ultrasonic signal analysis

procedures developed by using effective clusters and pattern analysis algorithms enabled detection and characterization of defects down to 1 % from 10 %. He explained in a lucid manner the use of these techniques in extracting information on microstructural features from micro to nano scale, residual stresses and textures. Prof. Nico F Declerecq (France) gave talk on ultrasonic diffraction phenomena at periodic structures caused by the use of phononic crystals for filtering devices.

Dr. Abhijit Mukherjee (Director, Thapar University, Patiala) described numerical modeling of ultrasonic waves. In his talk, he described beautifully the health monitoring of structures by recording the propagation of stress wave through them. Dr. Ashok Kumar (NPL, New Delhi) gave an illustrative talk on the applications of ultrasonics in making nano particles. Prof. Wolfgang Grill (Germany) described high resolution ultrasonic imaging done to microscopic scale by scanning confocal microscopy, microscopic technology and holography in variety of applications in material characterization and biomedical monitoring. He discussed the high resolution phase detection technique developed by him. Dr. Jacob Philip (Director, STIC, Cochin) discussed methodology and applications of Photoacoustic technique. Prof. N. N. Kishore (IIT, Kanpur) discussed on the application of composites in critical situations.

Prof. Udo Kaatze (Germany) in his tutorial talk spoke about ultrasonic measurement techniques for liquids. He pointed out that different techniques for the sound velocity measurements are available in wide frequency range covering about 10 decades of frequency and these are being widely used in basic research and in manufacturing processes.

Series of invited talks were also delivered during this symposium covering various aspects of ultrasound. Dr. P. Palanichamy (IGCAR, Kalpakkam) gave a systematic overview on the structure of recent developments in ultrasonic characterization of materials. Dr. E. Lamkamfi (Ghent University, Belgium) spoke about the use of the finite element method in the investigation of diffraction effects at the extremities of solid for Rayleigh and Scholte Stoneley waves. Dr. V.H. Patankar (BARC, Mumbai) summarized the results of his work on advances in ultrasonic instrumentation for NDE of materials and components. Prof. Rudra Pratap (I.I.Sc., Bangalore) delivered talk on ultrasonic MEMS and transducers. He discussed the design methodology of MEMS, ultrasound transducers, modeling issues, fabrications issues and their characterization. Dr. J.N. Som (NPL, New Delhi) discussed research and development in ultrasonic flow measurement. Prof. O.N. Srivastava (B.H.U., Varanasi) gave an overview of synthesis and characterization of various types of nanostructures such as nano rod, nano fullerene, CNT, MwCNT, Graphine etc.

Dr. M. Rizal Bin Arshed (Malaysia) covered several aspects of some recent attempts to develop bio-inspired underwater robotics platform with special emphasis on the application in underwater acoustic sensing for intelligent navigation. Dr. R.K. Shukla (NOPL, Kochi) discussed various aspects of underwater acoustics. Besides, a number of exciting talks were given by Dr. A.T. Sheshadri (IIT, Chennai), Dr. S. Jaykumar (Chennai), Dr. R.R. Yadav (Allahabad), Dr. Shruti Sharma & Dr. Sandeep Kumar Sharma (Thapar University Patiala), Dr. Prashant Dhise (IIT, Mumbai), Dr. Kailash (Hamirpur, U.P.) and others. Contributory papers were presented during parallel oral and poster sessions.

During the valedictory function, Dr. G. N. Pandey (Programme Director, BRNS, DAE) expressed happiness over the professional approach adopted in organizing this symposium. He stressed upon the need to pursue more R & D activity in this applied and vast expanding field of ultrasonics. He assured full co-operation from BRNS, DAE in sponsoring related Programmes/ Proposals/Activities while presiding over the valedictory session. All the participants had a good time during cultural evening on 4th Dec, 08 and on a trip to Ganga Arti-Darshan in the evening on 5th Dec, 08.

Rajendra Kumar Singh
Convener, NSU-XVII
Department Of Physics
B.H.U., Varanasi

Dr. T.K. Saksena

Dr. Tribhuwan Kumar Saksena was born on November 1, 1934. After getting his M.Sc. Degree in Physics from the Allahabad University in 1957, he joined NPL in 1958 to take up a scientific career in the Acoustics Division. He simultaneously worked for Ph.D. under the guidance of Dr. M. Pancholy. In 1966 he was awarded the PhD Degree by the University of Delhi for his thesis - "Ultrasonic study of rates and equilibria in chemical reactions".

While serving Acoustics Division as scientist, he continued to be interested in ultrasonic studies in liquids. In 1967, he went to France to work on ultrasonic absorption in aqueos solutions with Professor Cerf at the University of Strasbourg. Later he went to U.S.A. to work on sonochemistry and cavitation with Prof. Nyborg at the University of Vermont. After his return from U.S.A., he turned his interests towards applied ultrasonics. One of his valuable contributions was on development of an ultrasonic device for guiding blind persons. He also developed an ultrasonic method to study bond strength of adhesives.

In 1980, he left acoustics division to join ultrasonics section to work with his old colleague Dr. V.N. Bindal. A synergy between his expertise in ultrasonics and the facilities and experienced staff in the ultrasonics section helped Dr Saksena to bring out his best research output. Some of his significant contributions were in development of high power air ultrasonic transducers using ultrasonic horn coupled with stepped radiator. This development led him to demonstrate novel phenomena such as acoustic levitation in air, sub-harmonic generation in air and generation of directional sound using parametric acoustic arrays in air. His work on development of parametric acoustic arrays in air and subsequently in water was a pioneering contribution. In fact, the team working with him on this work won the best paper award of the Acoustical Society of India for the year 1989. During this period he worked on several projects sponsored by government departments such as DOD and DOE on development of high power ultrasonic devices for oceanographic applications. Dr T K Saksena also played an important role in the start of a new activity of ultrasonic standards at NPL.

He was associated with the Acoustical Society of India as Life Fellow and had also served the Ultrasonics Society of India as Vice President. Dr. Saksena, took over the Leadership of the Ultrasonics group from Dr. V N Bindal after his retirement in December 1990, and very ably carried on the activities of the team under his leadership till retirement. He had many research publications to his credit which were published in journals like Ultrasonics; J. Acoust. Soc. Amer.; Acustica, Appl. Acoust.; Archives Acoust.; Acoust. Lett.; Indian J. Technol.; Indian J. Pure Appl. Phys.; Indian J. Marine Sci.; J. Acoust. Soc. India; J. Phys. Soc. Japan; J. Chem Phys; J. Pure Appl. Ultrason.; Z. Ange. Phys; Nuovo Cimento etc, in addition to a large number of papers published in proceedings of various conferences, symposia and seminars. He also guided Rupa Mitra on 'Study on vibrational amplitude characteristics of ultrasonic transducers' and Mukesh Chandra on 'Studies of parametric acoustic arrays in water in presence of intercepting liquid media' leading to the award of doctorate degrees to them.

Dr Saksena was a keen experimentalist, a highly erudite person and an original thinker. In fact, he observed many new phenomena in a large variety of experiments he was involved in during the course of his scientific career. He was a thorough gentleman and a person of high integrity. By his nature he

would never offend anybody but would also not compromise on principles.

On 8th August 1998, he had a stoke which resulted in paralysis of the right side of the body, and in spite of all treatment he was unable to write with his right hand. But his indomitable spirit and the moral and physical support from his life partner Mrs Kanak Saksena, he started writing poems in hindi with his left hand. A collection of 128 of his poems was published as a book titled - 'Teri Yaad Nirvaan'.

From the year 2009, the Ultrasonics Society of India has instituted an award in his honour under the name 'Dr. T.K. Saksena Award'. The award has been initiated by Dr. Skand Saksena in the memory of his father and will be given from the interest proceeds of a donation of Rs 60,000/- made by him to the Society. The award carries a cash prize of Rs 5000/- along with a trophy and a certificate and will be given to one student of age below 35 years who has obtained a Ph. D degree, for his/her work in the field of ultrasonics or allied area, during the previous five years.

He breathed his last on 23rd December 2008. He is survived by his wife, two daughters and a son. His both daughters are medical doctors, married and well settled. His son is a PhD in Chemical Engineering.

S.K. Jain and G.K. Arora

R.N. 39355/81

18th National Symposium on Ultrasonics

(NSU-XVIII)

21-23 December 2009

Organized by

Ultrasonics Society of India

and

VIT

UNIVERSITY

(Estd. u/s.3 of UGC Act 1956)

Vellore - 632 014, Tamil Nadu, India

Venue

Physics Division
VIT University
Vellore - 632 104 (TN)

e-mail : ultrasonics2009@gmail.com, ultrasonic2009@yahoo.com
websites : www.vit.ac.in www.ultrasonicsindia.com.

Printed at : Alpha Printers, BG-2/ 38C, Paschim Vihar, New Delhi-110063, Ph : 9811848335

ISSN 0256-4637

VOLUME 31 NUMBER 2 April-June, 2009

Journal of Pure and Applied

Ultrasonics

Website : www.ultrasonicsindia.com

A Publication of — Ultrasonics Society of India

A Quarterly Publication of Ultrasonics Society of India

Journal of Pure and Applied

Ultrasonics

No. 2 **Volume 31** **April-June, 2009**

J. Pure Appl. Ultrason. 31 (2009) pp. 61-66

Anomalous ultrasonic attenuation of agarose hydrogel

MADHUSUDAN ROY* and SUPRATIC CHAKRABORTY
Microelectronics Division, Saha Institute of Nuclear Physics, 1/AF Bidhannagar,
Kolkata 700 064, India
e-mail: supratic.chakraborty@saha.ac.in

An anomaly in ultrasound attenuation of agarose hydrogel studied over a temperature range of 283 K to 311 K, is observed. Anomalous ultrasound attenuation occurs at ~ 290 K. A theoretical model has been worked out to explain the anomaly. A differential scanning calorimetry (DSC) study shows an endothermic peak at ~ 290 K, indicating phase transition when scanned over a temperature range of 282 to 330 K at different heating rates. The investigation helps identify the range of temperature over which a gelatin/agar-based phantom may be used in mimicking tissues. This effect may also be explored in temperature imaging.

Key words : Ultrasound attenuation, agarose, imonification, pulse echo, time of flight

INTRODUCTION

Measurement of ultrasonic properties in tissues and tissue phantoms carves a special area of importance in medical research in recent days because it serves as a competent technique to characterize tissues in non-invasive and non-ionizing ways, and provides information on various features compatible to clinical diagnosis. In biological tissues refraction, reflection, scattering and absorption contribute to total attenuation loss of ultrasound energy. In practice, any variations of acoustic parameters such as speed, impedance, absorption, scattering and attenuation are extracted to acquire information as regards tissue structure[1]. Precisely, they all contribute to the complicated process of formation, and, therefore, to the pulse-echo signal. Although attempts were made to measure attenuation of tissue with frequency choosing temperature as a parameter[1-3], temperature dependence of ultrasound properties for non-invasive measurements appears to have met with relatively little success primarily due both to the difficulties in measuring parameters accurately and to the biological changes in the temperature coefficients of interest[1]. The effect of temperature variation on the acoustic parameters is an important feature, as temperature mapping in tissues under insonification can be made possible non-invasively through their explicit thermal changes. Besides, the study of gelation mechanism and structure of hydrogels becomes an important area of research in the field of cellular and sub cellular biology and in polymer physics[4-6]. However, a few attempts have so far been made to study the acoustic parameters of tissues and hydrogel-based tissue phantoms as a function of temperature[2,3], no such systematic study has been made up to now to investigate the temperature variation of acoustic parameters, namely, attenuation. In this context, an experiment has been simulated to investigate the temperature dependence of acoustic parameters, namely, attenuation over the temperature range 282 to 311 K in agarose hydrogel, a phantom material that mimicks acoustic properties of soft tissues. Differential scanning calorimerty technique was employed to investigate the phase change, if any over the temperature range[7-11]. Thermogravity analysis technique was also employed to know the amount of water loss of the agarose hydrogel in this temperature range[11].

EXPERIMENTAL SETUP

An experimental arrangement designed for the work is shown in Fig. 1; the inset shows the

*Life Member, Ultrasonics Society of India

test chamber. The chamber ( ) was made of brass fitted with an upper lid. An opening in one of its sidewalls was made to mount the transceiver that was fitted with a removable plug. A computerized numerical control (CNC) machine [Model: Pilatus 20T L5, LMW Ltd., India] having an accuracy of 1 m was employed for mounting transceiver and making the slots. The slots were made in such a way that an aluminum plate, when fitted into a slot, became parallel to the flat surface of the transceiver. It is noteworthy to mention that the alignment between transceiver and flat surface of the aluminum plate was very critical to maximize echo signal. The position of the slot was so chosen that it remained in the focal zone of the ultrasonic transceiver to minimize the diffraction effects.

An unfocused transceiver of A682S series from Panametrics - NDT, USA with flat circular face of diameter 12.5 mm, focal length ~ 13 cm, central frequency 3.44 MHz and pulse duration of 1.28 μs at - 20 dB level was employed to the study the temperature dependence of attenuation coefficient. It was driven by a pulser (Model: 5800, Panametrics - NDT, USA).

Three Ni-Constantan thermocouple probes [Sable Systems International, Inc., Las Vegas, USA] were used at three different depths, covering central region through which the ultrasound beam propagated, to measure the temperature of agarose. The steady state temperature of the sample was recorded by a thermocouple meter (TC-1000, Sable Systems International, Inc., Las Vegas, USA). The probes of diameter of 1.5 mm were so placed that it would not obstruct the probing ultrasound beam. The accuracy of thermocouple probe is better

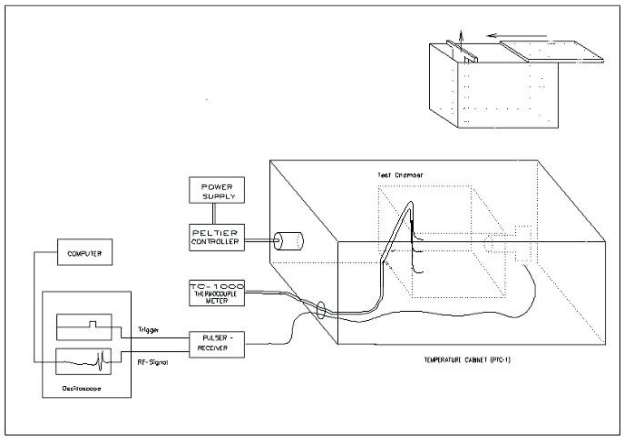

Fig. 1. Schematic diagram of the experimental arrangement; inset shows the details of test chamber

than 0.2 ^{o}C with a resolution of 0.01 ^{o}C.

Agar powder (3% by weight) in suspension with solid gelatin solution mixed with distilled water was heated at ~ 80 ^{o}C and stirred gently. Once the mixture was ready it was poured into the chamber fitted with the aluminum plate. When the agar got solidified at room temperature, the plate was withdrawn very carefully so as to create a cavity having plane surfaces within the agar. This cavity acts as the acoustic reflectorThe sample chamber along with sample, transceiver and thermocouples was then placed in a Peltier effect temperature cabinet driven by a microcomputer-based temperature controller (Pelt-4, Sable Systems International, Inc., Las Vegas, USA). The accuracy of the system was ±2 ^{o}C. The temperature of the cabinet was then set to a desired value and allowed the sample to reach a steady state.

The transceiver received multiple echoes from the interfaces, and was recorded by an oscilloscope (Tektronics TDS784 DPO) controlled through a computer program using Matlab 7.3.0. The record length and sample frequency were set to 50000 and 100 MHz respectively and the filter was set at 20 MHz during data acquisition. The data acquisition was done using Matlab by grabbing waveform from oscilloscope during acquisition in sample mode. The echo amplitude was taken for five times at a particular temperature. The ultrasound attenuation coefficient from the echo amplitudes and hence its mean value and standard deviation were estimated. The measurements were carried out at temperatures ranging from 283 K to 311 K. Other four transceivers of same type and dimensions of frequencies namely, 0.97, 2.25, 2.40, and 4.44 MHz were used to estimate attenuation at three different temperatures (308, 298 and 293 K) forming the cavity at suitable slots that corresponded to the focal zone of respective transceivers.

An independent investigation using Differential Scanning Calorimetry (DSC) (Netzsch, Germany, Model No 204 F1) was also employed to observe the phase transition of agarose hydrogel with temperature for explaining its anomalous ultrasound behavior. The sample was scanned from 282 to 330 K at different heating rates of 2, 5, 10 and 15 K min^{-1}. To investigate the loss of water content of agarose hydrogel, a thermo-gravimetry analysis (TGA) was carried out from 301 K to 318 K using

a thermo-gravimetric analyzer (Netzsch, Germany, model: STA 449C) at a heating rate of 10 K min^{-1}.

RESULTS AND DISCUSSION

The amplitude of an ultrasound signal propagating through a lossy medium such as agar follows an exponential decay when a transceiver is excited by a narrow excitation pulse width [12]. Accordingly, an equation for pressure amplitude undergoes attenuation while propagating through a distance d, is written as

$$p_e = p_o e^{-\alpha d} \quad (1)$$

where p_e is the attenuated pressure amplitude at d, p_o the incident pressure amplitude and α is the attenuation coefficient of medium. On simplification we may rewrite the above equation as:

$$ln\, p_e = ln\, p_0 - \alpha u t \quad (2)$$

where u is the speed of $ln\, p_e$ ultrasound and t is the time of flight.

A representative curve of vs. echo number was shown in Fig. 2. The good linear fit between lnpe and echo number verifies the plane wave approximation as enunciated in Eq. (1). The values of $\alpha[\frac{1}{2d} \times 8.6859 ln$ (ratio of two consecutive echoes)] in dB/m and u (= $2d/\Delta t$, Δt is the time interval between two consecutive echoes) in m/s were estimated at different temperatures at 3 wt-% agarose density and shown in Fig. 3 and Fig. 4 respectively. The experiment was repeated at 2 wt-% agarose density and a similar trend in

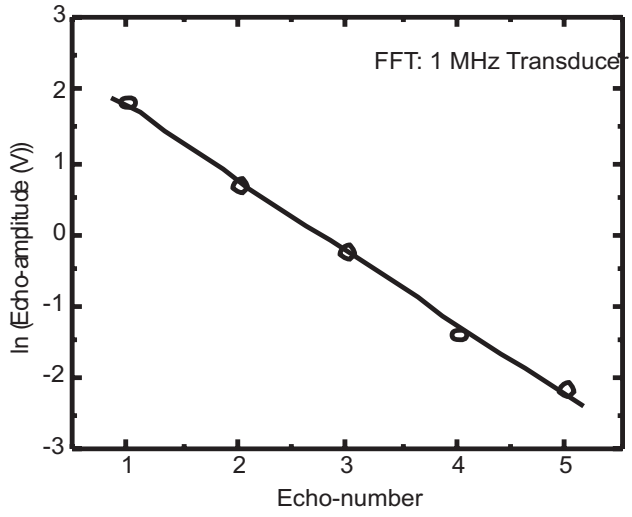

Fig. 2. Logarithmic variation of multiple echoes

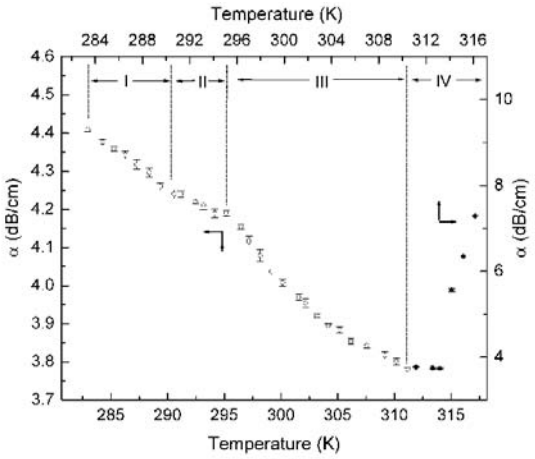

Fig. 3. Temperature dependent attenuation of agarose hydrogel

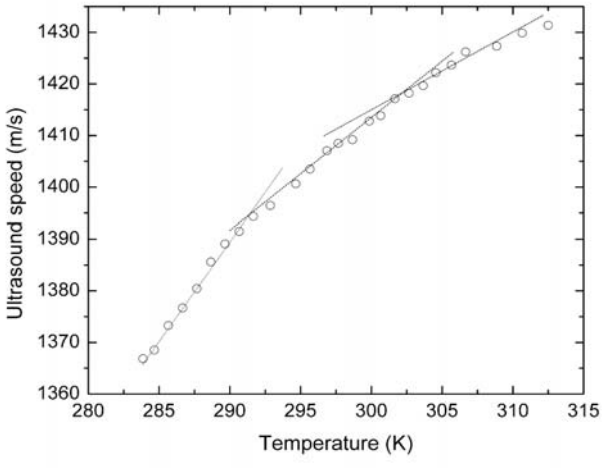

Fig. 4. Variation of speed of ultrasound with temperature in 3 wt-% agarose

variation of attenuation and velocity with temperature was observed. Since transmission of ultrasound through air is almost zero [13], the peak pressure amplitude is reflected from the agar/air interface without any transmission. Transmission of ultrasound through transceiver is also neglected, as it is negligibly small. Under this condition the pressure is construed to have suffered attenuation through propagation only. The transceiver received multiple reflected pressure amplitudes producing echo voltages from the interfaces.

Since agar is a bad conductor, energy loss by heat conduction due to ultrasound propagation is insignificant. Since there are evidences indicating the main contribution to attenuation is from absorption and not from scattering [14], the other sources of errors such as scattering are not considered. Moreover, at low frequencies, the wave parameter fluctuation is slow enough to

lead to additional absorption due to relaxation [15]. Therefore, the ultrasonic attenuation in agar phantom is primarily attributed to a combined effect of energy loss due to shear viscosity, α_{η_s} and bulk viscosity, α_{η_v}, where

$\alpha_{\eta_s} = (8/3)(\pi^2 f^2 / \rho_o u^3)\eta_s$ and

$\alpha_{\eta_v} = (2\pi^2 f^2 / \rho_o u^3)\eta_v$,

f denotes the sound frequency, η_s, the shear viscosity and η_v denotes the resistance of the sample to a pure expansion or compression [16]. Thus,

$$\alpha = \frac{2\pi^2 f^2}{\rho_o u^3}\left(\frac{4}{3}\eta_s + \eta_v\right) \quad (3)$$

with $\eta_s = (N_A h / \overline{V}) exp(\Delta\overline{G}_o^+ / RT)$ and

$\eta_v = (1/\psi)(N_A h / \overline{V}) exp(\Delta\overline{G}_o^+ / RT)$

where N_A is the Avogadro number, h, the Planck constant, $\overline{V}$, the molar volume of the liquid, $\psi (= n_h / N_A)$, the porosity (n_h, the number of 'holes'), R, the gas constant and $\Delta\overline{G}_o^+$ is the molar free standard energy of activation. To establish the validity of the proposed theoretical model, dependence of a with f^2 was studied using five transceivers. All the transceivers are of same diameter and narrow pulse width (in frequency domain). It is observed that the linear variation of a with f^2 at 300 K, shown in Fig. 5, proved experimentally the model based on classical absorption due to viscosity [see Eq. (3)]. At a given frequency, the expression of α may be written as

$$\alpha = K e^{\frac{\Delta\overline{G}_o^+}{RT}} \quad (4)$$

where $K = ((4/3)+(1/\psi))(2\pi^2 f^2 / \rho_o u^3)(N_A h / \overline{V})$.

Thus, Eq. (3) predicts that ultrasound attenuation decreases with the increase in temperature. It is observed in Fig. 3 that attenuation coefficient decreases over the temperature range; in regions I and III its variation with temperature follows the Eq. (3) having an inflexion in region II. The inflexion starts at ~ 290 K and continues up to ~ 296 K. Another sharp change in ultrasonic attenuation was observed at ~ 315 K as indicated in region IV. Like many other thermo-responsive polymer hydrogels, agarose has possibly the property of reversible volume change between shrinkage and expansion due to temperature and, in fact, the shrinkage in its volume under cooling has been noticed.

Eq. (4) may further be simplified under the approximation that the change in speed over the said temperature range is ~ 2% of its initial value and hence u is considered as a constant:

$$ln\,\alpha = \frac{\Delta\overline{G}_o^+}{RT} + ln\,K \quad (5)$$

The variation of with , shown in Fig. 6 is linear over regions I and III and hence, supports the theory based on energy loss by inner friction and energy loss due to inner changes.

Furthermore, a departure in speed as shown in Fig. 4 is observed at ~ 290 K and 301 K which is in accordance with the variation of ultrasound attenuation coefficient with temperature.

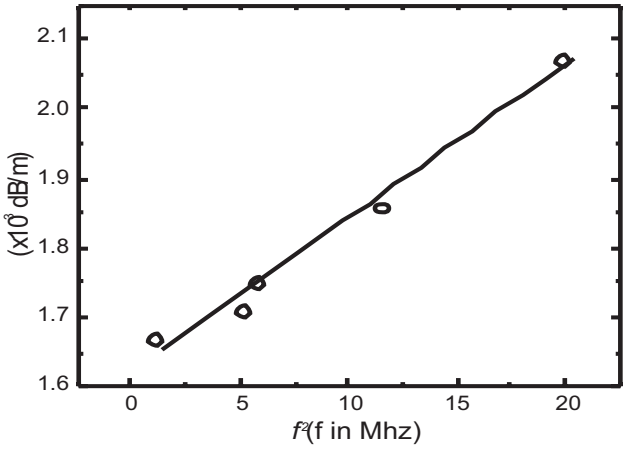

Fig. 5. Variation of with f^2

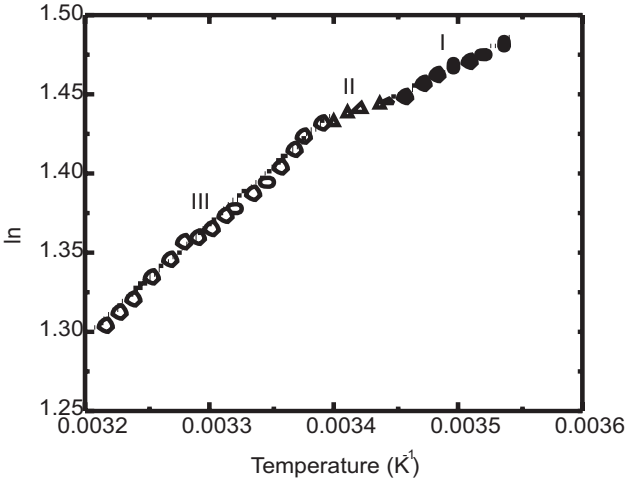

Fig. 6. Variation of with f^2

Independent experiments using differential scanning calorimetry and thermo-gravity analyzer were carried out to confirm the observations of anomalous ultrasound attenuation with temperature. The agarose sample was scanned over the temperature 282 to 330 K and endotherm peak was found at 289.89, 288.26, 289.76 and 290.56 K with heating rates 2, 5, 10 and 15 K/min respectively. Thus, the mean temperature corresponding to the endotherm peak is 289.6 K. Moreover, exotherm peaks are also observed at mean temperatures 295.6 and 315.5 K. A representative graph is shown in Fig. 7. The exotherm peaks showing transitions thus provided a concrete proof of the crystallites present in the gel [8]. Thermo-gravimetry analysis (TGA) was carried out at a heating rate of 10 oC min^{-1} and indicated in Fig. 8. A mass loss of ~ 2 % is observed due to release of water content from the agarose gel when the temperature changes from 301 K to 318 K. 2% mass loss in water content has been observed over the temperature ranges from 301 to 318 K. This change is negligibly small to affect the sample condition. Moreover, ultrasound attenuation in water is very small as compared to that of agarose. Thus the change in water content did not affect magnitude of attenuation coefficient of agarose hydrogel in this temperature range.

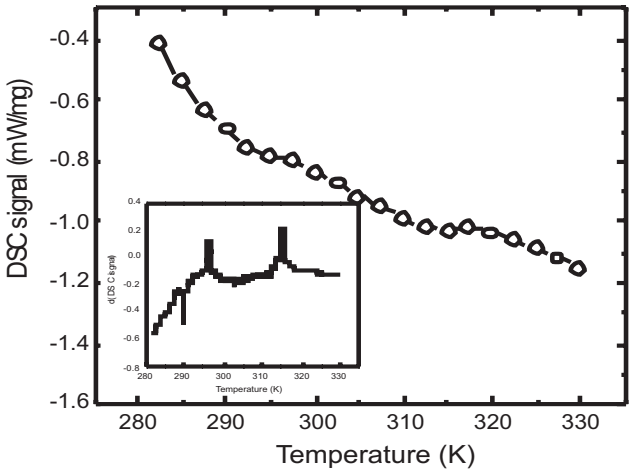

Fig. 7. DSC signal of agarose gel; inset shows first order derivative of the signal

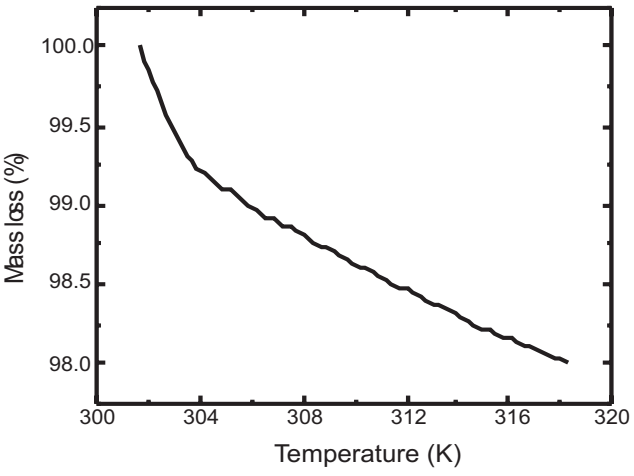

Fig. 8. Mass loss of the agarose gel with temperature

CONCLUSION

In conclusion, we propose a simulated experiment to investigate the anomalous attenuation of agar phantom with temperature. The anomaly has been explained using a classical absorption model on the basis of energy loss by inner friction and energy loss due to inner changes. The anomaly in ultrasound attenuation, is attributed to a phase transition in agarose used in designing phantom to mimick soft tissue acoustically, takes place at around 290 K. The DSC experiment shows endotherm peak at 289.6 K. The study has a profound importance that sheds light on the temperature limit of usages of agar as a phantom. This approach also finds its applicability in estimating a temperature profile in tissues non-invasively through attenuation.

Authors wish to thank all the members of Microelectronics Division, Saha Institute of Nuclear Physics for their encouragement.

REFERENCES

1. **Hill, C.R., Bamber, J.C.** and **Harr, G.R.,** Physical Principles of Medical Ultrasonics, *John Wiley & Sons, England,* (2004) 93.

2. **Bamber, J.C.** and **Hill, C.R.,** Ultrasonic attenuation and propagation speed in mammalian tissues as a function of temperature, *Ultrasound Med. & Biol.*, **5** (1979) 149-157.

3. **Gammell, P.M., Le Croissette D.H.** and **Heyser, R.C.**, Temperature and frequency dependence of ultrasonic attenuation in selected tissues, *Ultrasound Med. & Biol.* **5** (1979) 269-277.

4. **Burchard, W.** and **Ross-Murphy, S.B.,** Physical Networks, Elsevier, London, 1988.

5. **Clark, A.H.,** in Biopolymeric Mixtures, edited by S.E. Harding, S. Hills, J. R. Mitchell, Nottingham University Press, Nottingham, 1996.

6. **De Gennes, P.G.,** Scaling Concepts in Polymer Physics, Cornell University Press, Ithaca, 1979.

7. **Matsuo, M., Tanaka, T.** and **Ma, L.,** Gelation mechanism of agarose and κ-carrageenan solutions estimated in terms of concentration fluctuation, *Polymer,* **43** (2002) 5299-5309.

8. **Bulone, D., Giacomazza, D., Martorana, V., Newman, J.** and **San Biagio, P.L.,** Ordering of agarose near the macroscopic gelation point, *Phys. Rev.,* **E 69** (2004) 04101.

9. **Roy, M.** and **Chakraborty, S.,** Comment on 'gelation mechanism of agarose and κ-carrageenan solutions estimated in terms of concentration fluctuation' [Polym 2002;43:5299], *Polymer,* **46** (2005) 3535-3537.

10. **Matsuo, M.**, Reply to the paper 'Comment on Gelation mechanism of agarose and β-carrageenan solutions estimated in terms of concentration fluctuation' [Polym 2002;43:5299], *Polymer,* **46** (2005) 3538.

1.1 **Roy, M.** and **S. Chakraborty**, Note on the 'Reply to the paper "Comment on gelation mechanism of agarose and β-carrageenan solutions estimated in terms of concentration fluctuation" [*Polymer* **43** (2002) 5299]', *Polymer* **48** (2007) 5484-5485.

12. **Ophir, J., Shawker, T.H., Maklad, N.F., Miller, J.G., Flax, S.W., Narayana, P.A.,** and **Jones, J.P.,** Attenuation estimation in reflection: Progress and prospects, *Ultrasonic Imaging,* **6** (1984) 349-395.

13. **Skudrzyk, E.**, The foundations of Acoustics: Basic Mathematics and Basic Acoustics, Springer-Verlag, Wein, New York, 1971, p. 293.

14. **Pauly, H.** and **Schwan, H.P.,** Mechanism of Absorption of Ultrasound in Liver Tissue, *J. Acoust. Soc. Am.,* **50** (1971) 692- 699.

15. **Hill, C.R., Bamber, J.C.** and **Haar, G.R. ter.,** Physical Principles of Medical Ultrasonics, John Wiley & Sons, Ltd., West Sussex, England, 2004, p. 97.

16. **De Groot, S.R.** and **Mazur, P.,** Non-equilibrium Thermodynamics, North - Holland publishing company, Amsterdam, 1961, p. 331.

J. Pure Appl. Ultrason. 31 (2009) pp. 67-75

Effects of anisotropy on the longitudinal wave velocities in bone

MAMI MATSUKAWA
Laboratory of Ultrasonic Electronics, Doshisha University, 1-3 Tatara Miyakodani, Kyotanabe 610-0321, Kyoto, Japan
e-mail: mmatsuka@mail.doshisha.ac.jp

Ultrasonic wave properties of bone reflect elastic properties, which are closely-related to the bone strength. We have experimentally investigated the effects of anisotropic structure on the ultrasonic wave properties, focusing on the cancellous and cortical (compact) bovine bones. Both types of bone show interesting wave propagation phenomena. One is the two longitudinal waves – fast and slow waves – propagation in the cancellous bone. With the help of X-ray micro-computed tomography (CT), we have made clear the effects of anisotropic trabecular structure on the wave propagation. Wave properties of cortical bone also give us the clear information of elastic anisotropy. We can also find the nanoscopic effect of anisotropic orientation of polycrystalline Hydroxyapatite (HAp), on the longitudinal wave velocity in the cortical bone.

Key words : Longitudinal wave, anisotropy, cancellous bone, cortical bone

INTRODUCTION

In the area of bone studies, the gold standard for in vivo assessment of fracture risk has been bone mineral density (BMD) obtained by X-ray measurements[1]. BMD means the amount of mineral in bone. After the discussion at National Institute of Health (NIH) in 2000, however, the idea of "bone quality" has become widespread. Nowadays, the bone strength is considered to depend on both BMD and "bone quality". This idea of "bone quality" is still difficult to understand because it includes information of bone, e.g. microstructure,the existence of micro cracks, mineralization and bone metabolic turnover, which are difficult to evaluate from simple BMD values. In this point of view, quantitative ultrasound (QUS) has become an important technique to assess the status of bone[2-8]. QUS techniques are usually low cost, portable, and lack ionizing radiation, making it especially suitable for the assessment of children and pregnant women. QUS parameters, such as wave velocity (SOS), and broadband ultrasound attenuation (BUA) are closely related to the structural properties and elastic properties of bone, which can provide important information related to bone quality and bone strength[9-11]. This type of information cannot be obtained by X-ray measurements because X-ray techniques usually measure the amount of mineral[12].

Despite the aforementioned advantages and increasing use of the QUS technique, obtaining information about bones is still difficult. For characterization of bones to evaluate the status of osteoporosis, QUS clinical studies have focused mainly on SOS and BUA measurements. However, most current clinical QUS techniques still treat the bone as a homogeneous medium and provide averaged SOS and BUA values, even though the actual bone is inhomogeneous and anisotropic. Actually, bone exhibits complicated structure from microscopic to macroscopic levels [13-14]. For Example, the cancellous bone inside the epiphysis is composed of a complicated solid network structure called trabeculae in the bone marrow, showing strongly anisotropic and heterogeneous structure in the submilimeter range. It is greatly affected by bone metabolism, being highly active in remodeling, and is a good indicator of bone evaluation in osteoporosis[1-4]. From the mechanical point of view, the outside cortical (compact) bone mainly supports the body and has greater strength than the cancellous bone. The cortical bone also shows complicated

structure. For example, bovine cortical bone can be classified into two main microstructures in the submilimeter range, plexiform and Haversian. In addition, the elastic properties of cortical bone also depend on the structure in the smaller level, e.g. cell and bone matrix. Bone matrix is composed of organic components, which contain type I collagen, polysaccharide and mineral components, like calcium phosphate. The calcium phosphate constitutes 70% of total bone matrix mass, almost entirely in the form of (HAp) crystals, $Ca_{10}(PO_4)_6(OH)_2$.

In this point of view, I would like to introduce our recent experimental studies on the longitudinal wave propagation in bone, paying special attention to the anisotropy. First, two wave phenomenon in the cancellous bone is reported. Considering rather macroscopic structures of cancellous bone with the help of X-ray micro-computed tomography (CT), the interesting mechanism of two longitudinal wave propagation is discussed. The anisotropy in wave velocity is then investigated with structural parameters, such as the mean intercept length (MIL)[15-18], estimated from CT images.

In addition to the structural effect in the submillimeter range, cortical bone shows the strong effects of anisotropy of bone matrix, on the longitudinal wave velocities. One is the effects of HAp crystallites. The HAp crystal has a hexagonal system with uniaxial anisotropy, whose elasticity is the greatest in the c-axis direction[19-20]. With the help of X-ray diffractometry (XRD) to investigate the orientation of HAp crystallites, we have investigated the effects of preferred orientation of HAp on the longitudinal wave velocity.

ULTRASONIC WAVE PROPAGATION IN CANCELLOUS BONE

Materials and methods

Sample preparation

Cancellous bone specimens were obtained from a 30-month-old bovine left femur. At first, the cancellous bone in the distal part was removed and made into rectangular specimens. Most *in vivo* clinical techniques measure propagation of the ultrasonic waves perpendicular to the long axis. Therefore, we took rectangular samples the long axes of which were parallel to the bone axis (Fig. 1). The cylindrical specimens, which were about 40.70 mm in length and 11 ± 0.05 mm in diameter, were formed from these rectangular samples. The initial positions of the cylindrical specimens in the head of the femur are shown in the cross-section view in Fig. 1(c). The trabeculae were well aligned and often showed plate-like structures in the specimens. The diameter of each specimen was measured precisely using calipers (precision: 0.01mm), and the specimens were defatted carefully. To remove air bubbles trapped in the cancellous bone, the specimens were degassed in water for 60 minutes before ultrasonic measurements.

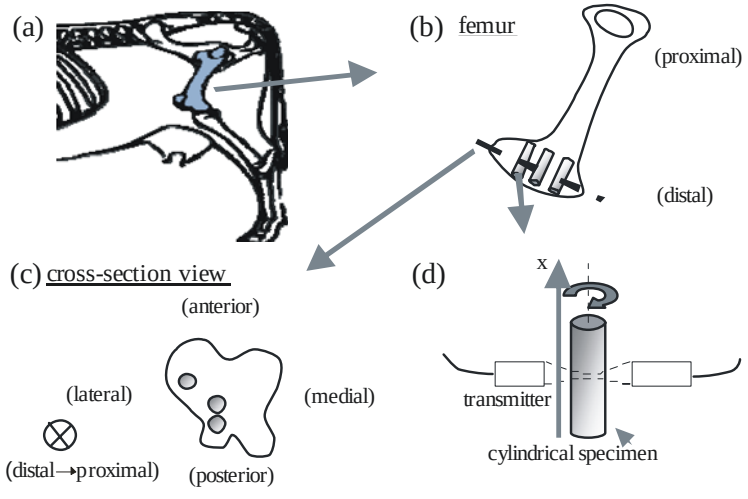

Fig. 1. Sample preparation and measurement direction of bovine cancellous bone

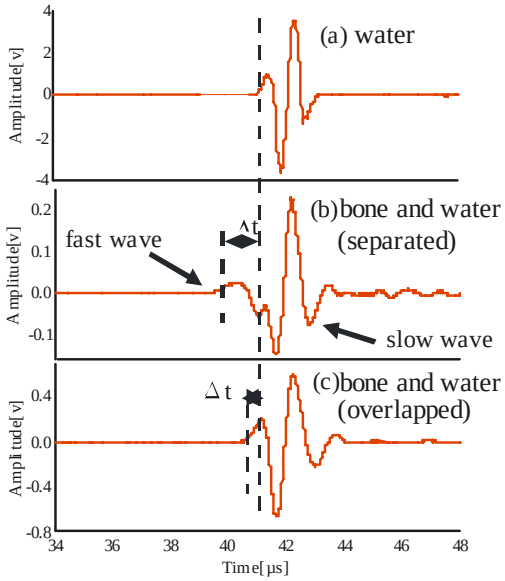

Fig. 2. Typical observed waveforms

Ultrasonic measurements

Measurements of longitudinal wave velocities were performed using a conventional ultrasonic pulse technique. A PVDF focus transmitter and a home-made PVDF receiver were used in this experiment. In water, the beam width at half maximum value of the wave amplitude was approximately 1.5 mm at the focal point[21]. Both PVDF transducers were mounted coaxially in degassed water at 22.0 ± 1.0 °C. A single sinusoidal signal with a center frequency of 1 MHz was applied to the transmitter. The longitudinal wave propagated through water, sample, and water. The other transducer received the wave and converted it into an electrical signal. The signal was amplified and visualized with an oscilloscope. We placed the focal point of sound on the central axis of the cylindrical specimen. The direction of the ultrasound incident wave was always perpendicular to the side surface of the cylindrical specimen. The measurements were performed by changing the measurement position along the cylindrical axis and the incident angle.

In these measurements, we found the separation of fast and slow waves in some parts of the specimens (Fig. 2). The fast waves were mostly related to propagation mode involving mainly the solid phase and reflected the characteristics of the trabeculae whereas the slow waves were related to the propagation mode in the liquid (bone marrow) phase[22-24]. In all observations, the wavefronts arrived faster than the waves passed through water shown in Fig. 2(a), indicating the existence of fast waves. Therefore, we focused on the arrivals of these fast waves in the cancellous bone. The fast wave velocity was calculated from the differences in the arrival time of longitudinal wavefronts that passed through the water and the water and specimen. The wave velocity in water was established based on the previous report by Greenspan and Tschiegg[25].

X-ray micro-CT measurements

The trabecular structure images of the specimens were obtained using X-ray micro-CT. The CT images were analyzed using TRI/3D-Bon software. In these specimens, ultrasonic waves propagate parallel to the circular cross-section. The structural anisotropy of cancellous bone can be expressed by mean intercept length (MIL) parameters[15-18]. We calculated both the main trabecular length, t_{lm}, and trabecular length orthogonal to the main trabecular orientation t_{l0}. We also defined the angle, θ, which was the angle of insonification relative to the trabecular orientation. A value of θ=0 indicates wave propagation parallel to the predominant trabecular orientation. The total bone volume (BV) normalized by the total specimen volume (TV), BV/TV, was also defined from the CT images at each region.

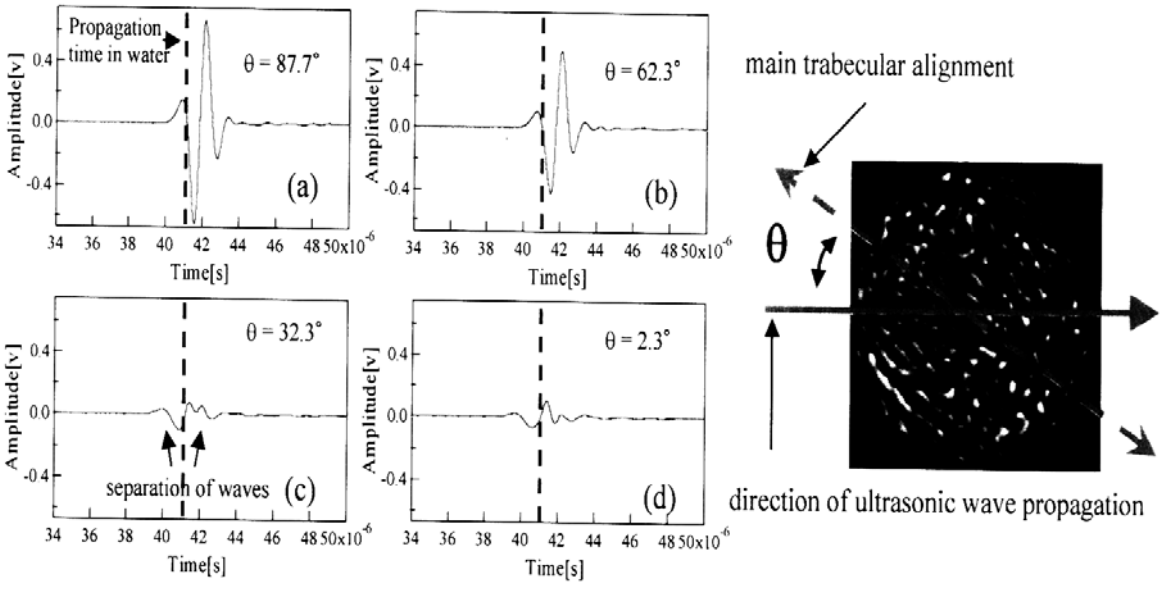

Fig. 3. Typical waveforms with different incident angle θ (BV/TV=0.33)

RESULTS AND DISCUSSIONS

Fig. 3 illustrates the data from regions with comparatively low BV/TV values, showing wave separation and clear effects of θ. In regions with low BV/TV, the fast and slow longitudinal waves were sometimes observed separately, which is the two-wave phenomenon. In any cases, the wavefronts were always faster than the propagation time in water. Fig. 4 shows examples of the periodic changes in the fast wave velocity as a function of θ. In this specimen, the fast wave velocities showed a maximum value when the ultrasonic waves propagated from the anterior medial part to the posterior lateral part or *vice versa*, corresponding to the predominant orientation of the trabeculae. These observations indicate that wave propagation is dominated by BV/TV and the angle between trabecular orientation and wave propagation direction.

The relationship between the velocity and trabecular length, t_{lm} and t_{l0} is shown in Fig. 5. Simple regression analysis revealed significant correlations between the maximum and minimum velocities of fast waves and averaged trabecular lengths, t_{lm} and t_{l0} (R^2 = 0.82, P<0.0001). These results demonstrate the quantitative effects of trabecular length on fast wave velocity.

Our data show that both the structural anisotropy and BV/TV have effects on the anisotropy of fast wave velocities. In addition, the dependence of wave velocity on the angle θ indicates that there is a considerable change of wave velocity due to small fluctuations in the incident angle and changes in the sensor position during measurements. For this purpose, however, it will be necessary to also investigate the characteristic structure of trabeculae in various parts, taking into account interindividual differences.

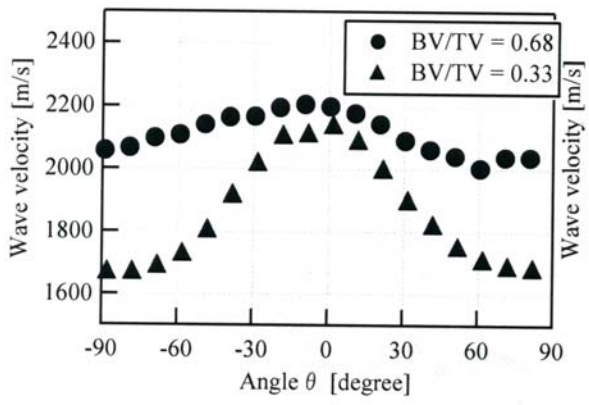

Fig. 4. Fast wave velocity as a function of θ

ULTRASONIC WAVE PROPAGATION IN CORTICAL BONE

Materials and methods

Sample preparation[26,27]

Left femora were obtained from two 36-month-old bovines. The femora were sectioned into five ring-shaped cortical bones, mid-diaphysis, 30 and 50 mm proximal and distal parts from the mid-diaphysis. Eight rectangular solids (anterior (A), posterior (P), medial (M), lateral (L) and four oblique parts) whose sides were perpendicular to the three orthogonal axes of the femur (axial, radial and tangential axes) were cut from the ring-shaped bones as shown in Fig.6 The final form of the samples was a rectangular cube with sides of 4~11 mm. We defined the surfaces perpendicular to the axial, radial and tangential directions as AD, RD and TD surfaces respectively. 40 specimens were made from each femur. The undecalcified thin bone sections were made to determine the microscopic structure of the samples. Bone sections were ground to 60μm thickness and were photographed under microscope (Olympus, BH-2). The area and length of the microstructure were measured using Image J software (NIH). The bone samples were usually stored in a deep freezer at -20°C. Fig. 7 shows two typical microstructures of the samples, plexiform and Haversian.

Plexiform structure is found in large animals, but rarely found in humans. This structure arises from brick like bone lamellae. Haversian structure is also found in human cortical bone. This structure is a uniaxial alignment of circular cylinders called osteon, which contains a blood vessel at the center of the bone lamellae[28]. We classified samples with more

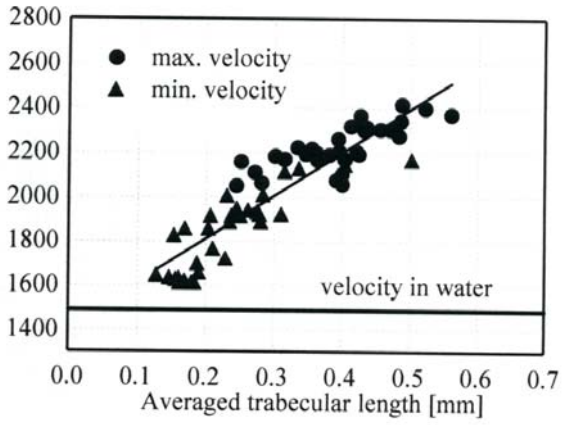

Fig. 5. Fast wave velocity and averaged trabecular length

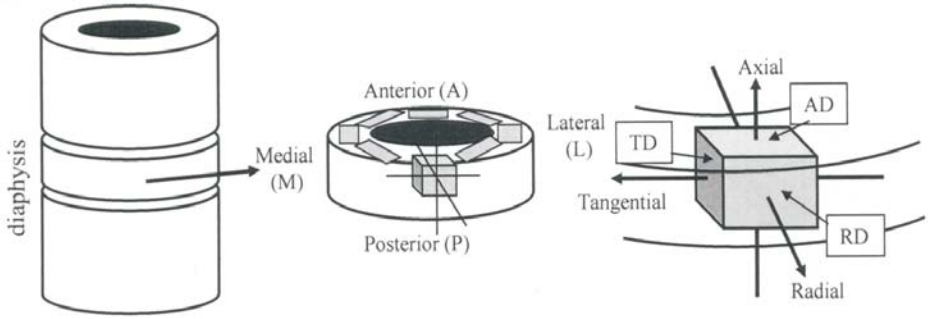

Fig. 6. Sample preparation from the diaphysis of bovine femur

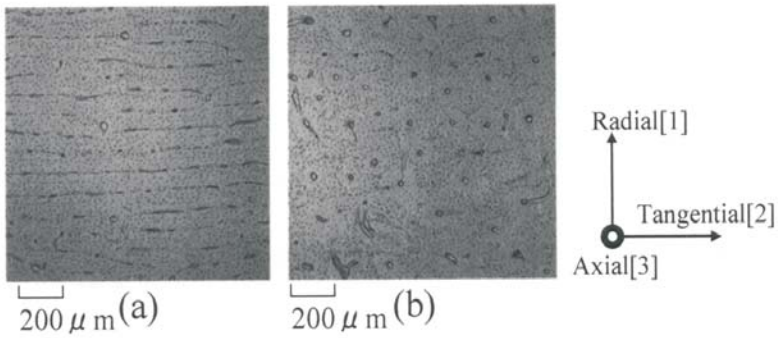

Fig. 7. Typical optical microscopic views of bovine cortical bone in cross section

than 80% area of plexiform structure as a plexiform sample, and with more than 70% area of Haversian structure as a Haversian sample. The number of plexiform samples was 44 whereas Haversian samples were 13.

Density and bone mineral density (BMD) measurements

The density of samples was determined by Archimedes principle, using an accurate balance. BMD measurements were performed using a bone densitometer. The data obtained were normalized as the value per unit volume, considering the thickness of each sample.

Ultrasonic measurement technique

Measurements of longitudinal wave velocity were performed using the same pulse system. A couple of PVDF flat transducers were used in this experiment. The transducers were placed on the opposite sides in a measurement cell, which was filled with normal saline solution (NSS) kept at temperature of 25.0 ± 0.1 ^{o}C. With a single period of sinusoidal wave with a center frequency of 10 MHz was applied to the transducer. The longitudinal wave propagated through the sample and NSS. The other transducer received the wave, which was converted into the electrical signal. The output signal was amplified and visualized in the oscilloscope. The arrival of the wave was determined from the position of wave front. The wave velocity was calculated by the difference of the arrival time of longitudinal waves between passing through the sample and NSS, or only NSS. Before measurements, first, the samples were defrosted for 60 minutes. Second, to exclude air effects on ultrasound transmission, the samples and NSS were degassed under vacuum for 60 minutes. The samples were then immersed in NSS at 25 ^{o}C for 60-120 minutes.

Measurement of X-ray diffraction (XRD)

Crystallographic properties of the cortical bone samples in AD, RD and TD surfaces were characterized using an X-ray diffractometer. This X-ray diffractometer was based on point focus Cu-Kα radiation X-ray source operated at 45 kV and 40 mA. An X-ray beam was irradiated to the sample surface through parallel beam optics with a 3mm x 3mm slit. 2θ–ω axis was scanned with a step size of 0.05^{o}, and time count per step of 0.4 second.

RESULTS AND DISCUSSIONS

As shown in Table 1, the distribution pattern of density and BMD were similar. Fig. 8 represents velocities in three orthogonal

directions of the plexiform and Haversian samples. The longitudinal velocity in the axial direction is always the highest of those in three orthogonal directions, which are consistent with some previous reports[28,29].

Typical XRD patterns from the AD, RD and TD surfaces of a plexiform sample are shown in Fig. 9. The peak patterns were in good agreement with the artificial HAp powder XRD pattern. For the AD surface, a more intensive {0002} peak was observed than any other peaks, showing that HAp crystallites c-axis preferentially oriented parallel to the bone axis. This result is also consistent with previous studies about HAp crystallites orientation in bone tissue[19,20,28,29]. Fig. 10 represents the intensity ratio of the (0002) peak in three orthogonal directions of the plexiform and Haversian samples. Here, the integrated intensity ratio of the (0002) peak, which was normalized with a (31-40) peak. Statistical analysis revealed the significant effect of the microstructure on the intensity ratio of (0002) peak.

To exclude the effect of structure types, each of the plexiform and Haversian samples were considered . Simple regression analysis revealed significant linear correlations between the velocity in the axial direction and the intensity ratio on the AD surface in both plexiform (R2 = 0.49, P < 0.001) and Haversian samples (R2 = 0.56, P < 0.001)(Fig.11). In the tangential direction, significant correlation between the velocity and intensity ratio was observed only in the plexiform samples (R2=0.54, P<0.001). No significant relationship is observed between the velocity and intensity ratio in the radial direction.

Significant correlation (P < 0.01) between velocity in the three orthogonal directions and BMD values are observed (axial: R=0.588, radial: R=0.422, tangential: R=0.656). BMD values clearly depend on their types of structures, for example, the plexiform samples have denser mineral properties than the Haversian samples.

However, if we focus on the plexiform samples, the correlation between velocity and BMD disappears in all directions.

These data tell us that, in cortical bones, differences in microstructure type have an impact on density and BMD, which clearly affects the velocity. In addition, at the nanoscopic level,

Table 1. Velocity, density and BMD in the different types of microstructure

	n	Density [g/cm³]	BMD [g/cm³]
plexiform	43	2.093 ± 0.012	1.471 ± 0.036
Haversian	13	2.022 ± 0.026	1.391 ± 0.050
others	24	2.034 ± 0.063	1.393 ± 0.102

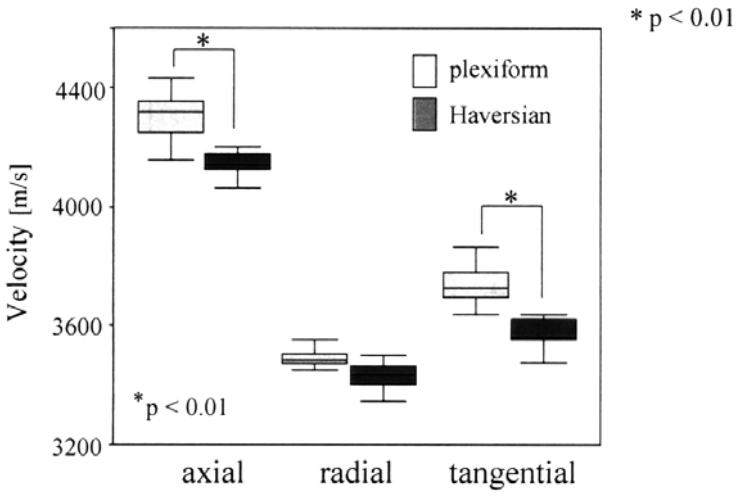

Fig. 8. Range of longitudinal wave velocities of plexiform and haversian samples

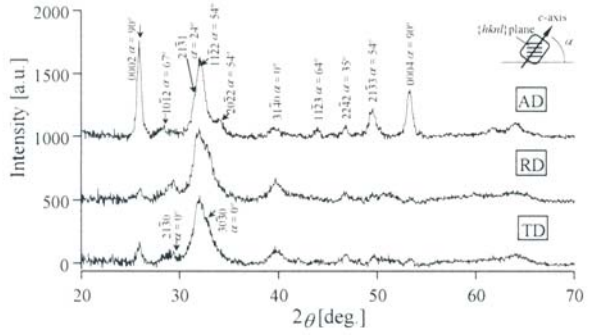

Fig. 9. Typical XRD patterns of a bovine cortical sample

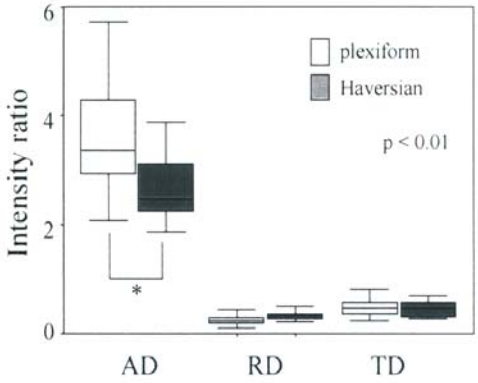

Fig. 10. Intensity ratio of the (0002) peak.

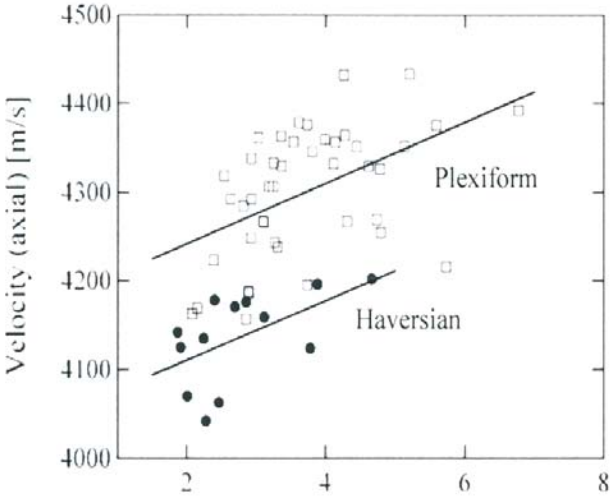

Fig. 11. Relationship between velocity and intencity ratio of the (0002) peak

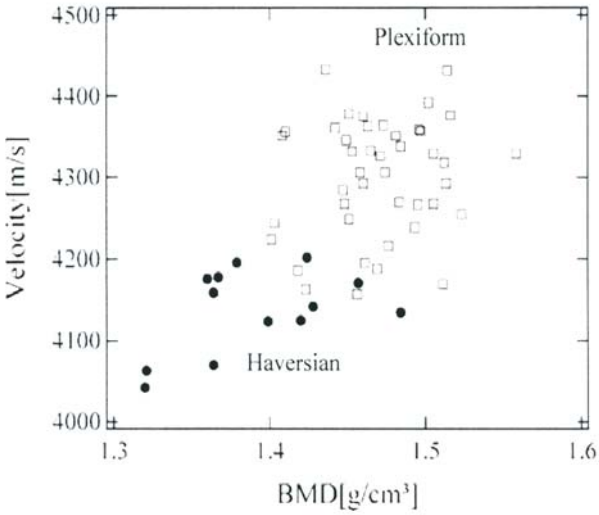

Fig. 12. Relationship between velocity in the axial direction and BMD

HAp crystallites that align in the axial direction also affect the velocity and anisotropy. This results in the velocity differences among samples with similar microstructures.

CONCLUSIONS

Focusing on the cancellous and cortical bovine bones, we have investigated the longitudinal wave velocities. In the cancellous bone, we could find clear wave separation into fast and slow waves, due to the large scale structural anisotropy. The trabecular structure strongly affected the fast wave propagation in the cancellous bone. Here, BV/TV and θ (the angle between trabecular orientation and wave propagation direction) were the main parameters for the two wave phenomena. These observations suggest that both trabecular orientation and length are strongly related to the propagation phenomena of waves in cancellous bone, especially with those of fast waves.

In cortical bones, the anisotropy of bone also affects the longitudinal wave velocities. The wave velocities showed strong dependence on the microstructure in the submilimeter range and the direction of wave propagation. If we focus on the much smaller level, the anisotropy of bone matrix was observed as the velocity changes. This anisotropy seems to come from the HAp crystallites alignment.

Ultrasonic velocities reflect the structure and elastic properties from macroscopic to nanoscopic level. We should then be very careful to understand the effects of each level. However, these results tell us the strong possibility of ultrasonic technique as a strong tool to evaluate the "bone quality", which cannot be obtained from simple BMD of X ray measurements.

REFERENCES

1. **Njeh, C., F., Hans, D., Fuerst, T., Gluer, C.-C.** and **Genant, H.K.,** Basic sciences. in

Quantitative Ultrasound: Assessment of Osteoporosis and Bone Status (Martin Dunitz Ltd., London), (1999) 101.

2. Ultrasonic bone assessment: The time has come, Bone, (editorial) **40**, (2007) 5-8.

3. **Njeh, C.F.,** Quantitative ultrasound: assessment of osteoporosis and bone status, 1st edition. (Taylor & Francis) 1999.

4. **Langton, C.M., Palmer, S.B.** and **Porter S.W.,** The measurement of broadband ultrasonic attenuation in cancellous bone. *Engineering in Medicine,* **13** (1984) 89-91.

5. **Laugier, P., Giat** and **P., Berger, G.,** Broadband ultrasonic attenuation imaging: A new imaging technique of the os calcis. *Calcified Tissue Int.,* **54** (1994) 83-86.

6. **Barkmann, R., Kantorovich, E., Singal, C., Hans, C., Genant, H., Heller, M.** and **Gluer, C.-C.,** A new method for quantitative ultrasound measurements at multiple skeletal sites. *J Clin Densitometry,* **3** (2000) 1-7.

7. **Barkmann, R., Lusse, S., Stampa, B., Sakata, S., Heller, M.** and **Gluer C.C.,** Assessment of the geometry of human finger phalanges using quantitative ultrasound in vivo. *Osteoporos Int.,* **11** (2000) 745-755.

8. **Bossy, E.,Talmant, M.** and **Laugier, P.,** Bi-directional axial transmission can improve accuracy and precision of ultrasonic speed measurement in cortical bone: a validation on test material. IEEE Transactions on Ultrasonics, *Ferroelectrics and Frequency Control,* **51** (2003) 71-79.

9. **Ashman, R.B.** and **Ryo, J.Y.,** Elastic modulus of trabecular bone material. *L. Biomech.,* **21** (1988) 177-181.

10. **Bouxsein, M.L.** and **Radloff, S.E.**, Quantitative ultrasound of the calcaneus reflects the mechanical Plexiform Haversian properties of calcaneal trabecular bone. *J B one Miner. Res.,* **12**, (1997)839-846.

11. **Njeh, C.F., Kuo, C.W., Langton, C.M., Atrah, H.I.** and **Boivin, C.M.**, Prediction of human femoral bone strength using ultrasound speed and BMD: an in vitro study. *Osteoporosis Int.,* **7** (1997) 471-477.

12. **Gluer, C.-C., Blake, G., Lu, Y., Blunt A. B., Jergas, H.** and **Genant, H.,** Accurate assessment of precision errors: how to measure the reproducibility of bone densitometry techniques. *Osteoporosis Int.,* **5** (1995) 262-270.

13. **Susan, F.L.** and **Katz, J.L.**, The relationship between elastic properties and microstructure of bovine cortical bone. *J Biomech* **17**(1984) 241-249.

14. **Martin, R.B.** and **Burr, D.B.,** Skeletal tissue mechanics. Springler-Verlag, New York (1980).

15. **Whitehouse, W.J.**, The quantitative morphology of anisotropic trabecular bone. *J. Microscopy,* **101** (1974)153-168.

16. **Whitehouse, W.J., Dyson, E.D.,** Scanning electron microscope studies of trabecular bone in the proximal end of the human femur. *Journal of Anatomy,* **118** (1974) 417-444.

17. **Harrigan, T.** and **Mann, R.W.**, Characterization of microstructural anisotropy in orthotropic materials using a second rank tensor. *J. Mat. Sci.,* **19** (1984) 761.767.

18. **Goldstein, S.A., Goulet, R.** and **McCubbrey, D.**, Measurement and significance of three-dimensional architecture to the mechanical integrity of trabecular bone. *Calcified Tissue Int.,* **53** (1993) 127-133.

19. **Nightingale, J.P.** and **Lewis, D.,** Pole figures of the orientation of apatites in bones. *Nature* **232** (1971) 334-335.

20. **Chen, H.L.** and **Gundjian, A.A.,** Determination of the bone-crystallites distribution function by X ray diffraction. *Med Biol Eng* **14** (1971) 531-536.

21. **Otani, T.**, Quantitative estimation of bone density and bone quality using acoustic parameters of cancellous bone for fast and slow waves, *Jpn. J. Appl.Phys.*, **44** (2005) 4578-4582.

22. **Hosokawa, A.** and **Otani, T.,** Ultrasonic wave propagation in bovine cancellous bone. *J. Acous. Soc. Am.,* **101**, (1997) 558-562.

23. **Hosokawa, A.** and **Otani, T.,** Acoustic anisotropy in bovine cancellous bone. *J. Acous. Soc. Am.,* **103** (1998) 2718-2722.

24. **Cardoso, L., Teboul, F., Sedel, L., Oddou, C.** and **Meunier, A.,** In vitro acoustic waves propagation in human and bovine cancellous bone. *J. Bone. Min. Res.,* **18** (2003) 1803-1812.

25. **Greenspan, M.** and **Tschiegg, C.E.,** Tables of the speed of sound in water. *J. Acous. Soc. Am.,* **31** (1959) 75.

26. **Yamato, Y., Kataoka, H., Matsukawa, M., Yamazaki, K., Otani, T.** and **Nagano, A**., Distribution of longitudinal wave velocities in bovine cortical bone *in vitro*. *Jpn J Appl Phys.,* **44** (2005) 4622-4624.

27. **Yamato, Y., Matsukawa, M., Otani, T., Yamazaki, K.** and **Nagano, A.,** Distribution of longitudinal wave properties in bovine cortical bone *in vitro*. *Ultrasonics,* **44** (2006) 233-237.

28. **Sasaki, N.** and **Sudoh, Y.,** X-ray pole figure analysis of apatite crystals and collagen molecules in bone. *Calcif Tissue Int.* **60** (1997) 361-367.

29. **Nakano, T., Kaibara, K., Tabata, Y., Nagata, N., Enomoto, S., Marukawa** and **E., Umakoshi, Y.,** Unique alignment and texture of biological apatite crystallites in typical calcified tissues analyzed by microbeam x-ray diffractiometer system. *Bone* **31** (2002) 479-487.

J. Pure Appl. Ultrason. 31 (2009) pp. 76-80

Ultrasonic and FTIR investigations of PbO-Bi_2O_3-SiO_2 glass system

RAJINDER SINGH KAUNDAL, SANDEEP KAUR, NARVEER SINGH and KANWAR JIT SINGH*
Department of Applied Physics, Guru Nanak Dev University, Amritsar-143005
*Email: kanwarjitsingh@yahoo.com

Recently, it has been found by the authors that heavy metal oxide based glasses are the potential candidates as substitute for conventional concretes as gamma-ray shielding materials[1,2]. Glasses have the advantage as compared to concrete due to (1) their transparency to visible light (2) they can be prepared in wide range of compositions thus enhancing the possibility of choosing the elements and their mole fraction as per choice. During the investigations, it has been found that there should be improvement in brittleness and elastic properties of the glasses. Aim of present study is to get the information regarding the acoustical behavior and structure properties of one of the heavy metal oxide glasses. Glass samples of the $xPbO(0.60\text{-}x)Bi_2O_3$ $0.40SiO_2$ system (x =0.10 to 0.50) were prepared by melt quenching technique and characterized by X-ray diffraction, ultrasonic velocity and FTIR measurements. Mole fraction percentage of PbO has been varied from 10 to 50%. The longitudinal velocities of ultrasonic waves were measured in these glass samples at 5 MHz using pulse echo technique. FTIR spectrum has been recorded in the wave number range of 400 to 2000 cm^{-1}. Their data for density, molar volume, infrared spectra and ultrasonic properties were analyzed in order to study their structure systematically. It is estimated that the data may provide the clues which may improve the mechanical properties of the glass samples.

Key words : Glass structure, ultrasonic velocity, acoustic properties, infrared spectroscopy

INTRODUCTION

Glasses containing Bi_2O_3 and PbO have many advantages due to their high density and high refractive index properties. These oxide glasses containing heavy metal cations like Pb^{2+} *and* Bi^{3+} have low melting points and find their applications in the field of solder and sealing materials. Lead oxide is an interesting component of silicate glasses because of its dual role[3] i.e. it can act as modifier and former in the glass structural lattice. The Pb^{2+} ions in lead borate and lead silicate glasses with the low content of PbO act as a modifier in the form of $[PbO_6]$ groups. At higher concentrations, its effect as a glass forming agent is manifested in the form of tetrahedral $[PbO_4]$ groups.

Heavy metal oxide glasses are one of the possible candidates as alternatives of concretes for gamma-ray shielding applications. Their commercial utilization is possible if they have better gamma-ray shielding and elastic properties. Keeping this objective in mind, authors have measured several parameters of PbO-Bi_2O_3-SiO_2 glass system. Measurement of ultrasonic velocity is directly related to the elastic properties of glasses. The calculation of elastic properties such as longitudinal modulus (L), packing density, Poisson's ratio and oxygen molar volume of glassy materials provide the information about the structure of the network units of the glasses and hence, elasticity of the glass system. FTIR spectra of the glass system can be used as complimentary technique to confirm the conclusions arrived at regarding the structure information of the glass system. Structural and elastic properties are related to each other.

In the present paper, structure of PbO-Bi_2O_3-SiO_2 glasses is discussed with the help of ultrasonic velocity measurements and infrared spectroscopy. Interest in the present system is

*Life Member, Ultrasonics Society of India

due to wide range applications of the *Pb* and *Bi* containing glasses[4-5] and their possible utility as commercial gamma-ray shielding materials

EXPERIMENTAL PROCEDURE

Glass samples of the system $xPbO(0.60-x)Bi_2O_3$ $0.40SiO_2$ system (x =0.10 to 0.50) were prepared by using melt and quenching technique. Appropriate amounts of *PbO*, Bi_2O_3 and SiO_2 (AR grade) were mixed thoroughly. Melting was performed in porcelain crucibles placed in an electric furnace for about 1h in the temperature region of 1000-1200°C. Dry oxygen was bubbled through melts using quartz tube to ensure homogeneity. The homogenized molten glass was cast in preheated copper mould at around 275°C and slowly cooled to room temperature. The compositions of the samples are given in Table 1. The density of the samples was measured using Archimede's principle with benzene as the immersion liquid. X-ray diffraction studies were carried out in order to study the amorphous structure of the samples. Absence of any sharp peak in XRD data shows that prepared samples are amorphous. FTIR spectra of the glasses were recorded at room temperature using KBr disc technique. In a wave number range between 400 to 2000 cm^{-1} with the resolution of $2cm^{-1}$. Ultrasonic measurements were carried out using Matec equipment. The samples taken for ultrasonic measurements were cylindrical in shape. The ultrasonic velocity measurements were carried out at 5MHz using ultrasonic jelly as the contact between sample and the transducer. Time of flight was measured between two successive echoes.

RESULTS AND DISCUSSION

The molar volume of the glass was calculated using the relation

$$V_m = M/\rho, \quad (1)$$

Where ρ is the density of the glass and M is the molar mass given by

$$M = x_1M_1 + x_2M_2 + (1-x_1-x_2)\ M_3, \quad (2)$$

Here, M_1, M_2 and M_3 are the molar masses of PbO, Bi_2O_3 and SiO_2 respectively and x_1 and x_2 are the mole fractions of *PbO* and Bi_2O_3. Fig. 1 provides the trends of density and molar volume. The densities increase steeply from 6.17 to 6.48 g cm^{-3} as mole fraction of *PbO* is increased from x= 0.10 to 0.30 and then decreases from 6.48 to 5.86 as mole fraction of *PbO* is further increased from x= 0.30 to 0.50 It is seen that molar volume decreases from 45.26 to 31.09 cm^3mol^{-1} with increase in mole fraction of *PbO* for x= 0.10 to 0.50 indicating that structure becomes compact with increase in mole fraction of *PbO* at the expense of Bi_2O_3. Values of longitudinal ultrasonic velocities increase with the replacement of bismuth by lead ions. The ultrasonic velocities increases from 3100 to 3422 ms^{-1} for x= 0.10 to 0.30 and then decreases from 3422 to 3260 ms^{-1} with further addition of *PbO* (Fig. 2). These trends may be due to fact that lead ions play the dual role of network modifier as well as network former. At higher mole fraction of PbO, their role in the glass network is of network former. This causes the formation of non bridging oxygens and results in the weakness of the network structure. This structural change is manifested by the decrease in the ultrasonic velocities at higher mole fraction of *PbO*.

The packing density of the glass system is calculated by the following relation[6,7];

$$V_T = (1/V_m)\Sigma V_i x_i \quad (3)$$

Where V_m is the molar volume and V_i is the packing factor of the component oxide i, which is obtained from an equation given for the oxide AnOm as

Table 1. Sample number (No.), the chemical composition (in mol. %), Packing density (V_T), oxygen molar volume (V_o), and Poisson's Ratio (s)

No	Chemical Composition			V_T	V_o (cm^3mol^{-1})	σ
	PbO	Bi_2O_3	SiO_2			
1	10	50	40	0.4430	18.8616	0.1865
2	20	40	40	0.4558	18.5478	0.1953
3	30	30	40	0.4814	17.8058	0.2115
4	40	20	40	0.4726	18.4434	0.2061
5	50	10	40	0.4577	19.4350	0.1966

$V_i = (4\pi/3)N_A\,[nR_a^3 + mR_o^3]$ (4)

Here, N_A is Avogadro's number, R_a and R_o are the respective Pauling's ionic radii of metal and oxygen. The calculated values of packing density (V_T), oxygen molar volume (V_o) and Poisson's ratio (s) are given in Table 1. The values of packing density increases from 0.4430 to 0.4814 for x= 0.10 to x = 0.30 and then decreases from 0.4814 to 0.4577 for x = 0.30 to x = 0.50. The values of Poisson's ratio (s) also show the similar trends i.e. they increase from 0.1865 to 0.2115 for x = 0.10 to 0.30 and then decreases from 0.2115 to 0.1966 with further addition of PbO from x=0.30 to 0.50. Poisson's ratio is the measure of the cross-link density of the structure. Trends of packing density and Poisson's ratio can be explained as follows. Cross linking density of glass samples increases from x = 0.10 to x = 0.30 resulting in higher value of elastic modulus of glass samples. Above x=0.30, it is speculated that cross link density decreases due to formation of non bridging oxygens which results in the weak structure causing the ultrasonic velocity to decrease.The longitudinal modulus of glass samples is calculated by the following relation,

$L = V_l^2.\rho$ (5)

Trends of longitudinal modulus are similar to longitudinal ultrasonic velocity, packing density and Poisson's ratio indicating the close relation between the structural information

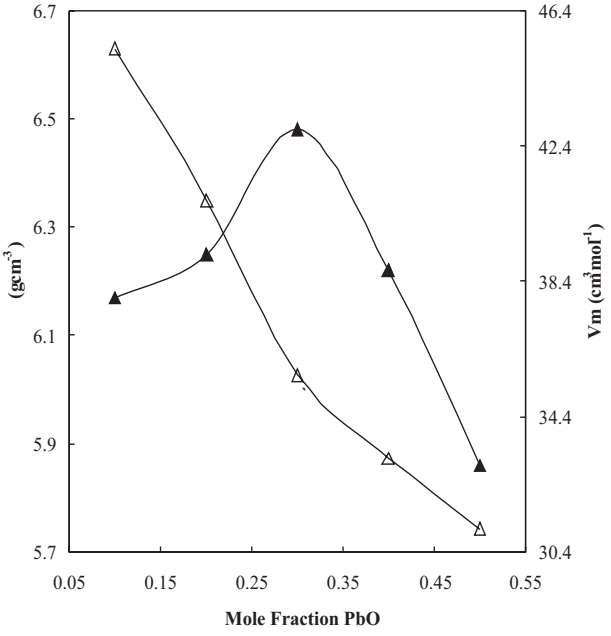

Fig. 1. Variation of Density (▲) and Molar volume ( ) as the function of mole fraction of *PbO in PbO-Bi_2O_3-SiO_2* glass system

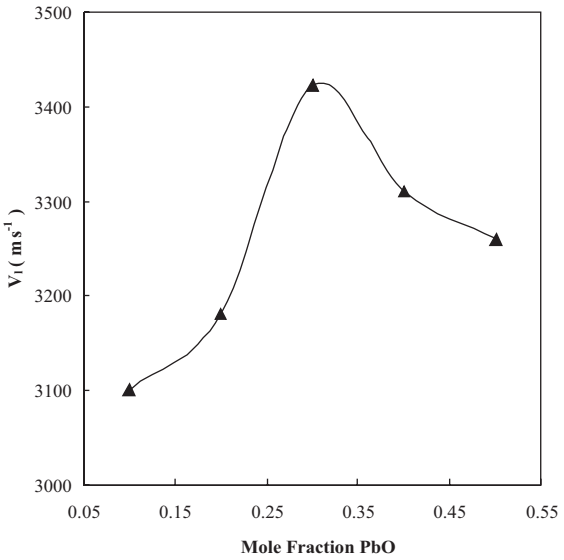

Fig. 2. Variation of Longitudinal ultrasonic velocity ( ) as the function of mole fraction of *PbO* in *PbO-Bi_2O_3-SiO_2* glass system

provided by these parameters. (Figs. 2, 3 and Table 1). In the light of this situation, it can be concluded conclusively that the glass structure has maximum elastic strength for 30 mol%*PbO* +*30* mol%Bi_2O_3 +*40* mol%SiO_2 composition.

FTIR spectra for the glasses have been plotted in Fig. 4. IR absorption band of the prepared glass samples in the range 450-600 cm^{-1} may be assigned to *Si-O-Si* and *O-Si-O* bending modes. This band is centered around 480 cm^{-1}. The IR absorption in the range 800-1000cm^{-1} is probably due to *Si-O-* stretching with non- bridging oxygens. The band around 1000-1300 cm^{-1} may be assigned to asymmetric stretching mode of *Si-O*. Absorption band around 450-600 cm^{-1} almost disappears during the change of composition of *PbO* from 30 to 40. Around the same composition change, absorption band of 800-1000cm^{-1} becomes shallow. These results indicate the structure change around 30mol%PbO +30mol%Bi_2O_3 +*40*mol%SiO_2 composition.

Gamma-ray mass attenuation coefficients of *PbO-Bi_2O_3-SiO_2* glass system have been evaluated by using XCOM computer software and results have been shown in Fig. 5. It is observed that the values of mass attenuation coefficient for the prepared glass samples is better than the conventional gamma-ray shielding material 'barite concrete' thus indicating that the prepared glass samples can be possible candidates as gamma-ray shielding materials. The additional advantage of the

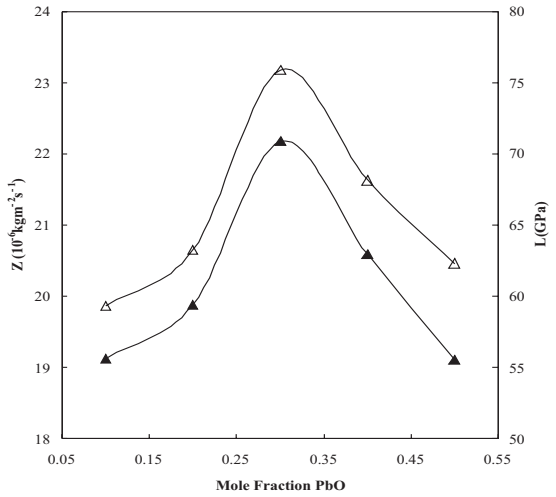

Fig. 3. Variation of Acoustic impedance ( ) and longitudinal modulus ( ) as the function mole fraction of *PbO* in *PbO-Bi_2O_3-SiO_2* glass system

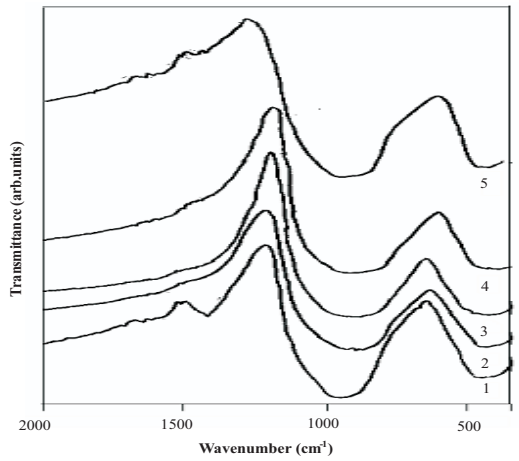

Fig. 4. FTIR spectra of *PbO-Bi_2O_3-SiO_2* glass system

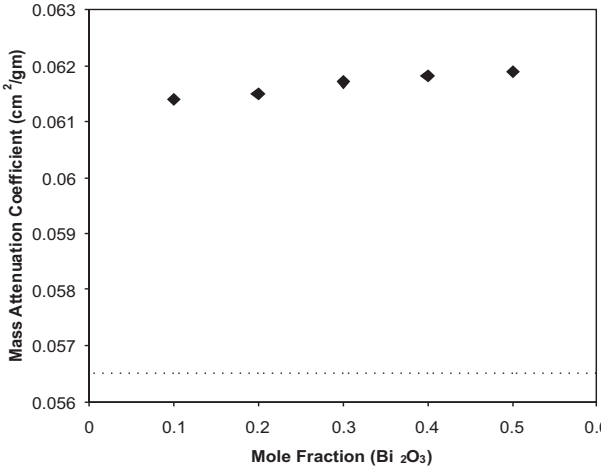

Fig. 5. Calculated values of Mass Attenuation Coefficient by using XCOM as a function of mole fraction of Bi_2O_3 in the *PbO-Bi_2O_3-SiO_2* glass system at 1173KeV for the prepared glass ( )samples. Theoretical values of barite concrete (--------) are included for comparison

prepared glass samples over concrete is their transparency to visible light. Chemical composition of barite concrete have been reported by authors elsewhere[10].

CONCLUSIONS

Glasses of the system *PbO-Bi_2O_3-SiO_2* with varying composition of *PbO* were prepared. Their structural and elastic properties have been analysed. It has been observed that the 30mol%*PbO* +*30*mol%Bi_2O_3 +*40*mol%SiO_2 glass composition provides the best elastic properties.

REFERENCES

1. **Singh, N.**, **Singh, K.J.**, **Singh, K.** and **Singh, H.**, Comparative study of lead borate and bismuth lead borate glass systems as gamma-radiation shielding materials, *Nucl. Instr. Meth. (B)*, **225** (2004) 305-309.

2. **Singh, N.**, **Singh, K.J.**, **Singh, K.** and **Singh, H.**, Gamma-ray attenuation studies of PbO-BaO-B_2O_3 glass system, *Radiat. Meas.*, **41** (2006) 84-88.

3. **Zahra, A.M.** and **Zahra, C.Y.**, DSC and Raman studies of lead borate and lead silicate glasses, *J.Non-Cryst. Solids*, **155** (1993) 45-55.

4. **Suzuki, S.** and **Abe, Y.**, The free volume of some oxide glasses at the transition temperature, *J. Non-Cryst. Solids*, **43** (1981) 141-143.

5. **Augustsson, T.**, Bragg grating-assisted MMI-coupler for add-drop multiplexing, *J. Lightwave Technol.*, **16** (1998) 1517-1522.

6. **Saddeek, Y.B.**, Ultrasonic study and physical properties of some borate glasses, *Mater. Chem. & Phys.*, **83** (2004) 222-228.

7. **Saddeek, Y.B.**, **Latif, L.** and **Abd, E.l.**, Effect of TeO_2 on the elastic moduli of sodium, borate glasses, *Physica* **B, 348** (2004) 475-484.

8. **Moneim, A., Abd, E.l., Daiem, A.M., Abd E.l.** and **Youssof, I.M.**, Ultrasonic and structural studies on T*i*O_2-doped *CaO-Al_2O_3-B_2O_3* glasses, *Phys. Stat. Sol.* **(a)** (2003) 192-201.

9. **Gaafar, M.S**. and **Marzouk, S.Y.,** Mechanical and structural studies on sodium borosilicate glasses doped with Er_2O_3 using ultrasonic velocity and FTIR spectroscopy, *Physica.,* **B 388** (2007) 294-302.

10. **Singh, K.J., Singh, N., Kaundal, R.S.** and **Singh, K.**, Gamma-ray shielding and structural properties of PbO-SiO_2 glasses, *Nucl. Instr. Meth.*, (B), **266** (2008) 944-948.

Prof. Ajit Ram Verma

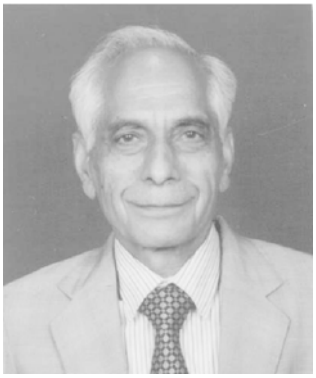

With great pain and anguish we have to report the sad demise of Prof. Ajit Ram Verma on 4 March 2009.

Prof. Ajit Ram Verma was an outstanding scientist with deep knowledge of fundamentals. He would only pick-up problems with strong impact on understanding of physical phenomena. He was a teacher par excellence just as he was endowed with extraordinary quality of communicating very difficult concepts in an understandable simple language. He made valuable contributions in school education as well as higher education. He had inspired three generations of researchers in three schools of research established by him, as well as scientists in general in national laboratories and academic centres. He was a highly elevated human being with deep spiritual base. His humility and understanding of human nature and treating even the junior most colleagues with respect and dignity endeared him to all. His administrative capability was of immense value to the growth of NPL as an internationally reputed centre. His experience and wise counsel benefited numerous national organizations, institutions and universities with which he had been associated either as a chairperson or a member of their Governing / Advisory bodies.

Professor Ajit Ram Verma was born on 20 September 1921 at Dalmau near Lucknow. After early education at several places including Allahabad and Meerut, he did M.Sc. in physics from Allahabad University in 1942. Even though he was a topper in M.Sc., he opted to pursue career in research rather than going for administrative services. After a short period as a research scholar at Allahabad, he was appointed as Lecturer in Physics at University of Delhi in 1947. During 1950-55, he worked at University of London and made well-known contributions on the observation and study of uni-molecular growth spirals on the surfaces of silicon carbide crystals. He was awarded Ph.D. in 1952 and D.Sc. in 1969 by the University of London. After serving as Reader in Physics for four years (1955-1959) at University of Delhi, he moved to BHU, Varanasi as Professor and Head, Department of Physics, in 1959. In 1965, he was appointed as Director, NPL, which he served till 1982. Thereafter, for three years, he served as Visiting Professor, IIT, Delhi and as Jawaharlal Nehru Fellow. Later, he was Emeritus Scientist of CSIR and INSA Sr. Scientist at NPL.

Academic and Research Contributions: Dr. Verma established three very active Schools of research in Crystallography, one each at University of Delhi, BHU (Varanasi) and NPL (New Delhi). In 1951, using Phase Contrast Microscopy, the first unequivocal experimental evidence in support of screw dislocation theory of crystal growth of millimetric sizes was provided by Dr. Verma. The correlation of the step heights of growth spirals with the dimensions of X-ray unit cell had helped in explaining the phenomenon of polytypism by the screw dislocation theory propounded by F.C. Frank. Professor Verma had also made valuable contributions in the pioneering work on direct measurement of metric thicknesses of Blodgett-Langmuir molecular films. At NPL, in collaboration with Dr. Krishan Lal, since 1966, he made several original contributions in the field of crystal growth and study of lattice imperfections.

As Director, NPL, from 1964-1982 Dr. Verma's efforts were focused on bringing Indian National Standards of Physical Measurement to International level. Also, with a view to replace artifact

standards, work was initiated by him on development of quantum standards. Dr. Verma laid the foundation of several new areas at NPL. These include: Quantum Metrology; Materials Science including work on electronic materials like silicon, phosphors, piezoelectric ceramics, liquid crystals, etc.; engineering materials like carbon fibers; synthetic hard materials, and consolidation of advanced materials characterization activities.

Support to Ultrasonics & USI: Prof. Verma had an unsurpassed ability to identify talent and nurture it, which resulted in NPL making great contributions and a strong impact at a National and International level. Impressed by a very successful development of Ultrasonic Interferometer at NPL, he created a new section on Ultrasonics, in late sixties. As Director, NPL, he took great interest in Ultrasonics activity, with the result that it became the largest (more than 35 people) and most active group in the country in ultrasonics during his time.

It was in this period (in 1974) that the Ultrasonics Society of India (USI) was founded. He gave all possible support and encouragement in its functioning at NPL. In 1979, the society started the publication of the Journal of Pure and Applied Ultrasonics. Prof Verma took considerable interest in its promotion and gave valuable guidance. In 1982, he became the First Patron of USI. After his passing away, USI lost a great admirer and a source of encouragement.

Professor Verma had authored 6 Books/Volumes, published more than 100 research papers in refereed journals and contributed numerous invited papers and book chapters. Professor Verma was recipient of several honours and awards. Notable among these are I.C.I. Fellowship (University of London) 1952-1955, Shanti Swarup Bhatnagar Prize in Physics in 1964, Fellow of Indian Academy of Sciences and National Academy of Sciences, Member of Editorial Board of Solid State Communications, Elected member of International Committee on Weights and Measures (CIPM) Paris 1966-1982, Member of Commission on Symbols, Units and Nomenclature of International Union of Pure & Applied Physics (IUPAP), Padma Bhushan in 1982, Atma Ram Puraskar in Hindi by Kendriya Sansthan, Agra in 1984.

Professor Verma was a person with many extraordinary qualities as mentioned above. He tried to practice what he preached. A most remarkable manifestation of this was the superb mental balance he exhibited during the last phase of his life, while battling the dreadful pancreatic cancer. He established strong human bond with numerous persons, from the highest to the modest. As a result he headed a very big family of people. His spiritual world was strongly influenced by the teachings of Geeta, Upanishads and Sant Kabir.

Dr Krishan Lal

ULTRASONICS SOCIETY OF INDIA

e-mail: info@ultrasonicsindia.com

ANNOUNCEMENT

Dr. T.K. Saksena Memorial Award For Distinguished Research

The "Dr. T.K. Saksena Memorial Award for Distinguished Research" has been instituted by the Ultrasonics Society of India, to recognize young researchers, who have made distinctive research contribution in the field of ultrasonics and allied areas. The award is initiated and sponsored by Dr. Skand Saksena, son of late Dr. Tribhuwan Kumar Saksena (01.11.1934 - 23.12.2008), whose pioneer contributions in the field of ultrasonics are milestones.

Award Highlights

* The Award will be given every year to one distinguished researcher, starting from the year 2009.
* A Trophy, a certificate, and a cash prize of Rs 5000/- will be presented to the awardee, a young researcher below 35 years of age, on the basis of the quality of his research work, carried out mainly in India, as reported in his Ph. D. thesis, and who has obtained his Ph. D. degree, during the previous two years.
* Brief details of all the applicants (names, title of thesis, synopsis, year, the University, the name of guide, etc.) will be published in the Journal of the USI "***Journal of pure and Applied Ultrasonics***".

How To Apply

Application shall be submitted on prescribed Application Form, obtainable from General Secretary, USI, along with the following documents.

1) Attested photocopy of the Ph.D. degree obtained.
2) Attested photocopy of the age proof.
3) Synopsis/ Summary of the thesis, and complete list of papers published.
4) Recommendation Certificate from the Ph. D. Guide, on his official stationary.

* The application should be mailed to:

Mr. S.K. Singhal
General Secretary (USI)
Deputy Director & Head
Shock & Vibration Sensors
National Physical Laboratory
Dr. K. S. Krishnan Road
NEW DELHI-110012.
e-mail : ssinghal@nplindia.org

* The last date of application for the award year 2009 is 31 October 2009.
* The award will be presented at the 18th National Symposium on Ultrasonics (NSU- XVIII) going to the held at the VIT-University, Vellore, Tamilnadu during 21-23, Dec. 2009.

ULTRASONICS SOCIETY OF INDIA

Room No. 106, Force Standard Building Annexe, National Physical Laboratory
Dr. K.S. Krishnan Road, New Delhi - 110 012
Phone : +91-11-45608694, 45608565
Fax: +91-11-45609310 e-mail : info@ultrasonicsindia.com

APPLICATION FORM

(Dr. T.K. Saksena Memorial Award For Distinguished Research)

To,
The General Secretary, USI

Sir,
I wish to apply for the Dr. T.K. Saksena Memorial Award for the year .....
My particulars are as given below :

Full Name ....
(in capitals) sir name first name middle name
Date of Birth ..... (DD/MM/YYYY) (Please also attach attested copy of age proof)
Title of Thesis .....
.....
Name of Supervisor .....
Name of University .....
Place of Research Work : .....
i) Name of Institution .....
ii) Address .....
Year of Award of Ph.D. ..... (Please attach photo copy of Degree)
Synopsis/Summary of Thesis : ..... (Please attach separate sheets)
Present Designation (If employed) .....
Organization with address .....
..... Pin : .....
Telephone Nos. (with STD code)
Mobile Phone no.: ..... E-mail I.D. .....

Please attach Recommendation Letter from your Guide on his Official stationary (with Phone numbers, email id, etc.)

Any other relevant information : .....
.....

RECOMMENDED

Signature of the Guide
Date .....
USI Membership No. (if any) .....

Signature of the Applicant
Date .....
USI Membership No. (if any) .....

Photocopies of this Application Form can be used.
The Applicatiion form can also be downloaded from www.ultrasonicsindia.com

R.N. 39355/81

18th National Symposium on Ultrasonics

(NSU-XVIII)

21-23 December 2009

Organized by

Ultrasonics Society of India

and

VIT

UNIVERSITY

(Estd. u/s.3 of UGC Act 1956)

Vellore - 632 014, Tamil Nadu, India

Venue

Physics Division
VIT University
Vellore - 632 104 (TN)

e-mail : ultrasonics2009@gmail.com, ultrasonic2009@yahoo.com
websites : www.vit.ac.in www.ultrasonicsindia.com.

Printed at : Alpha Printers, BG-2/ 38C, Paschim Vihar, New Delhi-110063, Ph : 9811848335